INTERMEDIATE TEMPERATURE PROTON CONDUCTING SYSTEMS BASED ON HETEROCYCLIC PROTOGENIC SOLVENTS

by

Fadime GÖKTEPE

August 2007

INTERMEDIATE TEMPERATURE PROTON CONDUCTING SYSTEMS BASED ON HETEROCYCLIC PROTOGENIC SOLVENTS

by

Fadime Göktepe

A thesis submitted to

the Graduate Institute of Science and Engineering

of

Fatih University

in partial fulfillment of the requirements for the degree of

Master of Science

in

Chemistry

August 2007

Istanbul, Turkey

APPROVAL PAGE

I certify that this thesis satisfies all the requirements as a thesis for the degree of Master of Science.

Assist. Prof. Dr. Metin TÜLÜ

Head of Department

This is to certify that I have read this thesis and that in my opinion it is fully adequate, in scope and quality, as a thesis for the degree of Master of Science.

Assoc. Prof. Dr. Ayhan BOZKURT

Supervisor

Examining Committee Members

Assoc. Prof. Dr. Ayhan BOZKURT _____

Assist. Prof. Dr. Metin TÜLÜ _____

Assist Prof. Dr. Abdülhadi BAYKAL _____

It is approved that this thesis has been written in compliance with the formatting rules laid down by the Graduate Institute of Sciences and Engineering.

Assist. Prof. Dr. Nurullah ARSLAN

Director

August 2007

INTERMEDIATE TEMPERATURE PROTON CONDUCTING SYSTEMS BASED ON HETEROCYCLIC PROTOGENIC SOLVENTS

Fadime Göktepe

M. S. Thesis - Chemistry
August 2007

Supervisor: Assoc. Prof. Dr. Ayhan BOZKURT

ABSTRACT

Anhydrous proton conducting polymer electrolytes were prepared by two different approaches. **In the first**, proton conducting polymer electrolytes have been synthesized by doping of Poly (styrene sulfonic acid), PSSA with 1H-1,2,4-Triazle, Tri and imidazole terminated triethyleneglycol, imi3. Polymer-dopant interactions were illustrated by FT-IR spectroscopy. The thermal properties of the blends were investigated by thermogravimetric analysis (TG) and found that the materials decompose when T> 200 ^{o}C. Differential scanning calorimetry (DSC) results demonstrated that dopants plasticized the host polymer. The proton conductivities of these materials changed with dopant type and increased with temperature. PSSATri$_1$ has a maximum proton conductivity of 0.016 S/cm measured at 150 ^{o}C. **In the second,** we have investigated proton conducting properties of anhydrous composites consisting of chitosan and poly (vinyl phosphonic acid), PVPA. The composites were prepared via in situ polymerization of vinyl phosphonic acid in the presence of chitosan. Homogeneous materials were produced and their compositions were analyzed by elemental analysis. Chitosan/PVPA interactions were studied by FT-IR and the morphology of the composites was investigated by XRD. Thermal properties of the composites were investigated by TGA and DSC techniques. Proton conductivity, activation energy and methanol permeability as well as water/methanol uptake of these membranes were also measured. Chitosan-PVPA composite material showed better proton conductivity compared to other ion-crosslinked materials in the anhydrous the state.

Keywords: Polystyrene sulfonic acid, Triazole, Thermal properties, Proton conductivity Chitosan, PVPA, polymer electrolyte.

HETEROSİKLİK PROTOJENİK SIVILARI TEMEL ALAN ARA SICAKLIKLI PROTON İLETKEN SİSTEMLER

Fadime Göktepe

Yüksek Lisans Tezi - Kimya
Ağustos 2007

Tez yöneticisi: Doç. Dr. Ayhan BOZKURT

ÖZ

Nemsiz proton iletken polymer elektrolitler iki farklı yaklaşıma göre hazırlandı. İlk olarak; proton iletken polymer elektrolitler, poli (stiren sülfonik asit)'e proton solvent olarak 1H-1,2,4-Triazol, Tri ve imidazol uçlu trietilenglikol, imi3 katılarak sentezlendi. Polimer-proton solvent arasındaki etkileşim FT-IR spektroskopi yardımıyla araştırıldı. Maddelerin termal sabitlikleri termal ağırlık analizi (TG) ile incelendi ve maddelerin T> 200 ^{o}C üzerinde termal bozulduğu bulundu. Diferansiyel taramalı kalorimetre (DSC) sonuçlarına göre katılan proton solventler polmer üzerinde plastifay etkisi gösterdi. Maddelerin proton iletkenlikleri katılan proton solvent türüne ve artan sıcaklıklara göre araştırıldı. En yüksek proton iletkenliği PSSATri$_1$ 150 ^{o}C de 0.016 S/cm ölçüldü. İkinci olarak; Citosan ve poli (vinil fosfonik asit), PVPA içeren nemsiz komposit maddelerin proton iletkenlikleri incelendi. Kompozitler çitosanın içerisinde vinil fosfonik asitin in situ polimerizasyon yöntemiyle hazırlandı. Homojen maddelerin içeriği elementel analiz ile incelendi. Çitosan/PVPA etkileşimi FT-IR ile incelendi ve maddelerin kristal yapısı XRD ile araştırıldı. Maddelerin termal sabitlikleri TGA ve DSC teknikleri ile araştırıldı. Bu maddelerin proton iletkenlikleri, aktivasyon enerjileri, methanol geçirgenlikleri, su/methanol tutmaları ölçüldü. Citosan-PVPA kompositlerinin proton iletkenlikleri nemsiz ortamdaki diğer iyonik çapraz bağlı maddelerle karşılaştırıldı.

Anahtar Kelimeler: Polistiren sülfonik asit, Triazol, Termal sabitlikleri, Proton iletkenliği, Çitosan, PVPA, Polimer elektrolit.

ACKNOWLEDGMENT

First of all, I would like to thank my thesis supervisor Assoc. Prof. Ayhan BOZKURT his motivation and will power kept me doing all the work. His academic activities will be references in my future studies.

I would like to thank Dr. Wolfgang Meyer from MPIP-Mainz/Germany where part of the characterizations were carried out.

This work is supported by TÜBİTAK under the contract number 104M220.

I would like to thank Şeyda T. Günday and for her help and other friends of my department for time support and patience.

Finally, I would like to thank my parents for their love, patience and encouragement.

TABLE OF CONTENTS

LIST OF TABLES

TABLE

LIST OF FIGURES

FIGURE

LIST OF SYMBOLS AND ABBREVATIONS

SYMBOLS/ABBREVATIONS

SPE	Solid Polymer Electrolytes
PVPA	Poly (vinylphosphonic acid)
PAMPSA	Poly (2-acrylamido-2-methyl -1-propanesulfonic acid)
PEM	Proton Exchange Membrane
PEMFC	Proton Exchange Membrane Fuel Cell
PTFE	Poly (tetraflouroethylene)
PBI	Polybenzimidazole
PEO	Poly (ethylene oxide)
PEI	Poly (ethyleneimine)
PAAM	Poly (acrylamide)
P-4VI	Poly(4-vinyl-imidazole)
Py	Pyrazole
MeIm	1-methylimidazole.
PAA	Polyacrylic Acid
MDP	Mono-dodecylphosphate
MP	Methanediphosphonic Acid
AFC	Alkaline Fuel Cell
PAFC	Phosphoric Acid Fuel Cell
MCFC	Molten Carbonate Fuel Cell
SOFC	Solid Oxide Fuel Cell
ECD	Electrochromic Device
EC	Electrochemical Cell
VTF	Vogel-Tammann-Fulcher
PSSA	Polystyrene sulfonic acid
imi3	1.12-diimidazol-2-yl-2,5,8,11-tetraoxa-dodecane

CHAPTER 1

INTRODUCTION

During last decade, the research activities in polymer electrolyte membranes increased progressively due to their potential application in advanced electrochemical devices such as polymer electrolyte membrane fuel cells (PEMFC). Hydrated perfluorosulfonic acid membranes such as Nafion® were successful in fuel cell application where these materials are typically segregate into hydrophobic and hydrophilic phases and conductivity occurs through latter phase via dissociated protons by the dynamics of water (Jannasch P 2003, Schuster MFH and Meyer WH 2003). However, these membranes have some weaknesses including complex external humidification, high material cost, high methanol crossover which have slowed down wide-spread industrial application (Bae B and Kim D 2003, Manthiram YFA and Guiver MD 2006). To overcome these limitations a number of studies have been performed to produce novel polymer based materials that can transport protons under anhydrous conditions.

The first approach toward alternative PEMFC was the polymer/acid complexes where the proton transport occur through phosphate ions ($H_4PO_4^+$, $H_2PO_4^-$) (Bozkurt A et al., 1999, Rikukawa M and Sanui K 2000). Another recent approach was the doping of the acidic polymers with amphoteric heterocyclic structures such as imidazole (Yang C et al., 2001, Sevil F and Bozkurt A 2004), pyrazole (Kreuer KD et al., 1998) and benzimidazole (Yamada M and Honma I 2003). In these systems, the host polymer improves the mechanical properties and thin free-standing films can be produced. Polymers also function as a proton source by means of supplying protons to heterocyclic protogenic solvents that enhance the defect type proton conductivity. In addition, polymers which have low glass transition temperatures may assist the proton transport through segmental motions of the chains (Bozkurt A and Pakula T 2006). Although the imidazole based membranes yielded more promising conductivity results, the electrochemical performance under fuel cell conditions seems to be lower than

1H-1,2,4-Triazole, Tri (Li S et al., 2005). The ionic conductivity of Tri is approximately $1x10^{-3}$ S/cm above melting point (T_m = 120 ^oC). This conductivity result can be related to the low pKa_1 value where the self dissociation of Tri also produces charge carriers similar heterocyclic structures (Li S et al., 2005, Günday ST et al., 2006). In that respect, Tri seems to be an alternative proton solvent that can be doped into acidic host polymers and may improve the anhydrous conductivity of the materials in the dry state.

Polystyrene sulfonic acid (PSSA) is a basic material in polyelectrolyte chemistry and can be prepared by sulfonation of commercially available polystyrene (Rikukawa M and Sanui K, 2000). Practically, hydrated PSSA ionomer exhibits high proton conductivity and have been utilized as polymer electrolytes in fuel cells (Smitha B et al., 2005, Sun J 2001), but the replacement of water by Tri in PSSA may result in the production of low cost anhydrous membranes that can maintain a stable high conductivity at higher temperatures.

Applications of biopolymers in electrical devices are not only interesting but also important for environmental safety. Additionally, the production cost can be optimized by using a biopolymer instead of expensive sulfonated aromatic polymers. In that respect, chitosan is a highly specialized basic biopolymer which was established as the main industrial derivative of chitin. Chitosan has many characteristic properties such as hydrophilicity, biocompatibility, and antibacterial properties (Rao P.S. et al., 2007, Osugi N. et al., 2007). Amino functional groups of chitosan have a polycationic character and form ionic-crosslinks in the presence of acidic units (Osugi N. et al., 2007).

PVPA is a simple polymeric diprotic acid which can be produced by free radical polymerization of vinylphosphonic acid (Bingöl B. et al., 2006). The blends of PVPA with imidazole illustrated high proton conductivity in the anhydrous state (Yamada M. and Honma I., Polymer, 2005; Sevil F. and Bozkurt A. 2004).

Recently, nanoporous composite membranes based on chitosan /poly (vinyl alcohol) (PVA) (Saxena A. et al., 2006) and polymer electrolytes based on chitosan/methanediphophonic acid were also reported (Yamada M. and Honma I., 2005).

In these work, Polystyrene sulfonic acid (PSSA) was produced by sulfonation of polystyrene. Then the anhydrous membranes were produced by doping of PSSA with Tri and imi3 at several compositions to get $PSSATri_x$ and $PSSAimi3_x$ electrolytes. The characterization results were interpreted in terms of composition and compared with previously reported systems.

Additional, novel polymer composites comprising chitosan and poly (vinyl phosphonic acid) were produced (Figure 5.4). The materials prepared by in situ polimerization of vinyl phosphonic acid (VPA) in the existence of chitosan. The materials were characterized by FT-IR, Elemental analysis, TGA, DSC and XRD. Proton conducting properties of these anhydrous polymer composite electrolytes were discussed according to PVPA composition.

CHAPTER 2

PROTON CONDUCTION

A proton conductor is an electrolyte where movable hydrogen ions (protons) are the primary charge carriers. Proton conductivity also plays a key role in other important processes as diverse as the photosynthesis in plants to the generation of clean electrical energy in fuel cell power plants. Such as extensive range of proton transport and transfer phenomena has therefore attracted interest from material through understanding of the mechanisms and procosses has been established. Hence, the identification and development of new proton conducting materials, especially for the solid electrolyte domain, relies heavily on this collective knowledge.

Proton transfer mechanisms are well-established phenomena in nature. Most biochemical reactions are very sensitive to changes in the pH of the surrounding environment so proton transfer serves as a vital route in the cell pH stabilization. In biological systems, while information is generally transferred via metal ions, all processes which convert energy from one form to another involve protonation and deprotonation reactions (Voet D. and Voet J.G., 1992).

2.1. PROTON CONDUCTION MECHANISMS

The proton is unique in that it is the only ion which possesses no electronic shell. It therefore strongly interacts with the electron density of its environment. In the case of metals, the proton interacts with the electron density of the conduction band, and is considered to be a hydrogen atom with a protonic or hydridic character. Metals are also unique in that they allow

the proton (hydrogen) to have a high coordination number, typically four or six at a tetrahedral or octahedral site (Kreuer, 1988).

Proton transfer phenomena follow two principal mechanisms where the proton remains shielded by electron density along its entire diffusion path, so that in effect the momentary existence of a free proton is not seen. The most trivial case of proton migration requires the translational dynamics of bigger species: this is the vehicle mechanism (Kreuer et al., 1982). In this mechanism the proton diffuses through the medium together with a "vehicle" (for example, with H_2O as H_3O^+). The counter diffusion of unprotonated vehicles (H_2O) allows the net transport of protons. The observed conductivity, therefore, is directly dependant on the rate of vehicle diffusion. In the other principal mechanism, the vehicles show pronounced local dynamics but reside on their sites. The protons are transferred from one vehicle to the other by hydrogen bonds (proton hopping). Simultaneous reorganization of the proton environment, consisting of reorientation of individual species or even more extended ensembles, then leads in the formation of an uninterrupted path for proton migration. This mechanism is known as the Grotthuss mechanism. Water is a good conductor of protons, because of the H-bonded networks between water molecules that give water its liquid properties in the physiological range. In ice, the H-bonded networks are more extensive, and ice is a better conductor than liquid water. Conduction occurs through a "hop-turn" mechanism, first suggested by Grotthuss, and often referred to as the Grotthuss mechanism in figure 2.1.

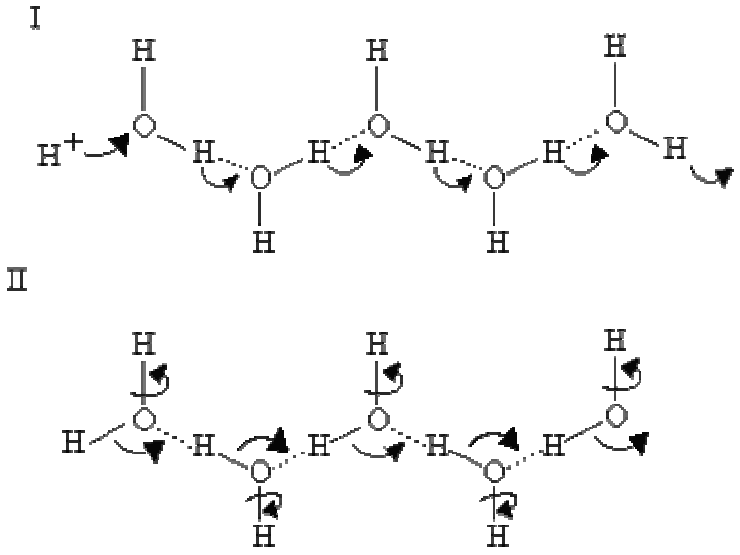

Figure 2.1. Grotthuss mechanism (Crofts A., 1996).

In the "hop" part of the mechanism, a proton first hops from the end of the H-bonded chain to an adjacent group (I, right); transfer of H-bond strength then allows it to be replaced by a H^+ binding at the other end, to give the structure in II. In the "turn" phase, rotation of the waters as shown in II then restores the starting structure (I). In this H-bonded chain, the waters can in principle be replaced by suitable protein side chains with H-bonding potential (Crofts A., 1996).

A fundamentally different approach toward high-temperature proton-conducting membranes points to materials with proton conductivity as an intrinsic property, i.e., functioning without any additional liquid phase. Theoretically, the path from a hydrated membrane to a single-phase polymer can be divided into two steps: First, water is substituted with another suitable proton solvent, which, in a second step, is integrated into the material by being covalently tethered to the polymer backbone (Figure 2.2). In principle, the second step aims at the immobilization of the proton solvent and thus may also be achieved by coulombic interactions (Schuster M.F.H. and Meyer W.H., 2003).

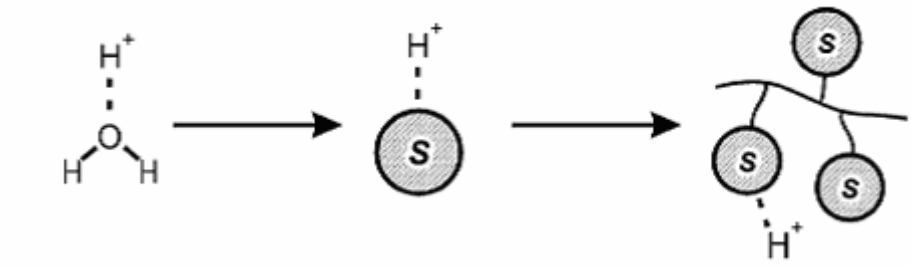

Figure 2.2. A hydrated membrane to an immobilized (polymeric) proton solvent (Schuster M.F.H. and Meyer W.H., 2003).

Recently, Kreuer emphasized the proton-conducting properties of nitrogen-containing aromatic heterocycles such as imidazole, pyrazole, and benzimidazole. In general, the behavior of these materials toward protons is very similar to that of water: The heterocycles are amphoteric molecules; they exhibit extensive hydrogen bond interactions that result in a fluctuating network, and, as mentioned above, to some extent undergo self-dissociation (Figure 2.3).

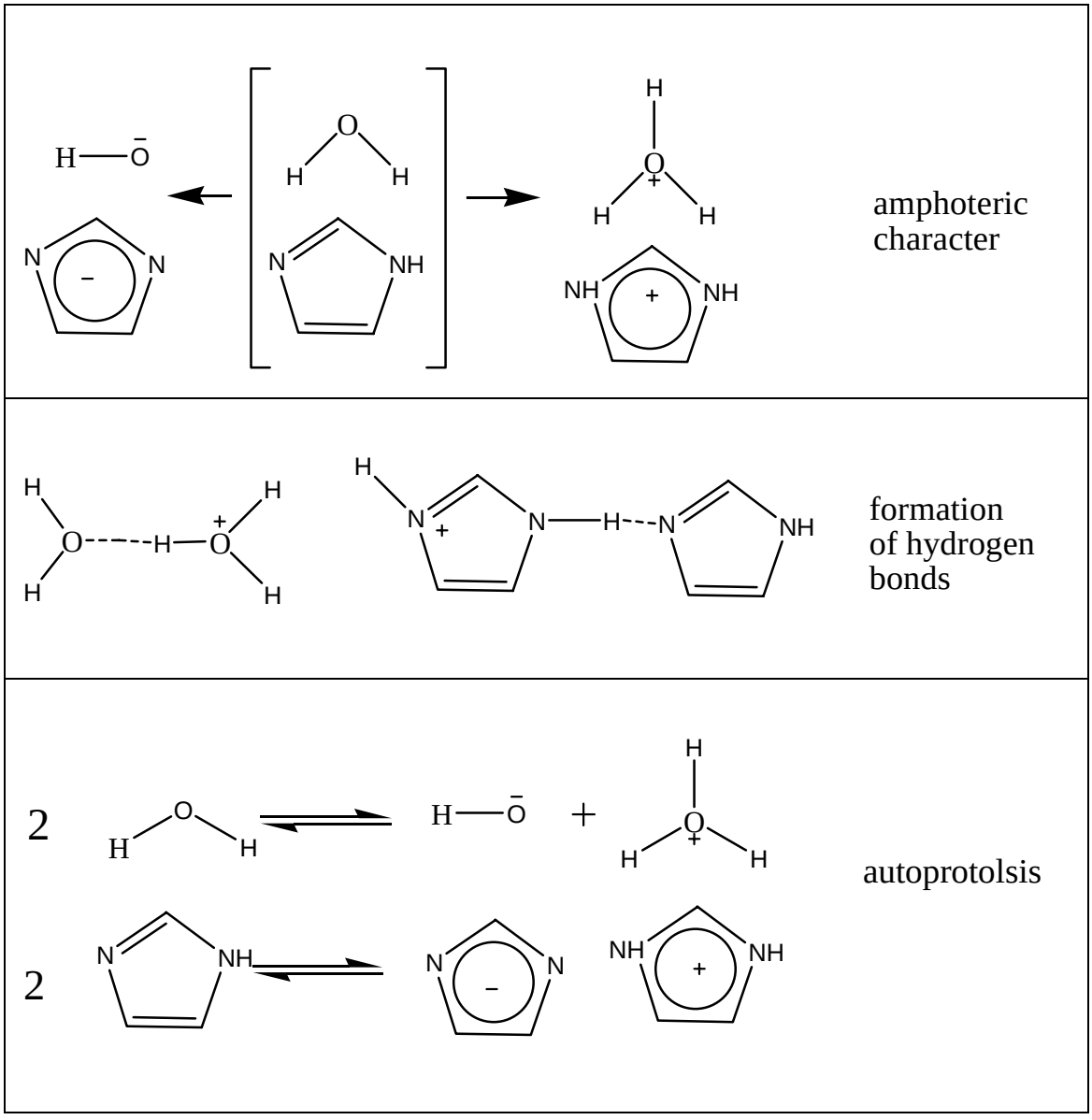

Figure 2.3. Imidazole and water exhibit similar behavior toward protons

These two principle mechanisms essentially reflect the difference in nature of the hydrogen bonds formed between the protonated species and their environment. In media which supports strong hydrogen bonding, the Grotthuss mechanism is preferred; the vehicle mechanism is characteristic of species with weaker bonding (Schuster M.F.H. and Meyer W.H., 2003).

CHAPTER 3

APPLICATION OF PROTON CONDUCTING ELECTROLYTES

3.1 FUEL CELLS

Fuel cells are electrochemical devices that convert the chemical energy of a reaction directly into electrical energy. The basic physical structure or building block of a fuel cell consists of an electrolyte layer in contact with a porous anode and cathode on either side. A schematic representation of a fuel cell with the reactant/product gases and the ion conduction flow directions through the cell is shown in Figure 3.1.

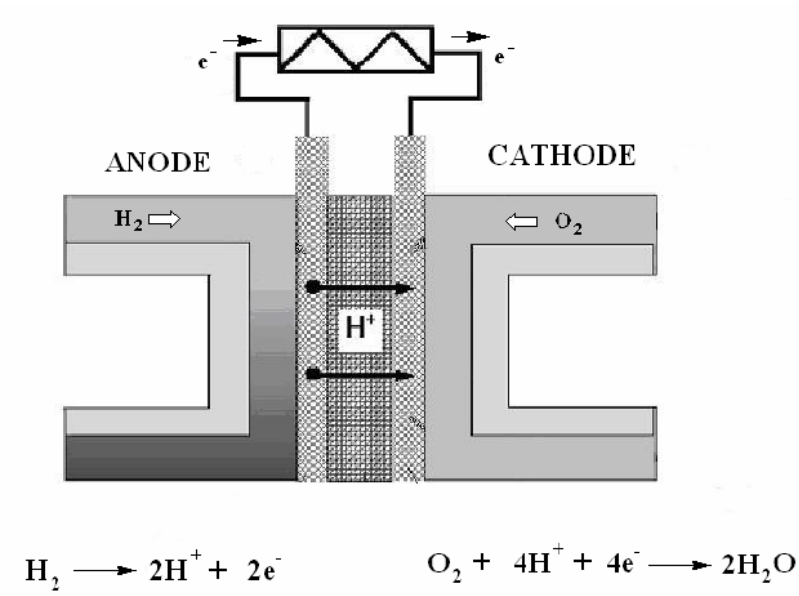

Figure 3.1. Schematic illustration of an Individual Fuel Cell(Fuel Cell Handbook,2000)

In a typical fuel cell, gaseous fuels are fed continuously to the anode (negative electrode) compartment and an oxidant (i.e., oxygen from air) is fed continuously to the cathode (positive electrode) compartment; the electrochemical reactions take place at the electrodes to produce an electric current. A fuel cell, although having components and characteristics similar to those of a typical battery, differs in several respects. The battery is an energy storage device. The maximum energy available is determined by the amount of chemical reactant stored within the battery itself. The battery will cease to produce electrical energy when the chemical reactants are consumed (i.e., discharged). In a secondary battery, the reactants are regenerated by recharging, which involves putting energy into the battery from an external source. The fuel cell, on the other hand, is an energy conversion device that theoretically has the capability of producing electrical energy for as long as the fuel and oxidant are supplied to the electrodes. Figure 3.2 is a simplified diagram that demonstrates how the fuel cell works. In reality, degradation, primarily corrosion, or malfunction of components limits the practical operating life of fuel cells (Fuel Cell Handbook, 2000).

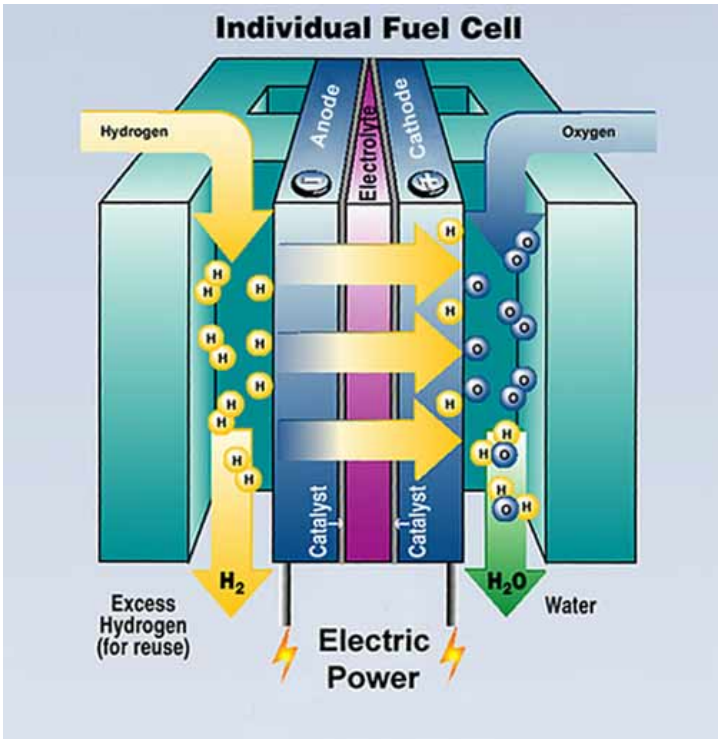

Figure 3.2 Simplified Fuel Cell Schematic (The Energy Policy Act, 2005)

Note that the ion specie and its transport direction can differ, influencing the site of water production and removal, a system impact. The ion can be either a positive or a negative ion, meaning that the ion carries either a positive or negative charge (surplus or deficit of electrons). The fuel or oxidant gases flow past the surface of the anode or cathode opposite the electrolyte and generate electrical energy by the electrochemical oxidation of fuel, usually hydrogen, and the electrochemical reduction of the oxidant, usually oxygen. In theory, any substance capable of chemical oxidation that can be supplied continuously (as a fluid) can be burned galvanically as the fuel at the anode of a fuel cell (Appleby and Foulkes, 1989).

Similarly, the oxidant can be any fluid that can be reduced at a sufficient rate. Gaseous hydrogen has become the fuel of choice for most applications, because of its high reactivity when suitable catalysts are used, its ability to be produced from hydrocarbons for terrestrial applications, and its high energy density when stored cryogenically for closed environment applications, such as in space. Similarly, the most common oxidant is gaseous oxygen, which is readily and economically available from air for terrestrial applications, and again easily stored in a closed environment. A three-phase interface is established among the reactants, electrolyte, and catalyst in the region of the porous electrode. The nature of this interface plays a critical role in the electrochemical performance of a fuel cell, particularly in those fuel cells with liquid electrolytes. In such fuel cells, the reactant gases diffuse through a thin electrolyte film that wets portions of the porous electrode and react electrochemically on their respective electrode surface. If the porous electrode contains an excessive amount of electrolyte, the electrode may "flood" and restrict the transport of gaseous species in the electrolyte phase to the reaction sites. The consequence is a reduction in the electrochemical performance of the porous electrode. Thus, a delicate balance must be maintained among the electrode, electrolyte, and gaseous phases in the porous electrode structure. Much of the recent effort in the development of fuel cell technology has been devoted to reducing the thickness of cell components while refining and improving the electrode structure and the electrolyte phase, with the aim of obtaining a higher and more stable electrochemical performance while lowering cost (Fuel Cell Handbook, 2000).

The electrolyte not only transports dissolved reactants to the electrode, but also conducts ionic charge between the electrodes and there by completes the cell electric circuit.

It also provides a physical barrier to prevent the fuel and oxidant gas streams from directly mixing.

The functions of porous electrodes in fuel cells are: 1) to provide a surface site where gas/liquid ionization or de-ionization reactions can take place, 2) to conduct ions away from or into the three phase interface once they are formed (so an electrode must be made of materials that have good electrical conductance), and 3) to provide a physical barrier that separates the bulk gas phase and the electrolyte. A corollary of item 1 is that, in order to increase the rates of reactions, the electrode material should be catalytic as well as conductive, porous rather than solid. The catalytic function of electrodes is more important in lower temperature fuel cells and less so in high temperature fuel cells because ionization reaction rates increase with temperature. It is also a corollary that the porous electrodes must be permeable to both electrolyte and gases, but not such that the media can be easily "flooded" by the electrolyte or "dried" by the gases in a one-sided manner (Fuel Cell Handbook, 2000).

A variety of fuel cells are in different stages of development. They can be classified by use of diverse categories, depending on the combination of type of fuel and oxidant, whether the fuel is processed outside (external reforming) or inside (internal reforming) the fuel cell, the type of electrolyte, the temperature of operation, whether the reactants are fed to the cell by internal or external manifolds, etc. The most common classification of fuel cells is by the type of electrolyte used in the cells and includes.

1) Polymer electrolyte membrane fuel cell (PEMFC),
2) Alkaline fuel cell (AFC),
3) Phosphoric acid fuel cell (PAFC),
4) Molten carbonate fuel cell (MCFC), and
5) Solid oxide fuel cell (SOFC),

These fuel cells are listed in the order of approximate operating temperature, ranging from ~80 °C for PEFC, ~100 °C for AFC, ~200 °C for PAFC, ~650 °C for MCFC, ~800 °C - 1000 °C for SOFC. The operating temperature and useful life of a fuel cell dictate the physicochemical and thermo mechanical properties of materials used in the cell components (i.e., electrodes, electrolyte, interconnect, current collector, etc.). Aqueous electrolytes are limited to temperatures of about 200 °C or lower because of their high water vapor pressure

and/or rapid degradation at higher temperatures. The operating temperature also plays an important role in dictating the type of fuel that can be used in a fuel cell. The low-temperature fuel cells with aqueous electrolytes are, in most practical applications, restricted to hydrogen as a fuel. In high-temperature fuel cells, CO and even CH_4 can be used because of the inherently rapid electrode kinetics and the lesser need for high catalytic activity at high temperature. However, descriptions later in this section note that the higher temperature cells can favor the conversion of CO and CH_4 to hydrogen then use the equivalent hydrogen as the actual fuel.

3.1.1 Polymer Electrolyte Fuel Cell (PEFC)

The idea of using an organic cation exchange membrane as a solid electrolyte in electrochemical cells was first described for a fuel cell by Grubb in 1959. At present the polymer electrolyte fuel cel (PEMFC) is the most promising candidate system of all fuel cell systems in terms of the mode of operation and applications. PEMFC consists of two electrodes and a solid polymer membrane, which acts as an electrolyte.

A schematic view of a polymer electrolyte membrane fuel cell is shown in Fig. 3.3. The H_2/O_2 fuel cell, commonly referred to as polymer electrolyte fuel cell (PEMFC), and the direct methanol fuel cell (DMFC) are the two types of fuel cells which use polymer electrolytes. DMFCs have higher energy density but exhibit shortcomings such as (a) slower oxidation kinetics than PEMFC below 100 ◦C and (b) significant permeation of the fuel from the anode to the cathode resulting in a drop in efficiency of fuel utilization upto 50% (Smitha et al., 2005).

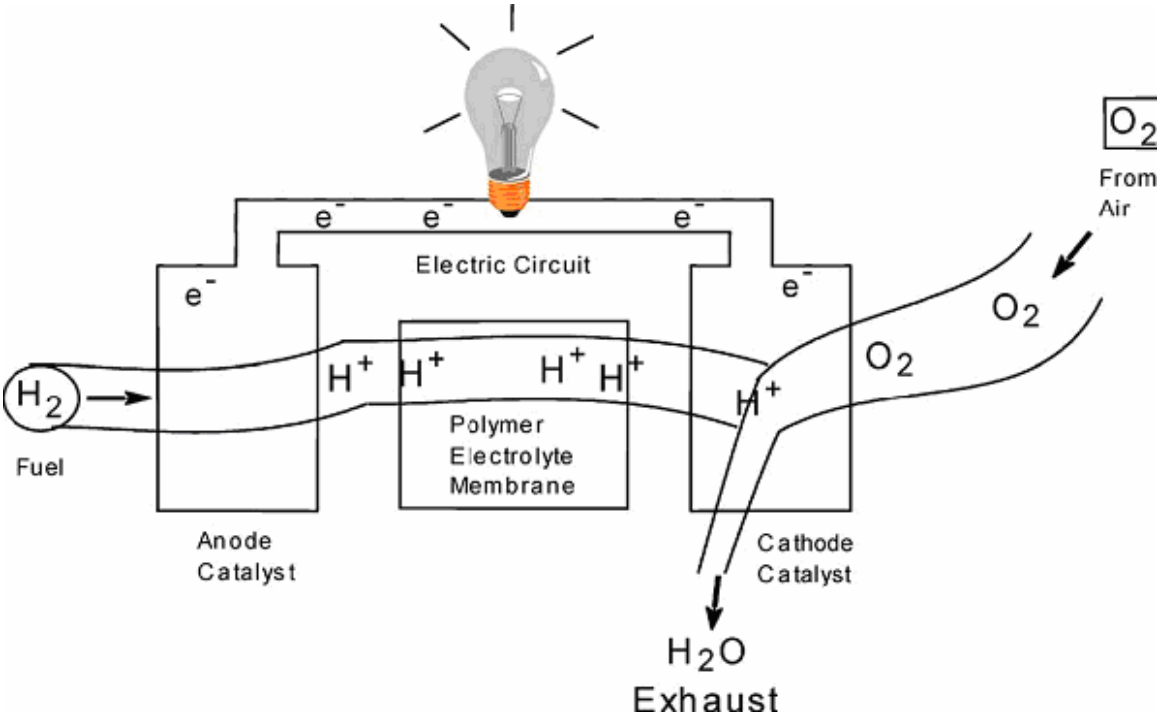

Figure 3.3 Schematic view of a PEM fuel cell (Smitha et al., 2005).

The polymer electrolyte membrane is sandwiched between two platinumporous electrodes such as carbon paper and mesh. Some single cell assemblies can be mechanically compressed across electrically conductive separators to fabricate electrochemical stacks. In general, PEMFCs require humidifed gases, hydrogen and oxygen (or air) as a fuel for their operation. The electrochemical reactions that occur at both electrodes are as follows:

Anode : $H_2 \rightarrow 2H^+ + 2e^-$

Cathode : $1/2\ O_2 + 2H^+ + 2e^- \rightarrow H_2O$

Overall : $H_2 + 1/2\ O_2 \rightarrow H_2O$ + Electrical Energy + Heat Energy

In recent years, PEMFCs have been identifed as promising power sources for vehicular transportation and for other applications requiring clean, quiet, and portable power. Hydrogen-powered fuel cells in general have a high power density and are relatively effcient in their conversion of chemical energy to electrical energy. Exhaust from hydrogen-powered fuel cells is free of environmentally undesirable gases such as nitrogen oxides, carbon monoxide, and residual hydrocarbons that are commonly produced by internal combustion engines. Carbon dioxide, a greenhouse gas, is also absent from the exhaust of hydrogen-powered fuel cells. Thus, transportation uses, especially fuel cell electric vehicles (FCEV), are

on attractive and effective application because of not only clean exhaust emissions and high-energy eficiencies but also effective solution to the coming petroleum shortage. While FCEV might provide the greatest societal benefts, its total impact would be small if only a few FCEVs are sold due to lack of fueling infrastructure or due to high vehicle cost. The major obstacles for the commercial use of FCEV are expensive materials and low performances at high temperatures (over 100C) and low humidities (Rikukawa and Sanui, 2000).

The factors affecting the performance of these alternatives, viz., level of hydration and thickness of the membrane, play an important role in deciding their suitability for application in fuel cell.

1) Hydration: The performance of a membrane is dependent on proton conductivity, which in turn depends on prevailing levels of hydration. Higher conductivity is supported by higher levels of hydration. However, for operations with wet membranes, there is a possibility of the cathode being flooded which slows down the oxidation reaction. This is in particular a problem with Nafion®, because of a phenomenon knownas electro-osmotic drag.

2) Thickness. One of the ways to avoid water drag or water crossover is to reduce the membrane thickness thereby enabling an improvement in the fuel cell performance. Other advantages of reduced thickness include lower membrane resistance (and therefore an enhancement in membrane conductivity), lower cost and rapid hydration. However, there is a limit to the extent to which membrane thickness can be reduced because of difficulties with durability and fuel by-pass. An ideal way to balance this would be to spatially control the acidic regions or increase the charge density in the chemical microstructure of the proton exchange membrane to obtain highly conductive materials (Smitha et al., 2005).

Proton-conducting polymer electrolyte membranes for high performance PEMFCs have to meet the following requirements, especially for electric vehicle applications (Higuchi, 1994).

1. Low cost materials;
2. High proton conductivities over 10^{o}C and under 0^{o}C;
3. Good water uptakes above 100^{o}C;
4. Durability for 10 years.

The electrolyte in this fuel cell is an ion Exchange membrane (fluorinated sulfonic acid polymer or other similar polymer) that is an excellent proton conductor. The only liquid in this fuel cell is water; thus, corrosion problems are minimal. Water management in the membrane is critical for efficient performance; the fuel cell must operate under conditions where the byproduct water does not evaporate faster than it is produced because the membrane must be hydrated. Because of the limitation on the operating temperature imposed by the polymer, usually less than 120 °C, and because of problems with water balance, a H_2-rich gas with minimal or no CO (a poison at low temperature) is used. Higher catalyst loading (Pt in most cases) than that used in PAFCs is required for both the anode and cathode design.(Fuel Cell Handbook, 2000).

3.1.2 Alkaline Fuel Cell (AFC)

The electrolyte in this fuel cell is concentrated (85 wt %) KOH in fuel cells operated at high temperature (~250 °C), or less concentrated (35-50 wt %), KOH for lower temperature (<120 °C) operation. The electrolyte is retained in a matrix (usually asbestos), and a wide range of electro catalysts can be used (e.g., Ni, Ag, metal oxides, spineless, and noble metals). The fuel supply is limited to non-reactive constituents except for hydrogen. CO is a poison, and CO_2 will react with the KOH to form K_2CO_3, thus altering the electrolyte. Even the small amount of CO_2 in air must be considered with the alkaline cell (Fuel Cell Handbook, 2000).

3.1.3 Phosphoric Acid Fuel Cell (PAFC)

Phosphoric acid concentrated to 100 % is used for the electrolyte in this fuel cell, which operates at 150 to 220 °C. At lower temperatures, phosphoric acid is a poor ionic conductor, and CO poisoning of the Pt electrocatalyst in the anode becomes severe. The relative stability of concentrated phosphoric acid is high compared to other common acids; consequently the PAFC is capable of operating at the high end of the acid temperature range (100 to 220 °C). In addition, the use of concentrated acid (100 %) minimizes the water vapor pressure so water management in the cell is not difficult. The matrix universally used to retain the acid is silicon carbide and the electrocatalyst in both the anode and cathode is Pt. (Fuel Cell Handbook, 2000).

3.1.4 Molten Carbonate Fuel Cell (MCFC)

The electrolyte in this fuel cell is usually a combination of alkali carbonates, which is retained in a ceramic matrix of $LiAlO_2$. The fuel cell operates at 600 to 700 °C where the alkali carbonates form a highly conductive molten salt, with carbonate ions providing ionic conduction. At the high operating temperatures in MCFCs, Ni (anode) and nickel oxide (cathode) are adequate to promote reaction. Noble metals are not required (Fuel Cell Handbook, 2000).

3.1.5 Solid Oxide Fuel Cell (SOFC)

Solid oxide fuel cells (SOFCs) use a hard, non-porous ceramic compound as the electrolyte. Since the electrolyte is a solid, the cells do not have to be constructed in the plate-like configuration typical of other fuel cell types. Solid oxide fuel cells operate at very high temperatures around 1,000°C (1,830°F). High temperature operation removes the need for precious-metal catalyst, thereby reducing cost. It also allows SOFCs to reform fuels internally, which enables the use of a variety of fuels and reduces the cost associated with adding a reformer to the system. SOFCs are also the most sulfur-resistant fuel cell type; they can tolerate several orders of magnitude more sulfur than other cell types. In addition, they are not poisoned by carbon monoxide (CO), which can even be used as fuel. This allows SOFCs to use gases made from coal.

High-temperature operation has disadvantages. It results in a slow startup and requires significant thermal shielding to retain heat and protect personnel, which may be acceptable for utility applications but not for transportation and small portable applications. The high operating temperatures also place stringent durability requirements on materials. The development of low-cost materials with high durability at cell operating temperatures is the key technical challenge facing this technology.

Scientists are currently exploring the potential for developing lower-temperature SOFCs operating at or below 800°C that have fewer durability problems and cost less. Lower-temperature SOFCs produce less electrical power, however, and stack materials that will function in this lower temperature range have not been

In low-temperature fuel cells (PEMFC, AFC, and PAFC), protons or hydroxyl ions are the major charge carriers in the electrolyte, whereas in the high-temperature fuel cells, MCFC, and SOFC, carbonate ions and oxygen ions are the charge carriers, respectively. Major differences between the various cells are shown in Table 3.1 (Fuel Cell Handbook, 2000).

Table 3.1. Summary of Major Differences of the Fuel Cell Types (Fuel Cell Handbook, 2000)

	PEMFC	**AFC**	**PAFC**	**MCFC**	**ITSOFC**	**TSOFC**
Electrolyte	Ion Exchange Membranes	Mobilized or Immobilized Potassium Hydroxide	Immobilized Liquid Phosphoric Acid	Immobilized Liquid Molten Carbonate	Ceramic	Ceramic
Operating Temperature	80°C	65-220°C	205°C	650°C	600-800°C	800-1000°C
Charge Carrier	H^+	OH^-	H^+	CO_3^{2-}	O^{2-}	O^{2-}
External Reformer for CH_4 (below)	Yes	Yes	Yes	No	No	No
Prime Cell Components	Carbon-based	Carbon-based	Graphite-based	Stainless-based	Ceramic	Ceramic
Catalyst	Platinum	Platinum	Platinum	Nickel	Perovskites	Perovskites
Product Water Management	Evaporative	Evaporative	Evaporative	Gaseous Product	Gaseous Product	Gaseous Product
Product Heat Management	Process Gas + Independent Cooling Medium	Process Gas + Electrolyte Calculation	Process Gas + Independent Cooling Medium	Internal Reforming + Process Gas	Internal Reforming + Process Gas	Internal Reforming + Process Gas

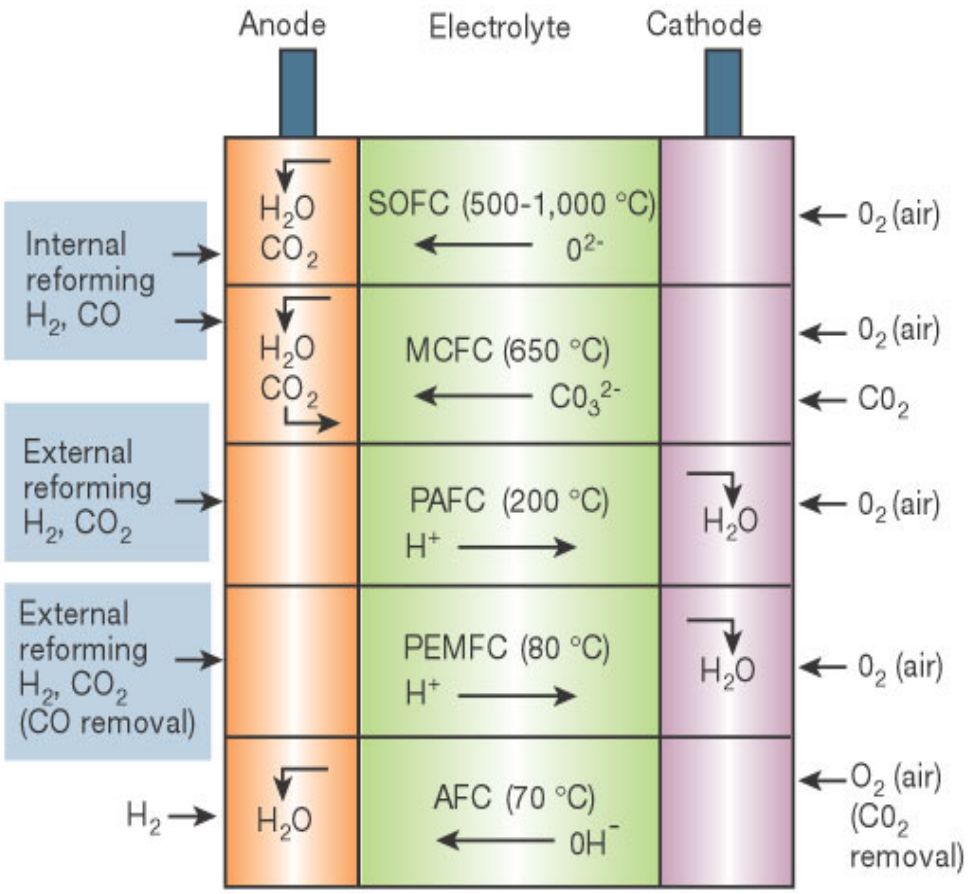

Figure 3.4. Overview of the different types of fuel cells. Temperature values indicate the maximum operating temperature (Steele B. C.H. and Heinzel A., 2001).

CHAPTER 4

POLYMER SYSTEMS

4.1. HYDRATED PROTON-CONDUCTING POLYMERS MEMBRANES

4.1.1. Perfluorinated membranes

The perfluorinated sulfonic acid membranes have been the subject of intense research. The key polymers used currently in portable fuel cell applications have perfluorinated structures with attached sulfonic acid groups. The perfluorinated polymer used most extensively and produced by DuPont goes by the trade name of Nafion®. Similar polymers are Flemion® produced by Asahi Glass and Aciplex-S® produced by Asahi Chemical (Fig.4.1). Among the three major types, the DuPont product is considered to be superior because of its high proton conductivity, good chemical stability and mechanical strength. Two research areas currently of interest on Nafion® are the transport phenomena within the membrane and modifications made to the membrane to increase its performance as well as water retention capacity. Proton transport in Nafion® in the presence of variations in operating parameters such as temperature, membrane thickness, and water content have been analyzed (Smitha et al., 2005).

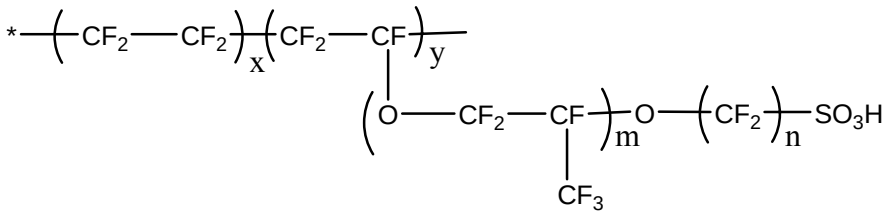

Nafion 117	m≥1, n=2, x=5-13.5, y=1000
Flemion	m=0, n=1-5
Aciplex	m=0, n=2-5, x=1.5-14
Dow membrane	m=0, n=2, x=3.6-10

Fig.4.1. Chemical structures of perfluorinated polymer electrolyt membranes(Rikukawa and Sanui 2000).

Level of hydration is a critical parameter in Nafion® membrane that has to be maintained in order to retain its performance at temperatures above 100 ◦C. In the presence of water, protons as well as the sulfonic acid groups are in the solvated form, and this greatly facilitates the "hopping mechanism of protons". To understand the transport of water in perfluorosulfonic acid membranes, quantitative and qualitative modeling studies have been conducted for supporting the optimization of not only the composition of the membrane but operating conditions, thereby yielding higher efficiencies and power densities (Smitha et al., 2005).

Nafion® membranes exhibit a protonic conductivity as high as 0.10 S/cm under fully hydrated conditions. For a typical membrane thickness of, say, 175 μm (Nafion 117), this conductivity corresponds to a real resistance of around 0.2 Ωcm^2, i.e. a voltage loss of about 150 mV at a practical current density. The structure model of Nafion membrane which comprises ionic hydrophilic clusters, an amorphous hydrophobic region is suggested previously (Figure 4.2) (Kreuer et al., 1993). The transport properties of perfluorosulfonic membranes largely influenced by the water content of the membrane, particularly when the membrane in the acidic form. The hydrophilic cluster swells with the water content. In the dry state Nafion membrane behaves like an insulator but, when hydrated the membrane becomes conductive (Yeo et al., 1983, Pourcelly et al., 1990). Proton conductivity reaches maximum over a temperature range 55-70 ^{o}C, even tough water content is minimum.Out with these temperature ranges, the conductivity decreases resulting from deionization of the sulfonic acid groups and perhaps a change of the hopping distance between cluster zones (Rieke and Vanderborgh, 1987).

Ionomer-based membranes intended for high-temperature PEMFCs should preferably retain a high conductivity at low levels of humidification. Thus, there is a need to improve water retention at high temperatures and to improve performance at low water contents, while simultaneously giving special attention to chemical as well as morphological stability to resist excessive water swelling. The membrane morphology is important for the performance, and is linked to the nature of the ionomer and the membrane formation process in a quite complex manner. It typically depends strongly on the water content, and on the concentration and distribution of the acidic moieties (Kreuer, 2001, Ding, 2002, Tang, 2001). For example, Kreuer has shown that hydrated membranes based on sulfonated polyetherketone have a less

pronounced separation into hydrophilic hydrophobic domains, as well as a larger distance between the acidic moieties, as compared to the Nafion membrane (Kreuer, 2001, Jannasch, 2003).

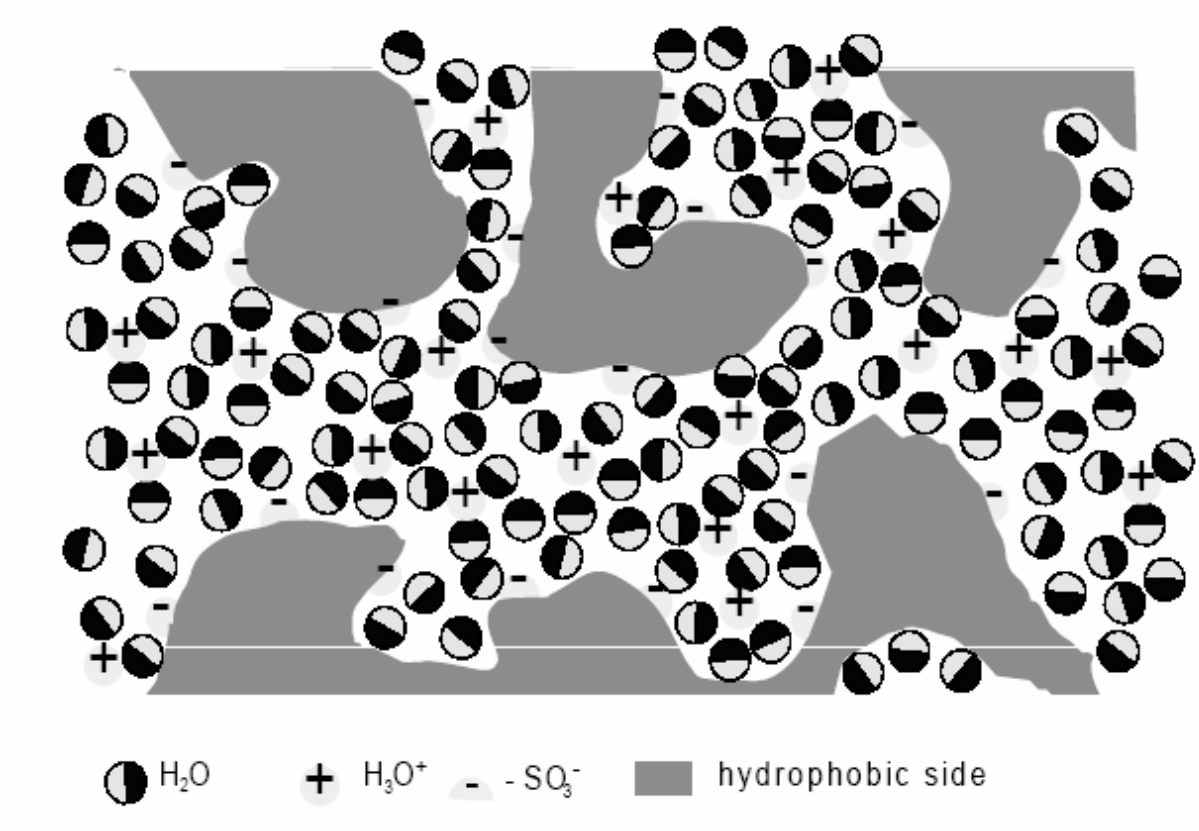

Figure 4.2 Structure model for Nafion perfluorosulfonic membrane (Kreuer, 2001).

Nafion® membranes also have disadvantages in DMFC applications: high methanol and ruthenium (for Pt–Ru anodes) crossover, high cost, low temperature limit (<80 ◦C), and high humidification requirements, among which MCO, which reduces the efficiency of the oxygen reduction reaction by the known mixed potential effect, is the major barrier preventing Nafion® membranes from being used successfully in DMFCs. Although Nafion® 112 is the most commonly used membrane for PEM fuel cells, Nafion® 117 is preferred for DMFC applications, in spite of higher ionic resistance, due to the significant reduction in MCO (Ball, 2005). A study of the crossover behavior of Nafion® 117, Nafion® 1135, Nafion® 1035, and Nafion® 112 was conducted using cyclic voltammetry (Ling and Savadogo, 2004). It was shown that the concentration of crossed methanol decreases with increasing thickness and equivalent weight (Neburchilov et al., 2007).

Perfluorinated PEMs have been developed by modification of the acid group (Hogarth and Glipa, 2001, Kotov et al., 1997). Thus, DesMarteau replaced the sulfonic acid group (-SO_3H) in Nafion with a sulfonyl imide group (-$SO_2NHSO_2CF_3$), which results in an increase in the water uptake while Kotov et al. developed membranes with a phosphonic acid group that has the potential for higher thermal stability (DesMarteau, 1995, Savett, 2002, and Kotov et al., 1997). Other perfluorinated PEMs include Gore-select which uses a PTFE matrix embedded in the perfluorinated PEM to provide mechanical strength, thus allowing membrane thickness to be reduced to below 20 mm. These membranes possess conductivity up to 0.01-0.1 S/cm depending on RH (Liu et al., 2001).

From the preceding discussion, it is clear that Nafion® and related polymers are still being intensely examined in view of the complex cell requirements of high proton conductivity and outstanding chemical stability combined with longevity of 60,000 h at 80 ◦C. The major disadvantages of these PFSA materials are the high cost of membrane; lack of safety during its manufacture and use; requirement of supporting equipment (Larminie and Dicks, 2000); and temperature related limitations (Rikukawa and Sanui, 2000). Degradation of PFSA membrane properties at elevated temperatures is another serious drawback (Smitha et al., 2005).

4.1.2. Sulfonated Hydrocarbon Polymer Membranes

Some sacrifce in material lifetime and mechanical properties may be acceptable, providing cost factors are commercially realistic. Good electrochemical properties over a wide temperature range may help the early marketing of PEFCs. Presently, one of the most promising routes to high-performance protonconducting polymer electrolyte membranes is the use of hydrocarbon polymers for polymer backbones. The use of hydrocarbon polymers as polymer electrolytes was abandoned in the initial stage of fuel cell development due to the low thermal and chemical stability of these materials. However, relatively cheap hydrocarbon polymers can be used for polymer electrolytes, since the lifetime of electrolytes required in FC vehicles are shorter when compared to use in space vehicles. Also, catalyst and FC assembly technologies have improved and brought advantages to the lifetimes of PEFCs and related materials (Rikukawa and Sanui, 2000).

There are many advantages of hydrocarbon polymers that have made them particularly attractive (Rikukawa and Sanui, 2000):

1. Hydrocarbon polymers are cheaper than perfluorinated ionomers, and many kinds of materials are commercially available.
2. Hydrocarbon polymers containing polar groups have high water uptakes over a wide temperature range, and the absorbed water is restricted to the polar groups of polymer chains.
3. Decomposition of hydrocarbon polymers can be depressed to some extent by proper molecular design.
4. Hydrocarbon polymers are easily recycled by conventional methods.

Over the last decade new proton-conducting polymer electrolyte membranes have been developed. These new membrane concepts include partially fluorinated membranes, composite membranes, and also aromatic polymer membranes. Poly(styrene sulfonic acid) is a basic material in this field. In practice, poly(styrene sulfonic acid) and the analogous polymers such as phenol sulfonic acid resin and poly(trifluorostyrene sulfonic acid), were frequently used as polymer electrolytes for PEFCs in the 1960s. Chemically and thermally stable aromatic polymers such as poly(styrene) (Gupta et al., 1993, Flint and Slade, 1997), poly(oxy-1,4-phenyleneoxy-1,4-phenylenecarbonyl- 1,4-pheneylene) (PEEK) (Bredas et al., 1982, Bailly et al., 1987), poly(1,4-phenylene) (Qi and Pickup, 1998, Kobayashi et al., 1998), poly(oxy-1,4-phenylene) (Chalk and Hay, 1968), poly(phenylene sulfide) (Qi et al., 1998), and other aromatic polymers (Johnson et al., 1984, Miyatake et al., 1996) can be employed as the polymer backbone for proton-conducting polymer electrolytes. These chemical structures are illustrated in Fig.4.3. These aromatic polymers are easily sulfonated by concentrated sulfuric acid.

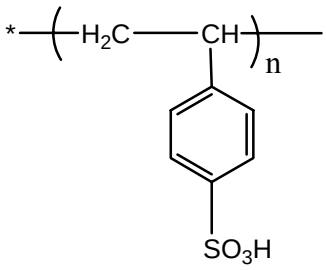

Poly(styrene sulfonic acid)

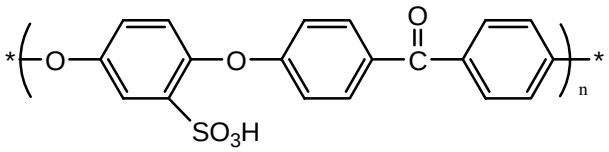

Sulfonated PEEK

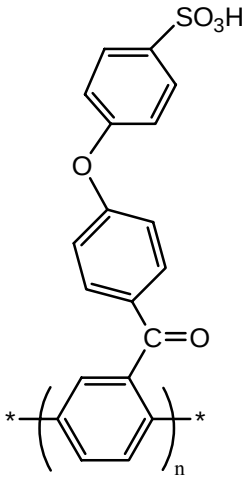

Sulfonated PPBP

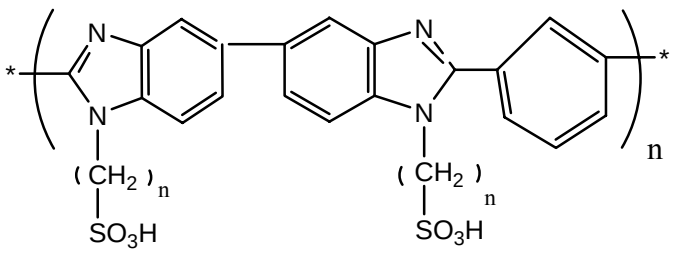

PBI-AS

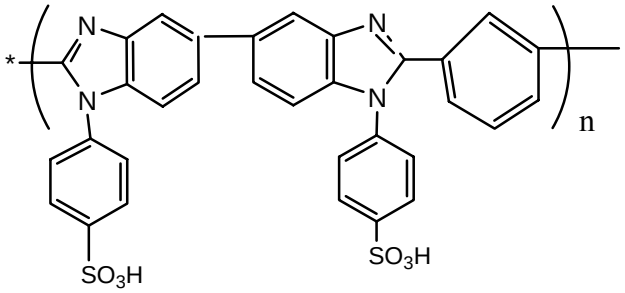

Sulfoarylated PBI

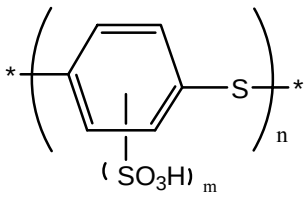

Sulfonated Poly(phenylene sulfide)

Figure 4.3. Chemical structure of polymer electrolyte membranes based on hydrocarbon polymers (Rikukawa and Sanui, 2000).

The thermal stabilities of S-PPBP investigated by TGA, S-PPBP showed an initial weight loss of about 20% of the original weight between 250 and 400^{o}C, which corresponds to a loss of sulfonic acid groups. Other proton-conducting polymer electrolytes based on sulfonated aromatic polymers also show thermal degradation between 200 and 400^{o}C.

The proton conductivity of sulfonated poly(thiopheneylene) is about 10^{-5} S cm^{-1} at 30% RH and it increases exponentially with relative humidity. The conductivity at 94% RH reaches up to 10^{-2} S cm^{-1}, where the water content of the polymer is 10.3 H_2O per sulfonic acid group. Films of S-PEEK and S-PPBP were placed in various relative humidities (0-100%) in order to absorb water into the films. The conductivity increased with a sigmoidal curve with increasing relative humidities and water uptake, and it reached almost 10^{-2} S cm^{-1} for S-PPBP with 65 mol% sulfonation, while that of S-PEEK for the same sulfonation level was 10^{-5} S cm^{-1}. A comparison of the proton conductivities of S-PEEK and S-PPBP for the same sulfonation level (65 mol%)(Rikukawa and Sanui, 2000).

In order to enhance stability at elevated temperatures, aromatic hydrocarbons can be (a) incorporated directly into the backbone of a hydrocarbon polymer or (b) polymers modified with bulky groups in the backbone to render them suitable for conduction of protons. Polyarylenes are high temperature rigid polymers with *T*g >200 ◦C owing to the presence of inflexible and bulky aromatic groups (Soczka-Guth et al., 1999). The aromatic rings offer the possibility of electrophilic as well as nucleophilic substitution. Polyethersulfones (PESF), polyether ketones (PEK) with varying number of ether and ketone functionalities (such as PEEK, PEKK, PEKEKK, etc.), poly(arylene ethers), polyesters and polyimides (PI) are some of the relevant examples of main chain polyarylenes (Gowariker et al., 1999). Studies reveal that polyesters must be avoided, as the ester group imparts instability in aqueous acids while polyaromatics are often preferred for fuel cell application due to their thermal stability. The specialty polymers on suitable modification are not only thermally stable but exhibit stability in oxidizing, reducing and acidic environments (Hoogers, 2003). Several research groups are working with different sulfonated polymers containing diarylsulfone units (Wang et al., 2002, Vogel et al., 2004). Direct sulfonated polyimides have also been extensively investigated (Guo et al., 2002, Besse et al., 2002). Asensio et al. have investigated sulfonated polybenzimidazoles and have found it to exhibit superior performance to Nafion at higher temperatures (Asensio et al., 2002, Bae et al., 2002). Poly(aryloxyphosphazene)s functionalized with phenyl phosphonic acid units and sulfonimide units (Hofmann et al.,

2002) have found application as candidate materials for fuel cells. Blending and radiation crosslinking of polyphosphazenes have also been investigated as means to reduce water swelling and methanol permeation of these ionomers (Carter et al 2002). Schuster et al. showed that imidazoleterminated ethylene oxide oligomers can reach conductivities of up to 10^{-5} S cm^{-1} at 120 ◦C (Schuster M. et al., 2001, Smitha, 2005).

Sulfonation with sulfuric acid, chlorosulfonic acid, sulfur trioxide, and acetylsulfate easily provides proton-conducting polymer electrolytes, but these sulfonated polymer electrolytes decompose on heating around 200-400^{o}C due to desulfonation. The introduction of alkylsulfonic substituents onto the backbone of aromatic polymers leads to thermally stable proton-conducting polymer electrolytes whose electrochemical properties can be controlled by the content of the substituent and the length of alkyl chain. These alkylsulfonic substituents can induce water uptake and proton conductivities similar to sulfonic acid groups without sacrificing desirable properties such as thermal stabilities, mechanical strengths, and chemical resistance. Alkylsulfonic substituents have synthesized poly(p-phenyleneterephthalamido-N-propanesulfonate),poly(p-phenyleneterephthalamido-N-methylbenzenesulfonate), poly[2,20-m-phenylene-5,50 bibenzimidazolyl-N-propanesulfonate], based on all-aromatic parent polymers, via a general method for attachment of alkylsulfonate or arenesulfonate side chains onto polymers containing reactive N-H sites .The alkylsulfonation and arenesulfonation of aromatic polymers are promising routes to the preparation of proton-conducting polymer electrolytes. For example, a solution of PBI in dimethylacetoamide (DMAc) is treated LiH or NaH, which deprotonates the nitrogen of the benzimidazole rings in the polymer backbone, and the addition of propanesulfonate side chains onto PBI was accomplished by the reaction of 1,3-propanesultone and the PBI anion, as shown in Fig.4.4.

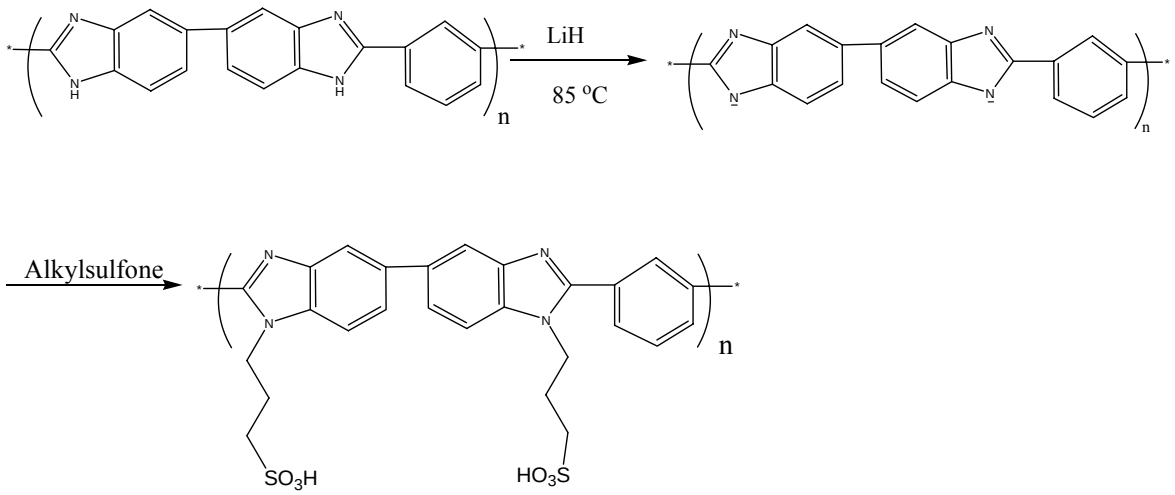

Figure 4.4. Synthesis of alkylsulfonated PBI.

Subsequent ion-exchange with H_3PO_4 or HCl provides proton-conducting polymer electrolytes based on PBI. The alkylsulfonation of PBI improved its solubility in organic solvents, where the solubility depended on the alkylsulfonation level. Alkysulfonated PBI was more soluble in polar aprotic solvents like methanol, DMAc, and DMSO when compared to the parent polymer (Kawahara et al., 2000).

The arenesulfonated and alkylsulfonated polymers based on all-aromatic backbones maintain high thermal stabilities when compared to the parent materials. The aim of derivatization of the parent polymers is to improve water absorption and to promote proton conductivity but retain a significant fraction of their high thermal stabilities.

Alkylsulfonated PBI is thermally more stable when compared with sulfonated aromatic polymer electrolytes whose degradation temperatures are in range of 200-350^{o}C. This thermal stability in alkylsulfonated polymer electrolytes is attributable to the strong chemical bond between the alkyl chain and the sulfonic acid groups. The addition of alkysulfonic acid groups to thermostable polymers with alkylsultone is one of the most important routes to synthesize thermally stable protonconducting polymer electrolytes. To design thermostable polymer electrolytes with hydrocarbon polymers, the additions of polar groups, as well as the choice of thermostable polymer backbones, are important factors.

The conductivity of a PBI-PS film containing 3.1 H_2O/SO_3H reached 10^{-5} S cm^{-1} at 80°C and decreased slightly at higher temperatures due to a small loss of water (about 10 wt%). The conductivity of PBI-PS containing more than 5.2 H_2O/SO_3H increased with an increase in temperature, and conductivity of the order of 10^{-3} S cm^{-1} was maintained over 100°C. The PBI-PS film containing 11.3 H_2O/SO_3H showed high proton conductivities on the order of 10^{-3} S cm^{-1} (Rikukawa and Sanui, 2000).

4.2. ANHYDROUS PROTON-CONDUCTING POLYMERS MEMBRANES

4.2.1. ACID-BASED COMPLEXES MEMBRANES

The development of novel proton-conducting polymers for various electrochemical applications is attracting considerable interest. There are still some limitations on the electrochemical properties and water uptake in proton-conducting polymers, especially at elevated temperatures. Complexes of basic polymers, such as poly(ethylene oxide) (PEO), poly(ethylene imine) (PEI), poly(acrylamide) (PAAM), and poly(vinylalchol) (PVA), i.e. with strong acids have been shown to possess high proton conductivities both in the dehydrated and hydrated states. Fig.4.5. shows some of the chemical structures for these materials (Rikukawa and Sanui, 2000).

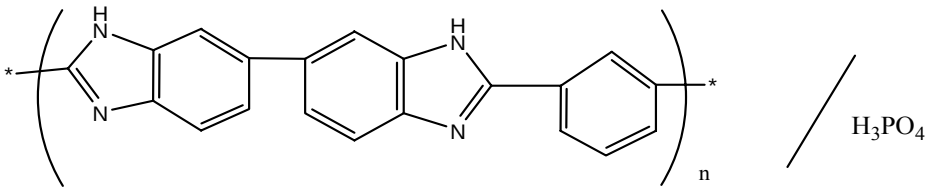

PBI/H_3PO_4

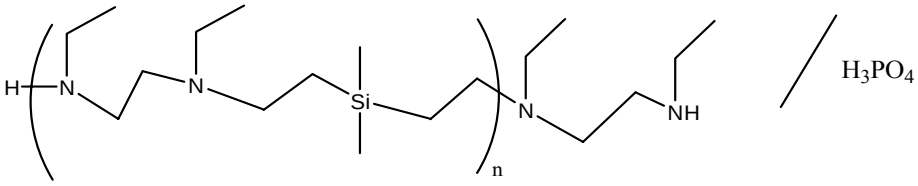

PSA/H_3PO_4

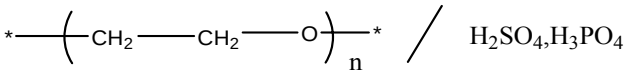

PEO/strong acid

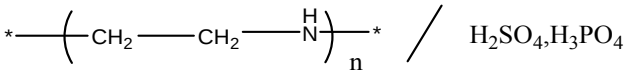

PEI/strong acid

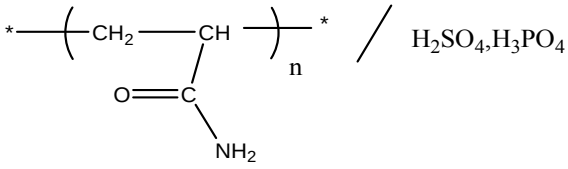

PAAM/strong acid

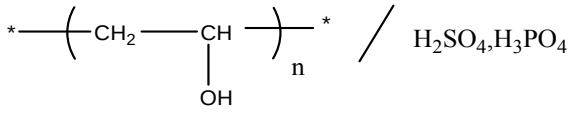

PVA/strong acid

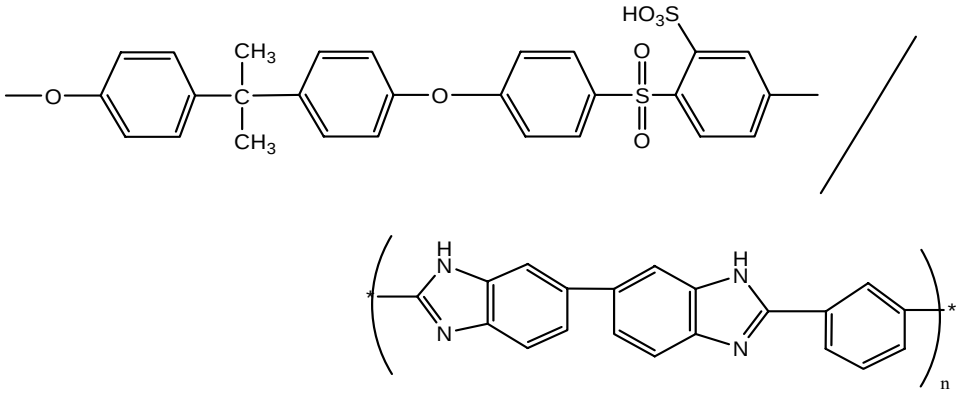

S-PSU/PBI

Figure 4.5. Chemical structures of polymer electrolytes based on acid-base polymer complexes (Rikukawa and Sanui, 2000).

Several research groups are currently developing high temperature PEMs based on complexes of strong acids, such as H_3PO_4 and H_2SO_4, with different basic polymers.

The property of phosphoric acid to interact via hydrogen bonds facilitates the preparation of blends with a large variety of polymers. In the case of basic polymers, proton transfer from phosphoric acid to the polymer helps for a wide miscibility of these complexes. However, the miscibility limits of phosphoric acid-polymer blends are often unknown, and some of the systems reported in the literature in reality may be inhomogeneous (Rikukawa and Sanui, 2000).

Phosphoric acid is a weak acid (pKa = 2.16) (Lide, 1995) that melts at 42^{o}C in the pure state and acts as an oxidant at elevated temperatures. With basic polymers, phosphoric acid undergoes hydrogen bond interactions or proton transfer reactions. In regard to its conductivity, phosphoric acid differs from water and many other solvents in two ways. First, conductivity is remarkably high in the pure state (Chin et al., 1989). Second, when strong electrolytes (e.g., H_2SO_4) are added, conductivity decreases rather than being improved (Munson et al., 1967). The first feature is due to the generation of charge carriers by self-dissociation ($5H_3PO_4 = 2H_4PO^+_4 + H_2PO^-_4 + H_3O^+ + H_2P_2O^{2-}_7$, where H_3PO_4 = 16.8 M, $H_4PO^+_4$ = 0.89 M, $H_2PO^-_4$ = 0.43 M, $H_3O^+ = H_2P_2O^{2-}_7$ = 0.46 M at 311 K) (Dippel et al., 1993, Munson 1964) and the fact that proton migration almost entirely results from structure diffusion (Dippel et al., 1993). The second feature is also closely related to the transport mechanism. The electrical field of extrinsic charge carriers causes a bias on hydrogen bonds and thus suppresses fluctuations within the dynamical hydrogen bond network (Kreuer 1996, Kreuer 2000). Addition of water, however, increases conductivity, which passes through a temperature-dependent maximum at compositions of 45 to 60% of H_3PO_4 (Chin et al., 1989).

4.2.1.1. PBI/ H_3PO_4

In 1995, a blend of poly(benzimidazole) and phosphoric acid was considered for hydrogen fuel cell and direct methanol fuel cell (DMFC) applications for the first time (Wainright et al.,1995). PBI is an amorphous (Singleton et al.,1967, Buckeley et al.,1988), basic polymer (benzimidazole:pKa = 5.5) (Lide, 1995) of extraordinary thermal stability and a

glass transition temperature of about 430^{o}C (Singleton et al.,1967, Gilham,1972). Qingfeng et al. found that the conductivity of PBI–H_3PO_4 complexes was insensitive to humidity, but strongly dependent on the acid content, reaching values of 0.13 S cm^{-1} at 160 ^{o}C and high acid-doping levels (Qingfeng et al., 2001). It was also shown that the water drag due to proton transport was almost zero in these PEMs. Wasmus et al. used solid-state NMR characterization of H_3PO_4 doped PBI to show that the phosphoric acid sorbed by the PBI membrane was relatively immobile as compared to free phosphoric acid, and revealed that there was an interaction between imidazole groups of PBI and phosphoric acid (Wasmus et al., 1995). Glipa et al. confirmed proton transfer from H_3PO_4 to the imino groups of PBI and the presence of undissociated H_3PO_4 at high doping levels with IR spectroscopy (Glipa et al., 1999). Li et al. measured conductivity as a function of temperature and a wide range of acid doping levels (x=3.0~16.0, where x is acid molecule per polymer repeat unit) at R.H. between 80%~85%. They obtained a conductivity of 4.6×10^{-2} S/cm at 165^{o}C. They suggested a useful H_3PO_4 doping level between 3.5~7.5, considering both conductivity and mechanical strength (Li et al., 2005). Kawahara et al. prepared H_3PO_4 doped PBI membranes by immersing the PBI membranes into a mixed solution of acid and methanol. The highest doping level observed was 2.9mol H_3PO_4/repeat unit. Based on FTIR data, they concluded that H_3PO_4 did not protonate the imidazole groups of PBI but interacted by hydrogen bonding between the OH and N groups. The presence of HPO_4^{2-} and $H_2PO_4^{-}$ anions, based on FTIR, implied that the proton conduction occurred according to the Grotthuss mechanism. The conductivity of the anhydrous PBIx2.9H_3PO_4 complex reached 10^{-4} S/cm at 160^{o}C. Fontanella et al. measured the isobaric conductivity data of PBIx6.H_3PO_4 membrane at temperatures of 25, 50, 75^{o}C. Based on the activation volume values (4~7 cm^3/mol), they proposed that proton transport in the acid doped PBI was mediated by segmental motions of the polymer (Fontanella et al., 1998). Pu et al. proposed that proton transport in phosphoric acid blended PBI was the consequences of the two contributions: one was based on rapid proton exchange (hopping) via hydrogen bonds between solvent molecules, which could be the phosphate, N-heterocycles of PBI and water molecules; and the other was based on the self-diffusion of phosphate moieties and water molecules (vehicle mechanism). They studied the temperature and pressure dependence of the conductivity of PBIxH_3PO_4 membranes (x=1.8~3.8) (Pu et al., 2002).

The PBI/strong acid polymer complexes were easily prepared by immersing PBI films into a strong acid/methanol solution (Kawahara et al., 2000, Rikukawa et al., 1996). The absorption level of strong acid molecule increased with increasing the concentration of the

strong acid, and the highest absorption level of 2.9 mol/unit was observed for PBI/H_3PO_4 polymer complexes.

All of the anhydrous PBI/strong acid polymer complexes exhibited proton conductions of 10^{-6}-10^{-9} S cm^{-1} at 100°C. The conductivity of PBI/H_3PO_4 polymer complex reached up to 10^{-5} S cm^{-1} at 160°C, while other PBI/strong acid polymer complexes showed a decrease in conductivity over 80°C. This result also reflects the good thermal stability of PBI/H_3PO_4 polymer complexes. The conductivity of the PBI/H_3PO_4 polymer complexes increased with increasing contents of H_3PO_4. The conductivity of PBI/H_3PO_4 complex (x ≈1.4) showed a different behavior, having relatively low conductivities over the entire temperature range. This phenomenon suggests that two H_3PO_4 molecules interact quantitatively with a PBI unit containing two imidazole groups and consequently an excess of H_3PO_4 to imidazole groups is necessary to give sufficient proton conductivity (Rikukawa and Sanui, 2000).

Compared with the established Nafion™ membranes, PBI is superior in several critical properties. PBI was reported (Savadogo and Varela, 2001) to be about 100 times cheaper than Nafion at present PBI is exclusively produced by celanese, who offer only complete membrane electrode assemblies (MEA) for operating temperatures of up to 200°C. Singleton et al. claim a considerably higher mechanical strength of doped PBI than that of Nafion (Singleton et al.,1967 , Wainright et al.,1995).

4.2.1.2. P-4VI/H_3PO_4

Poly(4-vinyl-imidazole), P-4VI, and phosphoric acid blends are reported (Bozkurt and Meyer, 2001).The number of moles of phosphoric acid per polymer repeat unit, x, was varied from 0 to 2 .These blends can be cast into homogeneous films. These blends are chemically stable up to about 150 °C. The softening temperature of the blends decrease from 77 °C for x = 1 to -8 °C for x = 2. Bozkurt and Meyer, 2001 was found the DC conductivity increases with x and reaches ~10^{-4} S/cm for x = 2 at ambient temperature.

4.2.1.3. PEO/H_3PO_4

PEO/H_3PO_4 complexes (x = 0.42 – 0.66) were described in 1988 by Donoso et al., who found conductivities of 2.5 x10^{-4} S/cm at 50 °C (x = 0.42) governed by segmental motion of

the polymer chains. Przyluski et al. reinvestigated these blends covering a wider range of compositions ($0.06 \leq x \leq 2.8$) by means of differential scanning calorimetry (DSC), IR, Vogel-Tamman-Fulcher (VTF), and impedance spectroscopy and found VTF behavior for small x and Arrhenius behavior for larger x. The molar amount of acid per mol of polymer repeating units is described by x.

4.2.1.4. PEI/H_3PO_4 or H_2SO_4

Anhydrous acid-base polymer complexes (PEI/x and PEI/xH_3PO_4) can also be obtained by protonation of branched commercial poly(ethylene imine) with H_2SO_4 or H_3PO_4. For partially protonated PEI ($x \leq 0.35$), only SO_4^{2-} or HPO_4^{2-} anions are present and the conduction seems to occur by proton exchange between protonated and unprotonated amine groups. Above $x \approx 0.35$, HSO_4^- or $H_2PO_4^-$ anions appear and the conductivity, likely to occur along the SO_4^{2-}/HSO_4^- or $HPO_4^{2-}/H_2PO_4^-$ anionic hydrogen-bonded chains, increases up to values of about 10^{-4} S cm^{-1} for PEI/0.5H_2SO_4 and about 10^{-5} S cm^{-1} for PEI/0.5H_3PO_4. Thin transparent films can be produced for $x \leq 0.35$, and they lose their mechanical properties and become very hygroscopic above this value because of the presence of excess acid. Fig.4.5. shows some of the chemical structures for these materials (Senadeera et al., 1996).

PEI/H_3PO_4 blends ($x \leq 0.5$) were introduced by Daniel et al., 1988, who found conductivities of 1 to $3x10^{-3}$ S/cm at 100 °C. At x = 0.35, a precipitate was formed from the aqueous solution, which redissolved upon further addition of H_3PO_4 (x = 0.58). Schoolman et al. characterized blends of higher acid contents ($x \leq 2$) that were applied as electrolytes for electrochromic devices. Whereas these researchers(Daniel et al., 1988, Schooleman et al., 1992) used branched commercial PEI. Tanaka et al., 1995, compared branched and linear PEI and found somewhat higher conductivities for the latter; however, compared with the results from Daniel et al., conductivities of the branched materials were about two orders of magnitude lower, which were attributed to the different preparation and purification procedures.

Composition-dependent conductivities of branched and linear PEI blends (Daniel et al., 1988, Tanaka et al., 1995) exhibited a local maximum at $x \approx 0.2$ and dropped to a minimum at $x \approx 0.4$, where the formation of PEI-H^+ 1/2 HPO_4^{-2} was completed (the maximum degree of protonation of PEI is ~ 80%) (Bloys and Staverman, 1974). This behavior is in accordance

with a maximum Tg of the blend (Daniel et al., 1988, Lassegues et al., 1989) and the precipitation from aqueous solution (Daniel et al., 1988) at $x \approx 0.35$. At higher acid levels, conductivity increased again and achieved values of 1.4 x 10^{-3} S/cm (^{l}PEI, $x = 2.05$; 100 ^{o}C) (Tanaka et al., 2000).

Properties of the hygroscopic, deliquescent linear PEI blends could be improved by crosslinking, which moderately influences conductivity at high x, but nearly reverses its dependence on composition at low x (Tanaka et al., 2000).

4.2.1.5.PAAM/H_3PO_4 or H_2SO_3

PAAM/H_3PO_4 blends showed relatively high conductivities ($4x10^{-3}$ S/cm, 20^{o}C, x= 2). However, condensation of the amide groups was observed at 100 ^{o}C in dry air (Rodriguez et al., 1993). Acid-base polymer complexes of PAAM and strong acids such as H_3PO_4 or H_2SO_3 exhibit a high proton conductivity in the range of 10^{-4}-10^{-3} S cm $^{-1}$ at ambient temperatures. The proton conductivity increases with temperature to about 10^{-2} S cm^{-1} at 100^{o}C. However, the mechanical and chemical stability of these complexes is relatively poor, and chemical degradation is often observed after humidification (Stevens et al., 1997, Wieczorek and Stevens, 1997).

4.2.2. POLYMER/HETEROCYCLE HYBRID MATERIALS

4.2.2.1. PVPA-Heterocycle Composite Material

Anhydrous proton conducting polymer electrolytes have been prepared by doping of poly(vinylphosphonic acid) (PVPA) with imidazole (Im). FT-IR results indicate the transfer of acidic protons to imidazole units to form imidazolium ions. Thermogravimetric analysis illustrates that these blends are thermally stable up to about 150 ^{o}C. The glass transition temperatures of the blends were detected via differential scanning calorimetry. The Tg of the homopolymer is -23 ^{o}C shifted to-15 ^{o}C for x = 0.5 and 5 ^{o}C for x = 1. For x = 2 there is excess imidazole in the material which plasticized the material shifting the Tg to -36 ^{o}C. DC conductivity increases with doping ratio of Im reaching ,$5x10^{-3}$ S/cm for x = 2 at 130 ^{o}C (Sevil and Bozkurt, 2004).

Yamada and Honma have prepared the acid–base composite materials by mixing of a strong phosphonic acid polymer poly(vinylphosphonic acid) (PVPA) with the high proton exchange capacity and an organic base heterocycle, such as imidazole (Im), pyrazole (Py), and 1-methylimidazole (MeIm)(Figure 3.4). This PVPA-heterocycle composite material exhibited a large proton conductivity of $7x10^{-3}$ S cm^{-1} at 150 ^{o}C under anhydrous condition. Additionally, the thermal stability of composite material was found to increase with the mixing ratio of the heterocycle.

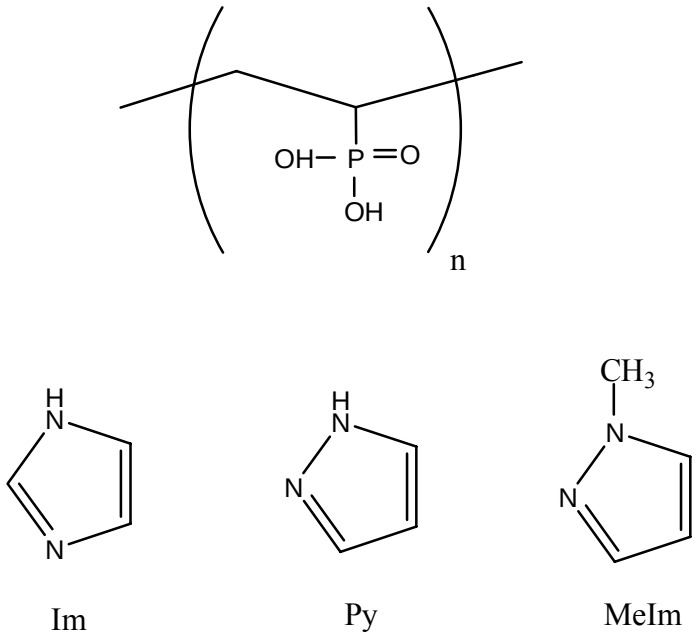

Figure 4.6. Molecular structures of poly (vinylphosphonicacid) (PVPA), imidazole(Im), pyrazole (Py), and 1-methylimidazole(MeIm).

Anhydrous proton conductivity of PVPA-heterocycle composite materials showed differences of approximately one order of magnitude, depending on the molecular structure of basic heterocycles. These different conductivities of composite materials are due to the pKa value of heterocyclic molecules. The pKa values of heterocycle molecules (Acheson,1976) and the maximum proton conductivity at 150 ^{o}C under anhydrous condition are listed in Table 1. The basicity of heterocycle molecules of Im is larger than that of Py (see the pKa_1 value in Table 1). Clearly, the conductivity of PVPA-Im composite material is larger than PVPA-Py composite material. These results suggest that pyrazole molecule with the low basicity do not act as a proton donor and acceptor in composite material since the free proton from the PVPA molecule could not strongly interacts with non-protonated –N═ group of pyrazole ring. In contrast, the pKa_1 value of MeIm molecules is as same as that of Im molecules. However, the conductivity of PVPV-MeIm composite material is lower than that of PVPA-Im. This

phenomenon is due to the molecular structure of imidazole. The Im molecules have been reported the construction of molecular cluster, consisting of approximately 20 molecules, (Acheson, 1976) through the intermolecular hydrogen bonding.

As a result, PVPA-Im composite material might possess fast proton transfer of inter-heterocycle molecules in the composite material. However, MeIm molecules do not construct the molecular cluster with the intermolecular interaction in membrane and cannot provide fast proton transfer kinetics in inter heterocycle molecules. Based on the basicity and clustering mechanism, PVPA-Im composite material are supposed to possess the highest proton conductivity of $7x10^{-3}$ S cm^{-1} at 150 ^{o}C under anhydrous condition in many different types of PVPA-heterocycle composite materials. These results suggest that the basicity and molecular structure of heterocycle in acid-base composite material are important factors to obtain the anhydrous proton conductivity at the intermediate temperature condition (Yamada and Honma, 2005).

Table 4.1 Maximum proton conductivities of PVPA-heterocycle composite material and acid dissociation constant (pKa values of various heterocycle molecules).

PVPA-heterocycle	Maximum conductivity [a] (S cm^{-1})	Pka value of heterocycle[b]	
		Pka1	pka2
PVPA-Im	7 x 10^{-3}	7.2	14.5
PVPA-Py	8 x 10^{-4}	2.5	14
PVPA-MeIm	1 x 10^{-3}	7.4	

[a] maximum proton conductivity 150^{o}C under anhydrous condition

[b] Referans (Acheson, 1976)

4.2.2.2. PAA/Imidazol

In 2003, anhydrous proton conducting polymer electrolytes have been prepared by entrapping imidazol (Im) in polyacrylic acid (PAA) with various stoichiometric ratios, x, to form PAAxIm (x is the number of moles of Im per polymer repeat unit) (Meyer et al., 2003). Polymer electrolytes, PAAxIm (with x = 0.5 and 1) can be cast into transparent, homogeneous

films which are thermally stable up to 200 ◦C. From FT-IR spectra it is evident that hydrogen bonds exist between protonated and unprotonated Im units (Figure 3.5). With increasing Im content the glass transition temperature decreases while their conductivity increase, reaching 10^{-3} S/cm at 120 ^{o}C.

It was previously mentioned that the membrane materials based on carboxylic acid groups shows no significant proton conductivity even at higher level of hydration. Because –COOH groups are less sensitive to hydrolysis and higher pKa values (Kreuer, 1996).

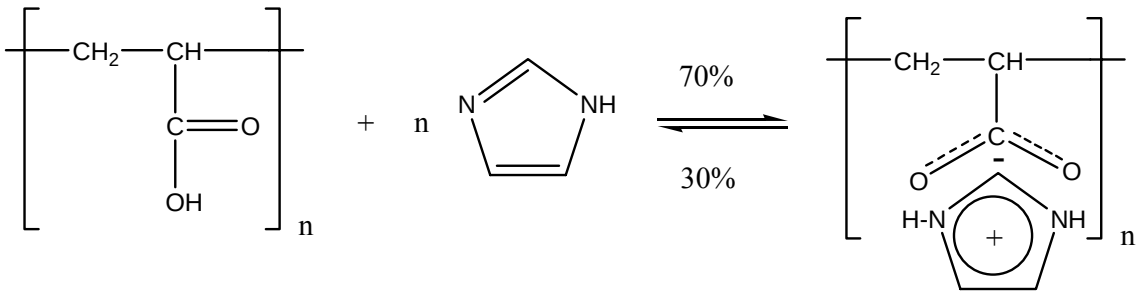

Figure 4.7. Illustration of the protonation of imidazol upon blending with PAA.

The intercalation of imidazol with different doping ratio, x into PAA as Brønstedt acid increased the conductivity PAAxIm membranes. The reason may be imidazol, like water, acts as proton donor and acceptor in the proton conduction process. In this sense it behaves amphoteric but with respect to other compounds they are more basic than water (Kreuer, 1998). FT-IR of PAAxIm confirmed that imidazol is partially protonated from “free” nitrogen side. A Grotthuss type diffusion mechanism may explain the proton diffusion process within protonated and unprotonated heterocycles. Because the protonic defect may cause local disorder by forming (. . . Him-(HimH+)-imH. . .) configuration as discussed in the literature (Münch et al. ,2001). The use of imidazol in a suitable acidic host polymer to increase the concentration of defect protons may also technological interest. Further systems like PAMPSA-imidazol are under investigation and will be communicated soon.

4.2.2.3 Alginic Acid-Imidazole Composite Material

Other anhydrous proton conductor consisting of alginic acid (AL), one of the acidic biopolymers, and imidazole (Im) molecules, one of the basic heterocyclic molecules was

reported by Yamada et al. in 2004. This AL-Im ($r \geq 20$) composite material indicated the high proton conductivity of $2x10^{-3}$ S/cm at 130 °C. On the other hand, the activation energy, such as 1.2-1.6 eV, at $r \leq 1$ is extremely larger than that of other reported materials. This high activation energy is due to the long distance between the hopping sites. Additionally, the proton hopping distance of pure AL or small mixed material ($r \leq 0,5$) was too long to hop to neighboring site, as a result, these materials could not show any measurable proton conductivity ($< 10^{-8}$ S/cm) (Yamada and Honma, 2004).

The bimolecular composite material, such as chitin phosphate-hetrocyclic molecules composite materials as an anhydrous proton conducting membrane was reported by (Yamada and Honma 2004). In these cases, the composite materials showed the high proton conductivity of $\geq 10^{-3}$ S/cm at 150 °C under anhydrous condition. Additionally, these materials had a high thermal stability. However, AL-Im composite materials did not indicate the satisfactory conductivity and thermal stability in comparison with the reported materials (Yamada et al., 2003, Yamada et al., 2004). One of the reasons might be the effect of pKa value (pKa = 3.1) of –COOH group in AL (Jang et al., 1996). Phosphonic acid is stronger than carboxylic acid. The phosphonic acid group and basic group forms a strong acid-base complex in the composite membrane, as a result the free proton from phosphonic acid strongly interacts with non-protonated –n═ (Yamada et al., 2003, Yamada et al., 2004). However a weak acid, such as –COOH group in AL, cannot form the strong acid-base in composite membrane and not provide enough mobile-protons to Im molecules, so that AL-Im composite showed the lower anhydrous proton conductivity than the phosphonic acid composite materials (Yamada and Honma, 2004).

4.2.2.4 Anhydrous Proton Conductive Membrane Consisting of Chitosan

Other anhydrous proton conducting membrane using a composite of chitosan, one of the basic biopolymers with an amino group, and methanediphosphonic acid (MP), which possesses a large proton Exchange capacity was prepared by Honma and Yamada, in 2005 (Figure 4.10). This chitosan–MP composite material showed the high proton conductivity of 5×10^{-3} S/cm at 150 °C under anhydrous (water-free) conditions. The proton conducting mechanism of the chitosan–MP composite material was due to proton transfer to the proton

defect site without the assistance of diffusible vehicle molecules. The utilization of a biopolymer, such as chitosan, for PEMFC technologies is novel and challenging where biological products are usually considered as waste, non-hazardous, and environmentally benign. Especially, the low production cost of the biopolymer is an attractive feature. Anhydrous proton conducting biopolymer composite membranes may have potential not only for PEMFCs operated under anhydrous conditions, but also for bio-electrochemical devices including an implantable battery, bio-sensors. Additionally, the thermal stability of this composite material was found to increase with the mixing ratio of the MP molecule (Yamada and Honma, 2005).

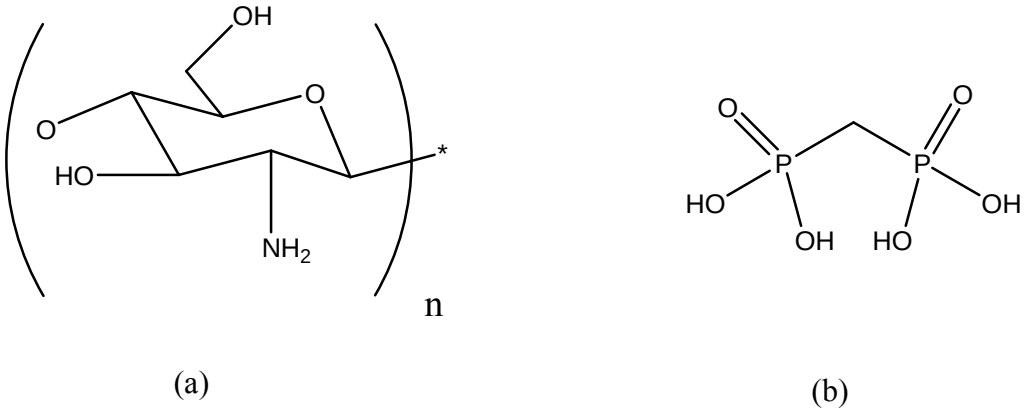

(a) (b)

Figure 4.8. Molecular structures of chitosan (a) and methanediphosphonic acid (b) (MP).

Also chitosan acetate–salt complexes were used to obtain some insight on the mechanism of ionic conductivity in chitosan-based polymer electrolytes (the chitosan acetate plasticized chitosan acetate, chitosan acetate containing salt and plasticized). The conductivity was due to the mobile ions from the salt. Highest proton conductivity in plasticized film containing salt was $4{,}0\times10^{-5}$ S cm^{-1} and for the plasticized films not containing salt was $3{,}0\times10-^{10}$ S cm^{-1} (Osman et al., 2001).

4.2.3. MODEL HYBRIDS MATERIALS

4.2.3.1. Benzimidazole/Monododecyl Phosphate Molecular Hybrids

It had been reported that a glass-filter supported monododecyl phosphate/benzimidazole mixed material shows a high proton conductivity of $1x10^{-3}$ S/cm at T = 150 ^{o}C underwater-

free conditions along with a high thermal stability (Yamada and Honma, 2003). Even other acid–base hybrid materials resulted in the same anhydrous conductor at elevated temperatures (Yamada and Honma, 2004,). Kim and Honma investigated the effects of monododecyl phosphate (MDP) doping to benzimidazole (BnIm) by IR, TG, XRD, proton conductivities. The XRD results showed new phases different from the crystal structures of MDP and BnIm (Figure 4.8), and the doping of MDP displayed the peaks of BnIm due to the extinction rule of reflection. The hybrids showed a high proton conductivity of $1x10^{-2}$ S/cm above 100 ^{o}C under a non-humidified (anhydrous) condition (Kim and Honma, 2005).

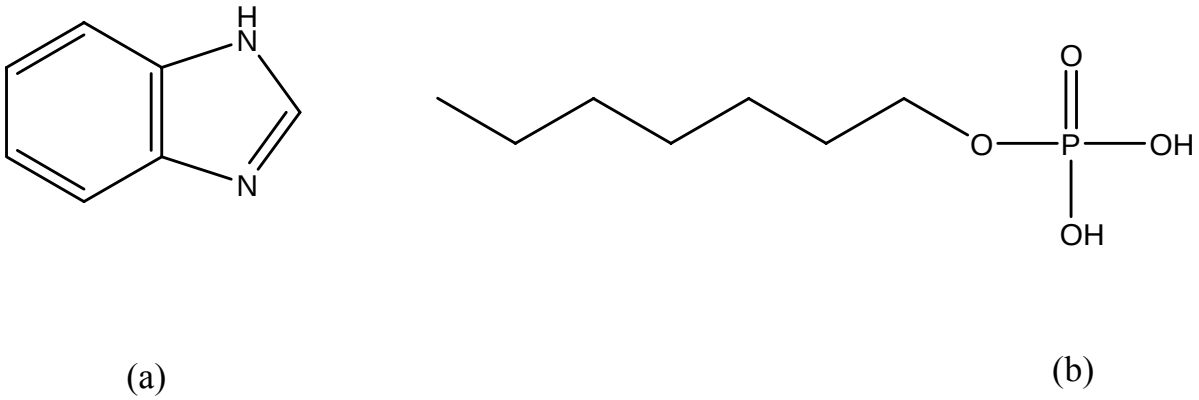

(a) (b)

Figure 4.9. Molecular structures of (a) benzimidazole and (b) monododecyl phosphate.

4.2.3.2. Adipic Acid/Benzimidazole Hybrid Electrolytes

Bozkurt et al. investigated several blends of a diacid, adipic acid (AA) (Figure4.9) and heterocyclic base, benzimidazole (BnIm). Adipic acid has very low proton conductivity (1^{-11} S/cm) in crystalline form. The conductivity of the blends increased with BnIm and reached a maximum conductivity of $4x10^{-3}$ S/cm at 130 ^{o}C (Karadedeli et al., 2005).

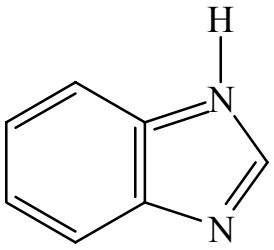

BnIm

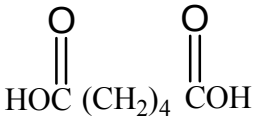

AA

Figure 4.10. Molecular structure of AA and BnIm.

From DSC results, it can be concluded that such conductivity increase within this temperature regime may be the effect of first-order transition (melting) onto the ionic conductivity of the samples. At higher temperatures, (T > 373 K) the conductivities of these samples are very close to each other irrespective of their BnIm content. High BnIm doping levels ($BnIm_2AA$) result in higher conductivity even at lower temperatures. This behavior may reflect the ambivalent role of hydrogen bonding as already observed for the proton mobility in heterocyclic systems (Kreuer et al., 1998). Previously the proton conductivity in anhydrous heterocycles, i.e. imidazole and pyrazole, and their mixtures with H_2SO_4 and H_3PO_4 were investigated (Kreuer et al., 1998, Schuster et al., 2003).

The protonic defects are created by protonation of heterocycles which act as solvent for protons and it is the dynamics of these solvent molecules which lead to the mobility of the protonic defects, i.e. intermolecular proton transfer and structural reorganization by hydrogen bond breaking and forming processes (structure diffusion). The IR spectra of the BnImxAA indicate the partial protonation of benzimidazole which occurs from the free N side forming benzimidazolium ion. Therefore, at higher temperatures, protons can be rapidly transferred to neighbor molecule with small activation energy. Similar behavior was observed in PAA-imidazole and mono-dodecylphosphate (MDP)-benzimidazole mixed materials (Bozkurt et al., 2003, Yamada et al., 2003). The BnImxAA blends showed a maximum conductivity of $4x10^{-3}$ S/cm at 130 °C in anhydrous state. The materials which comprise $–CO_2H$ acidic functional groups as part of their constitutional unit have not been preferred as proton conductors since these units are less sensitive to hydrolysis, have higher pKA values and hence yield low conductivity. This work was demonstrated that anhydrous, high proton

conductive organic electrolytes can also be obtained when $–CO_2H$ containing materials are doped with benzimidazole (Karadedeli et al., 2005).

4.2.4. ORGANIC-INORGANIC COMPOSITES

Incorporation of submicron particles of metal(IV) phosphates such as zirconium phosphate (ZrP) and tin phosphate (SnP) in polymer matrices tend to increase the proton conductivity of the polymers. For this purpose, precipitation from a solution containing M(IV) ions, within an appropriate polymer matrix, can offer a number of advantages:

i. elimination of the dissolution of the membrane material formed by the direct swelling of the polymers selected;
ii. proper mixing of inorganic and organic components at molecular level offering good mechanical stability compared with purely organic membrane;
iii. since proton conductivity is the result of transport of protons on the surface of the proton conductor particles, an increase in surface area (smaller particle size) will increase the conductivity obtained for a mixed matrix membrane;
iv. these membranes may cost the same as the conventional polymers;
v. with increasing proportion of metal particles, appreciable degree of improvements in proton conductivity specially at high temperature can be anticipated. However, the influence of metal particles on mechanical characteristics needs to be investigated (Smitha et al., 2005).

4.2.4.1. Benzyltriethoxysolane, n-hexyltrimethoxysilane, and triethoxysilane.

Gautier-Luneau et al. prepared an organic-inorganic proton-conducting polymer electrolyte to be used as a membrane for DMFC (Gautier-Luneau et al., 1992). They synthesized the electrolytes by hydrolysis-co-condensation of three different alkoxy silanes; benzyltriethoxysolane, n-hexyltrimethoxysilane, and triethoxysilane. After co-condensation and solvent evaporation, sulfonation was achieved in dichloromethane by adding chlorosulfonic acid in a stoichiometric amount, with respect to the benzyl groups. The cross-linking was performed in THF by hydrosilyation of the silane groups with divinylbenzene using a divinyltetramethyldisiloxane platinium complex as catalyst. The TGA data showed one broad endothermic peak with a maximum at 103^oC due to the loss of water. They reported

that these polymer electrolytes were thermally stable until 250^{o}C and that the cabonization of the organic chains started at 375^{o}C. The proton conductivity of these materials was about 1.6 x 10^{-2} S cm^{-1} (Rikukawa and Sanui, 2000).

4.2.4.2. SiO /PEO

Another alkoxy silanes based polymer electrolyte was reported by Honma et al. (Honma et al., 1999). Their organic-inorganic hybrid electrolyte membranes have been synthesized by the sol-gel process. Poly(ethyleneglycols) (Mw = 200; 300, 400, 600, 2000) were reacted with 3-isocyanatopropyltriethoxy silane in an N_2 atmosphere at 70^{o}C to obtain alkoxy end-capped poly(ethyleneoxide) precursors. The hybrid electrolyte membranes were fabricated by hydrolyzing the end-capped precursor with monophenyltriethoxysilane. A composition of the monophenyltriethoxysilane of 20% was found to be the most flexible and chemically stable composition for the hybrid electrolyte membranes. The TGA showed that decomposition of the hybrid membrane started near 300^{o}C. They reported that the thermal stability of the electrolyte membranes were enhanced enormously compared with poly(ethyleneoxide), which was the base material of the hybrid membranes due to structural confinement of the poly(ethyleneoxide) chain between the nano-sized silicate domains. Proton conductivity within the hybrid membranes was provided by incorporating acid molecules such as monododecylphophate and phosphotungstic acid. The proton conductivity as a function of humidifier temperature against the constant cell temperature at 80^{o}C was measured for the electrolyte membrane doped with 20 wt% of monododecylphophate. The proton conductivity was very small at low humidifier temperatures and increased with temperature and reached a maximum value of 10^{-3} S cm^{-1} above 80^{o}C. The hybrid electrolyte membranes needed almost saturated humidities to afford maximum proton conductivities. They also attempted to measure the conductivity of hybrid electrolyte membranes containing phosphotungstic acid. This system showed a specific conductivity of 0.17 S cm^{-1} at room temperatures. The maximum conductivity of $5x10^{-3}$ Scm^{-1} was observed for the hybrid electrolyte membrane incorporating phosphotungstic acid of 10 wt% at a humidifier temperature of 80^{o}C (Rikukawa and Sanui, 2000).

4.2.4.3. Polyvinylidene fluoride /SiO_2 (or SiO_2 gel) acid membranes

The modified polyvinylidene fluoride (PVDF) membranes (24% PVDF–16% SiO_2 with 60%–3M H_2SO_4 (vol%)) are nanoporous proton-conducting membranes (NP-PCM). The membranes, which utilize PVDF as the polymer binder to implant SiO_2 powder and acid into the polymer matrix to provide proton conductivity, can have very high surface area and thus two to four times higher ionic conductivity than Nafion®. Meanwhile, the MCO of PVDFmembranes are two to four times lower than Nafion® due to smaller pore sizes (1.5–3 nm compared to 3 nm for Nafion®) (Peled et al., 2000). Impregnation of the NP-PCM pores with Na_2SiO_3 solution and hydrolyzing the silicate in sulfuric acid (forming silica gel) decreases the MCO further to almost an order of magnitude lower than Nafion®. These membranes operate in a wider temperature range than Nafion® (from 0 to over 90 ◦C). They are also less sensitive to iron impurities (Fe > 500 ppm) than Nafion®, which allows for the use of Pt–Fe catalysts or stainless steel fuel cell hardware. MEAs utilizing these membranes have achieved power densities of 85mWcm−2 (at *T*=80◦C, 1Mmethanol, and a Pt–Ru anode with a loading of 4–6 mg cm^{-2}) (Peled et al., 2000). Modified PVDF membranes have good mechanical properties and can be bent 180◦ without breaking. They can be manufactured with 50–90% (by volume) acid solution, have a high thermal stability (from subzero to over 100 ◦C) and have stable dimensions which do not change with absorption of water (Neburchilov et al., 2007).

4.2.4.4. Silanes/silica modified sulfonated poly(ether ether ketone)

SPEEK-based membranes were developed to contain heteropolyacids and an oxide phase that was either produced by hydrolysis of amino-modified silanes or by dispersion of a surface-modified fumed silica. The degree of sulfonation ranged from 65 to 66%. The heteropolyacid was based on lacunary divacant $[\_\gamma\text{-}SiW_{10}O_{36}]^{-8}$ and contained epoxy groups. The reaction provided a covalent bond between the heteropolyacid and the insoluble oxide phase, resulting in its fixation within the membrane (Ponce et al., 2004). The organic–inorganic materials are mechanically more stable than membranes without inorganic compounds in alcohol solutions. Heteropolyacid has good proton conductivity but degradation was shown to be an issue for DMFC applications due to its dissolution in water. The stability has usually been increased through silica modification, which increases the strength of the covalent bonds or columbic interactions but reduces the acid strength. Heteropolyacid

bleeding can also be reduced through the addition of silanes (S66/$RSiO_{3/2}$/H4) and the dispersion of surface-modified, fumed silica (S66/Aerosil 380/H4) (Ponce et al., 2004). In comparison with non-modified sPEEK S66 (with 65–66% sulfonation and IEC: 1.66 mequiv. g^{-1}) the modified membranes have:

• lower methanol permeability (0.3×1016 m^2 s^{-1} Pa^{-1} for silane modified and 0.8×10^{16} m^2 s^{-1} Pa^{-1} for silica modified) at T=55°C and 20% methanol (MCO is lower than that of the plain membrane when alkoxysilane was used to generate the oxide phase);
• proton conductivities of 4, 10, and 12mScm^{-1}, respectively (at RH= 100% and T=70◦C). The silane modified sPEEK membrane has lower methanol crossover but also lower conductivity than that modified by silica. The inorganic phase decreases the water and methanol crossover, in addition to fixing of the heteropolyacid to the membrane. The stability of these membranes is higher than unmodified sPEEK due to their higher stability in alcohol solution. The modification of sPEEK by ZrP (10%) and PBI (5.6%) produces a membrane with (Silva et al., 2005):
• maximum power density of 50.1mWcm^{-2} at j = 250mAcm^{-2} and T = 130 °C;
• improved chemical stability and DMFC efficiency over unmodified sPEEK. (Neburchilov et al., 2007).

CHAPTER 5

EXPERIMENTAL

5.1. CHEMICALS

Imidazole (>99), formaldehyde (37%) and benzylchloride (>99%) were received from Merck. Tri (ethyleneglycol) di-p-toluene sulfonate (98%) was obtained from Alfa Aesar. Polystyrene (M_n = 140,000), 1H-1, 2, 4-Triazole and Vinylphosphonic acid were purchased from Aldrich. Other common chemicals (sulfuric acid (98%), phosphorus pentaoxide) and organic solvents (toluene, acetonitrile, Dimethylsulfoxid and cyclohexane) are Merck reagent grade and were used as received. THF (Merck) was dried over sodium prior to use.

Low molecular weight Chitosan, alpha, alpha'-Azodiisobutyramidin Dihydrochlorid (AIBHC, >%98) were obtained from Fluka.

1.12-diimidazol-2-yl-2,5,8,11-tetraoxa-dodecane (Imi3), chitosan, vinylphosphonic acid and 1H-1, 2, 4-Triazole were showed in Figure 5.1

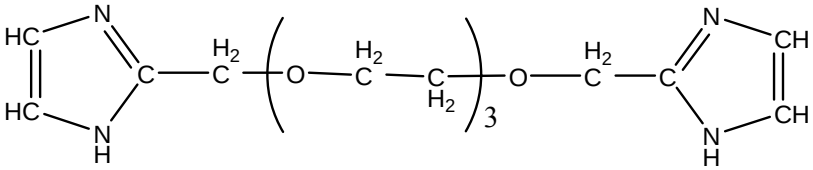

imi3

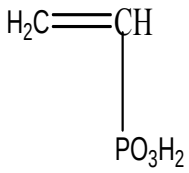

vinylphosphonic acid

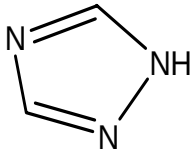

1H-1,2,4-Triazole

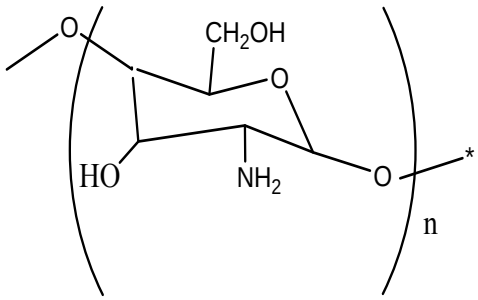

Chitosan

Figure 5.1. Chemical structures of imi3, Chitosan, vinylphosphonic acid and 1H-1, 2, 4-Triazole.

5.2. SYNTHESIS OF HOMOPOLYMERS

5.2.1. Free Radical Polymerization

PVPA was produced by free radical polymerization technique. The addition of a monomer molecule to an active chain end regenerates the active site at the chain end. Hence, a large number of monomer molecules are 'consumed' for each active site introduced into the system. In chain reaction, four distinct types of processes are recognized.

a) Chain Initiation: A process in which highly reactive transient molecules or active centers are formed.

b) Chain Propagation: The addition of monomer molecules to the active chain end, accompanied by regeneration of the terminal active site.

c) Chain Transfer: Involving the transfer of the active site to another molecule (e.g., monomer). The molecule that has lost the active site is now "dead" from a chain propagation point of view. The molecule that has accepted the active site can start a new chain.

d) Chain Termination: A reaction in which the active chain centers are destroyed. Chain reactions are found in free radical, anionic and cationic vinyl type polymerizations. In-free radical process all of the four steps listed above can usually be identified.

Schematically, a free-radical polymerization sequence can be represented by reactions shown in equation 5.1. In this equation, M represents a molecule of monomer; R'· is an initiating free radical from the initiator; R_n is the propagating free radical with a degree of polymerization, n; YZ is a chain transfer agent that may be solvent, monomer, initiator, or polymer molecules; and P_n is the final inactive polymer. It should be noted that in some cases the initiator molecule may be the monomer itself.

$$
\begin{aligned}
&\text{Initiator}(I_2) \longrightarrow 2\,I\cdot \\
&I\cdot + M \longrightarrow IM\cdot \qquad \text{Initiation} \\
&IM\cdot + M \longrightarrow IMM\cdot \longrightarrow R_n\cdot \\
&\cdots\cdots\cdots\cdots \qquad \text{Propagation} \\
&R_n\cdot + M \longrightarrow R_{n+1}\cdot \qquad (5.1) \\
&R_n\cdot + R_m\cdot \longrightarrow R_{n+m} \\
&R_n\cdot + R_m\cdot \longrightarrow R_n + R_m \qquad \text{Termination}
\end{aligned}
$$

5.2.2. In Situ Polymerization

Another method is in-situ polymerization. Here, nanoscale particles are disappeared in the monomer or monomer solution, and the resulting mixture is polymerized by standard polymerization methods. One fortunate aspect of this method is the potential to graft polymer on the particles surface. Many different type of nanocomposites have been processed by in-situ polymerization. The key to in-situ polymerization is appropriate dispersion of the filler in

the monomer. This often requires modification of the particle surface because, althoughdispersion is easier in liquid than in a viscous melt, the settling process is also more rapid (Ajayan et al., 2006).

The composite polymer electrolyte of $CHPVPA_x$ was produced in situ polymerization with vinyl phosphonic acid (VPA) of in the existence of chitosan.

5.3. PREPARATION OF POLYMER BLENDS

5.3.1. Synthesis of poly (styrene sulfonic acid)

The synthesis of sulfonated polystyrene was performed according to following procedure described by Vink (Vink, 1981): 1.5 g of polystyrene in cyclohexane was introduced into the solution of sulfuric acid/ phosphorous pentoxide in a 500 ml three-necked flask. After stirring the mixture for about 30 min, the reaction was stopped and kept at 40 ^{o}C for about 1 h. Then crushed ice was slowly added until PSSA completely precipitated out as a pale yellowish sticky mass. The precipitate was collected and dialyzed against water. The percent sulfonation of PSSA was approximately 95%, which is confirmed by elemental analysis.

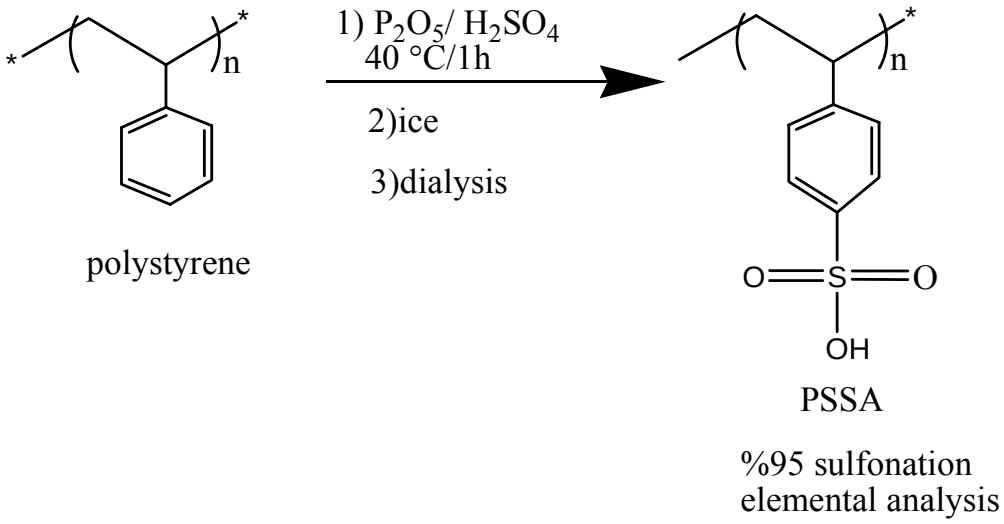

Figure 5.2 Reaction of Synthesis of poly (styrene sulfonic acid).

5.3.2. Synthesis of imi3

The synthesis of imi3 was carried out using a similar procedure as described in a previous literature (Schuster et al., 2001). N-benzyl-2-imidazoyl-methanol was synthesized starting from imidazole. The NH group of imidazole was first protected using benzylchloride and then the product was crystallized from toluene to get N-benzylimidazole. The protected compound was heated in aqueous formaldehyde solution in an autoclave at 150 ^{o}C, and then it was crystallized from ethyl acetate to get N-benzyl-2-imidazoyl-methanol. The product was deprotonated with sodium hydride in dry THF and reacted with tri(ethyleneglycol) di-p-toluene sulfonate (98%, Alfa Aesar). The deprotection of benzyl groups was carried out by catalytic hydrogenation. The viscous oil was dissolved in acetonitrile and filtered (three times) through aluminum oxide (for column chromatography, Merck). The solvent was removed by a rotary evaporator and further dried under vacuum. The structure at every step was confirmed by ^{1}H NMR and FT-IR. For final product imi3: ^{1}H NMR, $CDCl_3$: δ = 7 (s, 2H), δ = 4.65 (s, 2H), δ = 3.6–3.7 (m, 4H).

5.3.3. Doping of PSSA with Tri

PSSATri_x polymer electrolytes membranes were prepared by doping of PSSA with Tri at several molar stoichiometric ratios x that is the number of moles Tri per polymer repeating unit. The x was varied from 0.5 to 1.5 for PSSATri_x. The mixing ratio x are summarized in Table 1. The films were cast onto polished PTFE plates and dried under vacuum at 70 ^{o}C and then stored in the glove box. Transparent, hygroscopic and free standing films (Figure 5.3) were obtained for all the samples.

Figure 5.3. Photograph of PSSATri$_x$ film with a thickness ca. 200 µm.

Table 5.1 PSSA and Tri amounts to obtain the ratio x.

X	PSSA(g)	Tri(g)	H_2O(ml)
0,5	1	0,178	10
1	1	0,356	10
1,5	1	0,534	10
2	1	0,713	10

5.3.4. Doping of PSSA with imi3

PSSAimi3$_x$ polymer electrolytes membranes were prepared by doping of PSSA with imi3 at several molar stoichiometric ratios x that is the number of moles imi3 per polymer repeating unit. The x was varied from 0.5 to 1 for PSSAimi3$_x$. The mixing ratio x are summarized in Table 5.2. The films were cast onto polished PTFE plates and dried under vacuum at 70 ^oC and then stored in the glove box.

Table 5.2 PSSA and imi3 amounts to obtain the ratio x.

X	PSSA(g)	Imi3(g)	H_2O
0,5	1	0,8	10
1	1	1,6	10

5.3.5. Preparing composite membrane of Chitosan and poly (vinylphosphonic acid)

The polymer composite membrane has been produced by swelling of Chitosan in vinylphosphonic acid. A few milliliters of DMSO were added to homogenize the mixture Polymer composites comprising chitosan and poly (vinyl phosphonic acid) were produced (Figure 5.4).

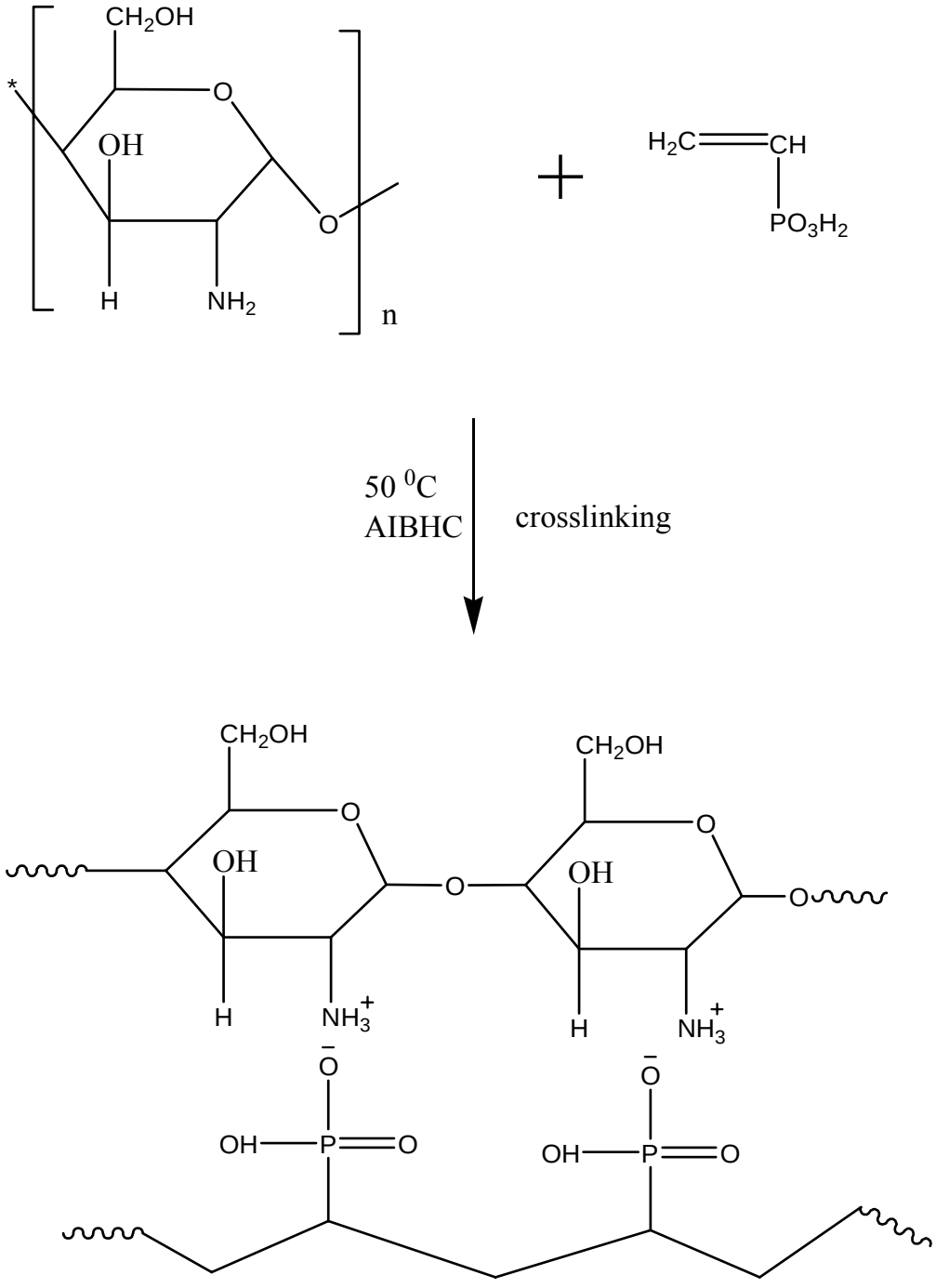

Figure5.4. Structure of the polymer salt formation of chitosan and poly (vinylphosphonic acid).

The feed ratios x which is the molar ratio of vinylphosphonic to chitosan repeat unit, was varied from 1 to 5. Chitosan and vinylphosphonic acid composites amounts to obtain the ratio x were summarize in Table 5.3.

Table 5.3 Chitosan and vinylphosphonic acid composites amounts to obtain the ratio x of vinylphosphonic acid.

X	Chitosan (g)	vinylphosphonic acid (g)	Initiator	DMSO (ml)
1	1	0,67	0,0134	4
2	1	1,342	0,051	4
3	1	2,013	0,0674	4
4	1	2,684	0,084	3
5	1	3,356	0,102	3

The resulting mixture was cast onto polished PTFE plates in the glove box. The materials were produced in situ polymerization of VPA in the presence of chitosan using AIBHC as initiator at 60 ^{o}C. After polymerization free standing films were washed in boiling THF and the films were dried under vacuum at 50 ^{0}C. The materials were stored in the glove box. (Figure 5.5)

Figure 5.5. Photograph of CHPVPA$_x$ film and glove box.

5.4. INSTRUMENTATION AND PROCEDURE

Fourier-Transform IR (FT-IR) spectra of the samples were scanned using a Mattson Genesis II spectrophotometer (4000-400 cm $^{-1}$). Thin films of PSSATri$_x$ and PSSAimi3$_x$ were cast onto silicon wafers and dried under vacuum at 60 ^{o}C prior to measurements. Composite material of CHPVPA$_x$ was scanned with KBr pellet.

The carbon, hydrogen and nitrogen compositions were measured by elemental analysis using LECO, CHNS–932 instrument at METU, Ankara. The compositions of the composite electrolytes, CHPVPA$_x$ were measured through nitrogen analysis.

X-Ray diffraction (XRD) patterns chitosan and CHPVPAx composite membranes were obtained by X-Ray Diffraction Instrument, Rigaku Dmax 2200 (Cu K$_\alpha$).

Thermal stabilities of the PSSATri$_x$ and PSSAimi$_x$ polymer electrolytes were examined by TG analyses with a Mettler-Toledo TG-50. Thermal stabilities of the CHPVPA$_x$ polymer electrolytes were examined by TG Perkin Elmer Pyris 1. The samples (~ 10 mg) were heated from room temperature to 700 ^{o}C under N_2 atmosphere at a scanning rate of 10 ^{o}C/min.

DSC measurements were carried out on a Mettler-Toledo DSC 30 differential scanning calorimeter under nitrogen atmosphere. The samples were loaded into aluminum

pans and heating-cooling curves were recorded at a rate of 10 ^{o}C/min. The glass transition temperatures were determined from the second heating curves.

The AC proton conductivity studies of the samples were performed using a SI 1260-Schlumberger impedance spectrometer at the Max-Planck Institute for Polymer Research, Mainz, Germany. The samples were placed between gold electrodes and their conductivities were measured in the frequency range 1 Hz to 1 MHz at 10 ^{o}C intervals. The temperature was controlled with a Novocontrol cryosystem, which is applicable between -150 and 400 ^{o}C with a precision of 0.01 ^{o}C. The DC conductivities were obtained by linear fitting of the AC conductivities measurements.

CHAPTER 6

CHARACTERIZATION OF PROTON CONDUCTING POLYMER ELECTROLYTES

6.1. FT-IR SPECTROSCOPY

FTIR (Fourier Transform Infrared) spectroscopy, or simply FTIR Analysis, is a failure analysis technique that provides information about the chemical bonding or molecular structure of materials, whether organic or inorganic.

6.1.1 .FT-IR studies of PSSATri$_x$

The FT-IR spectra of PSSATri$_x$ electrolytes are shown in Figure 6.1. Sulfonated polystyrene gives a strong and broad absorption band near 1200 cm^{-1} corresponding asymmetric O=S=O stretching vibration of the $–SO_3H$ unit. The peaks at 1005 cm^{-1} result from the vibration of the phenyl ring substituted with a sulfonic group (Ismail et al., 2005). After doping of PSSA with Tri, the broadening of these peaks indicates the presence of phenyl ring attached sulfonate anion, $-SO_3^-$ (Bozkurt, 2005). FT-IR bands which are located at 1559 cm^{-1} (C=N) and 1436 cm^{-1} (C-N) are due to the stretching vibrations between carbon and nitrogen atoms of the heterocyclic ring. The proton exchange reactions can be proved by the increase in the intensity of the (C-N) peak at 1436 cm^{-1} and correspondingly the decrease in the intensity of the C=N at 1590 cm^{-1}. Relative increase in the intensity of the N-H stretch at

3100cm^{-1} as well as the broad band at 1943cm^{-1} can be the additional evidence of the salt formation (Günday et al., 2006). A broad band in the region of 3400-2500 cm^{-1} indicates hydrogen bonding network formation.

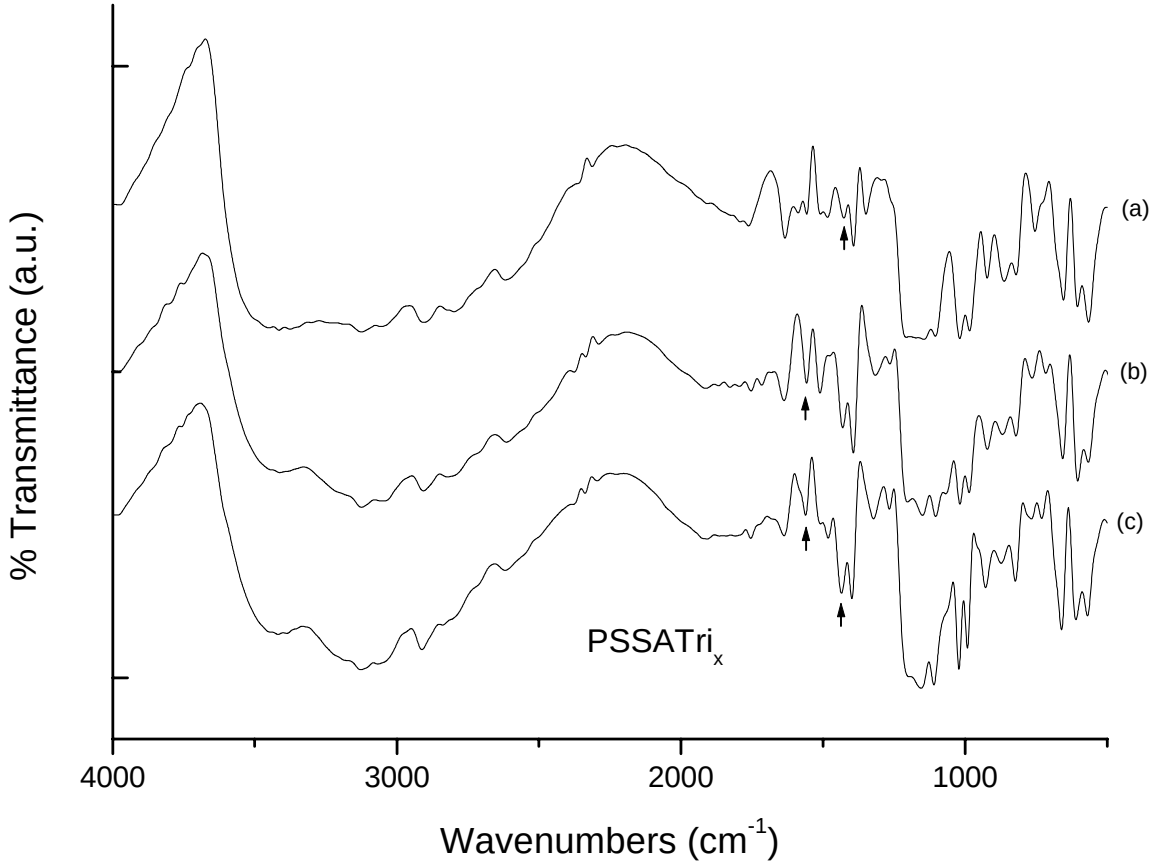

Figure 6.1. FT-IR spectra of (a) PSSATri$_{0.5}$, (b) PSSATri$_1$,c) PSSATri$_{1.5}$.

6.1 2.FT-IR studies of PSSAimi$_x$

The FT-IR spectra of PSSAimi3$_{0.5}$ and PSSAimi3$_1$ are presented in Figure 6.2. In this system, the protonation can be proved by the characteristic imidazolium ion (HImH$^+$) peak located near 1630 cm^{-1} (Sevil and Bozkurt, 2004). The intensity of the peak increased for PSSAimi3$_1$. The broadening of the band at 2500-3400 cm^{-1} indicates the hydrogen bonding

network formation that plays a significant role in the proton conductivity of the polymer/heterocycle systems.

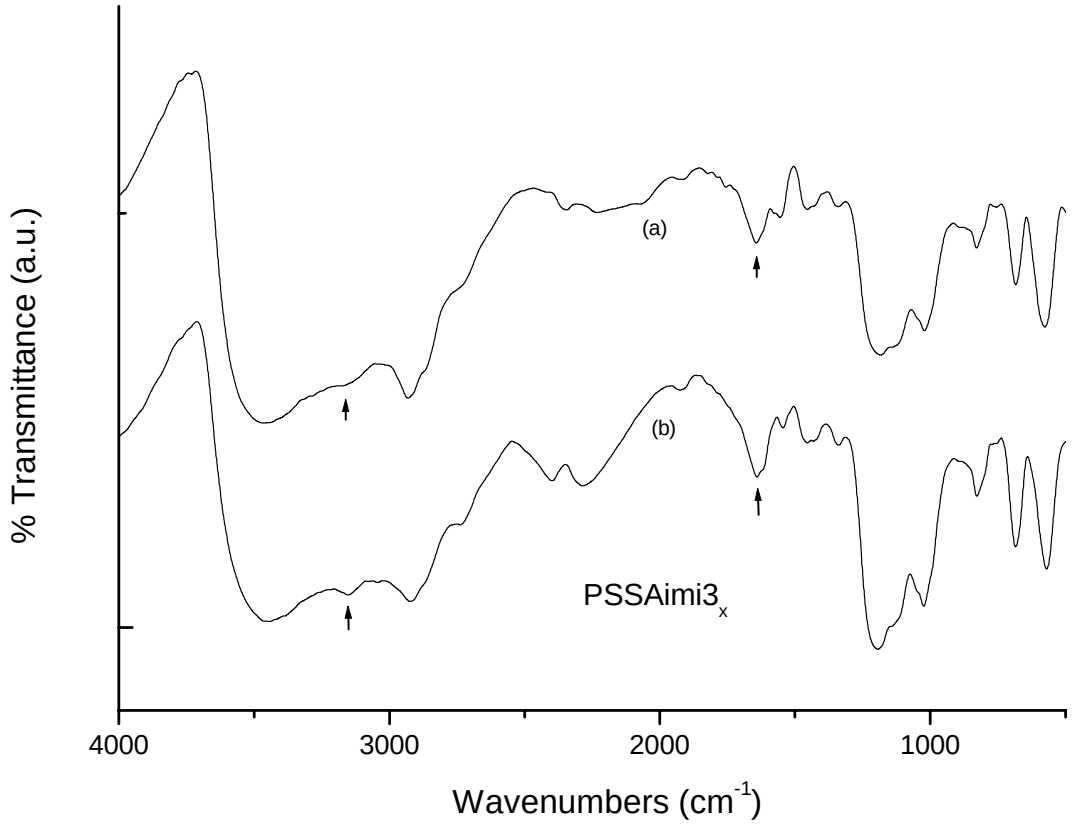

Figure 6.2. FT-IR spectra of (a) PSSAimi3$_{0.5}$, (b) PSSAimi3$_{1.}$

6.1. 3. FT-IR studies of CHPVPA$_x$

The interactions as well as proton exchange reactions between chitosan and PVPA were characterized by FT-IR studies (Figure 6.3). The absorption band at 1636 cm^{-1}, related to the C=O stretching peak of the chitin form. The broad absorption between 950 and 1150 cm^{-1} may be due to the presence of three distinct vibrational modes of C-O-C, C-OH, and C-C of the ring. Additionally, band at 1577 cm^{-1} was attributed to characteristic N-H bending

vibrations of pure chitosan (Kolhe and Kannan, 2003). The biopolymer also exhibits broad N-H and O-H stretching vibrations between 3200–3500cm^{-1}. For the composites (CHPVPA$_1$ and CHPVPA$_3$), the band which is located at 1577 cm^{-1} shifted to 1540 cm^{-1} was attributed to –NH_3^+ bending vibration. Additionally, the intense absorption band at 990 cm^{-1} correspond to P-O$^-$ formation for CHPVPA$_1$, indicating the inter polymer complexation via proton exchange reactions, i.e., (chitosan)-NH_3^+...$^-$O-P-(PVPA). However, at higher PVPA compositions (CHPVPA$_3$) the P–O-H vibration appeared near 930 cm^{-1}. These results indicate the 'polysalt' formation as shown in figure 5.4.

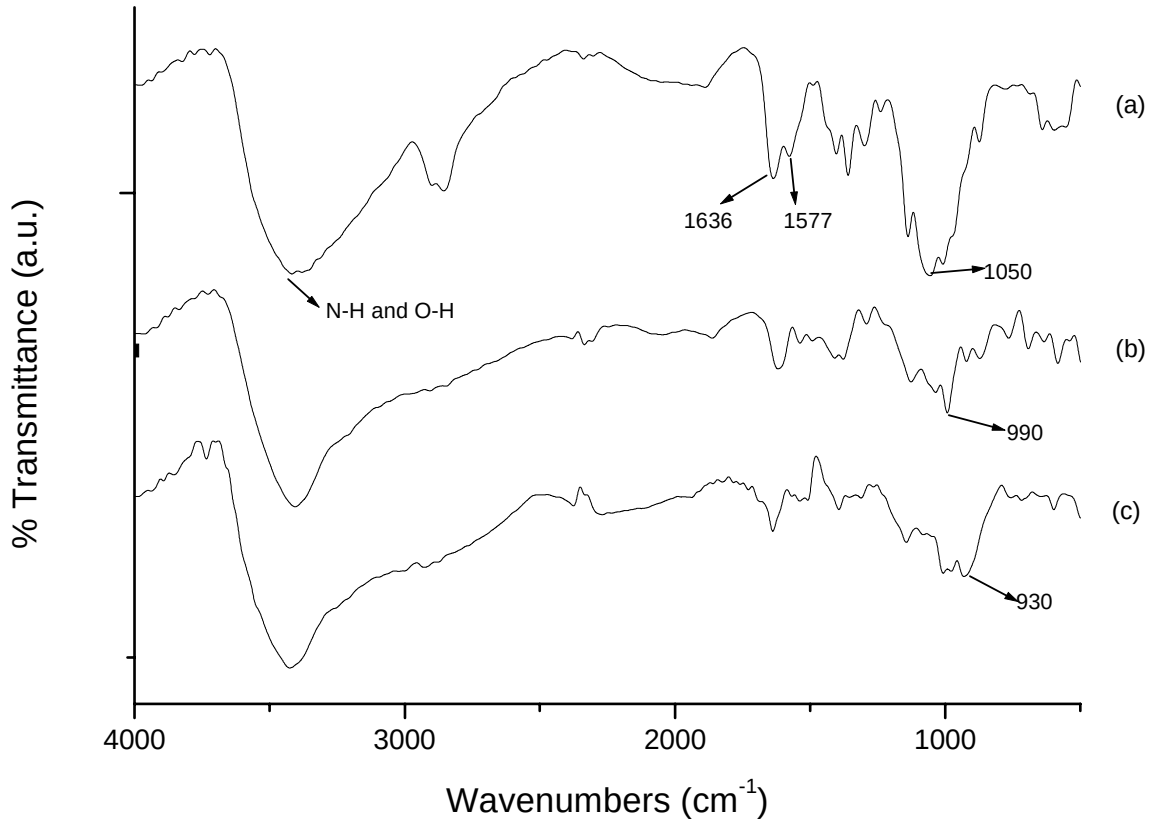

Figure 6.3. FT-IR spectra of (a) pure chitosan, (b) CHPVPA$_1$, (c) CHPVPA$_3$.

6.2. ELEMENTAL ANALYSIS (EA)

Elemental analysis or determination of functional groups is especially valuable for copolymers or chemically modified polymers. For homopolymers where the elemental analysis should agree with that of the monomer, deviations from the theoretical values are an indication of side reactions during polymerization. However, they can also sometimes be caused by inclusion or adsorption of solvent or precipitant, or, in commercial polymers, to the presence of added stabilizers. The preparation of the sample for analysis must, therefore, be very carefully carried out (several reprecipitations, if necessary using various solvent/precipitant combinations; through drying) (Braun et al., Polymer Synthesis).

6.2.1Elemental analysis (EA) of $CHPVPA_x$

The compositions of the composite electrolytes were calculated using nitrogen analysis and the results are compiled in Table 6.1. The composition of the composite material is depending on the monomer feed ratio so that we controlled the PVPA composition in the resulting materials. When the VPA mole percent in the feed was varied from 50% to 84%, the percent PVPA content is changed from 49% to 82%.

Table 6.1. The EA results of the composite electrolytes

Samples	N % (g)	mole % VPA in the feed	PVPA moles % ratio
$CHPVPA_1$	4,73	50	49
$CHPVPA_3$	3,08	75	72
$CHPVPA_4$	2,67	80	76
$CHPVPA_5$	2,04	84	82

6.3. THERMAL ANALYSIS

6.3.1. 1. Thermogravimetric Analysis (TG) of PSSATri$_x$

Prior to the thermal measurements the materials were dried under vacuum until constant weight and stored in the glove box. The thermal measurements of the polyelectrolyte, poly(4-styrene sulfonate) was reported in a previous work (Jiang et al., 1999). They reported that the decomposition of polymer occurs in two steps within 200-500 ^{o}C. The first step occurs from 100 to 280 ^{o}C and approximately 5 % weight loss was attributed to loss of absorbed humidity in these hygroscopic polyelectrolytes. The decomposition of the polyelectrolyte appeared above this temperature range. The TG thermograms of PSSATri$_1$ and PSSATri$_{1,5}$ are shown in Figure 6.4 and Figure 6.5.

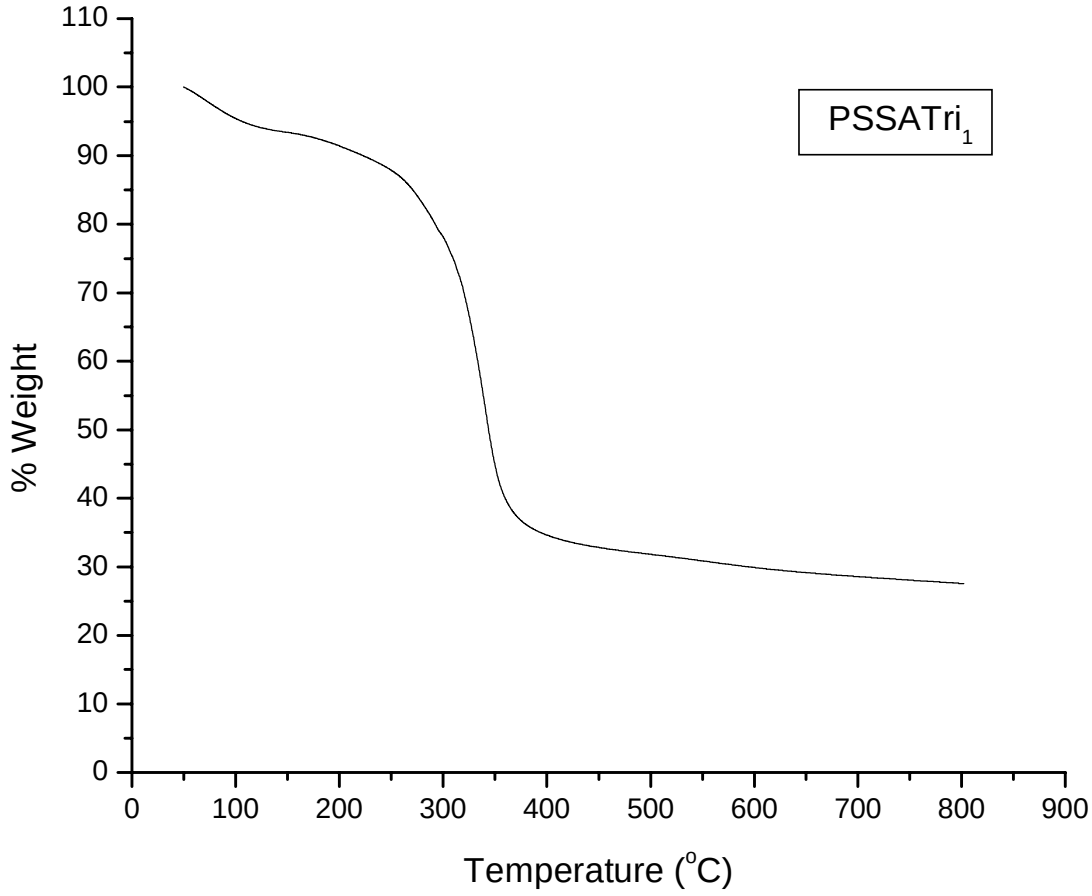

Figure 6.4. TG thermograms of $PSSATri_1$ recorded at a heating rate of 10^oC/min under a nitrogen atmosphere.

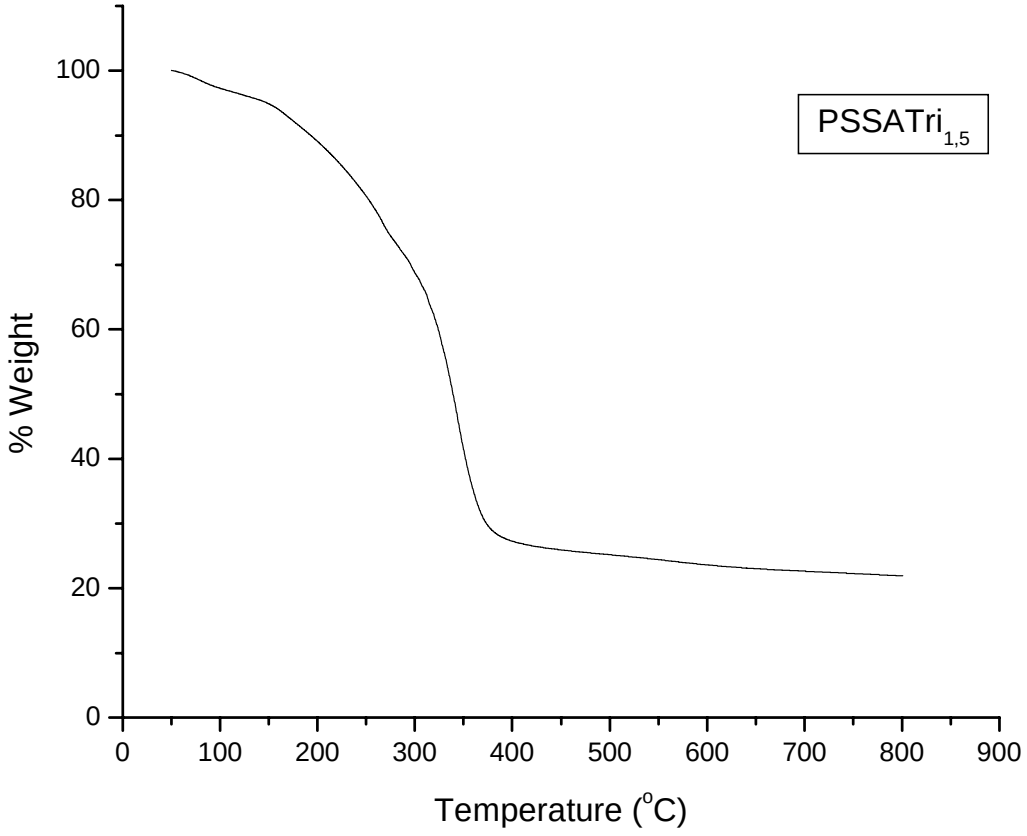

Figure 6.5. TG thermograms of $PSSATri_{1,5}$ recorded at a heating rate of 10 °C/min under a nitrogen atmosphere.

6.3.1.2. Thermogravimetric Analysis (TG) of $PSSAimi3_x$

Prior to the thermal measurements the materials were dried under vacuum until constant weight and stored in the glove box. The decomposition of polymer occurs in two steps within 200-600 °C. The first step occurs from 100 to 240 °C and approximately 5 % weight loss was attributed to loss of absorbed humidity in these hygroscopic polyelectrolytes. The decomposition of the polyelectrolyte appeared above this temperature range. The TG thermograms of $PSSAimi3_{0,5}$ and $PSSAimi3_1$ are shown in Figure 6.6 and Figure 6.7.

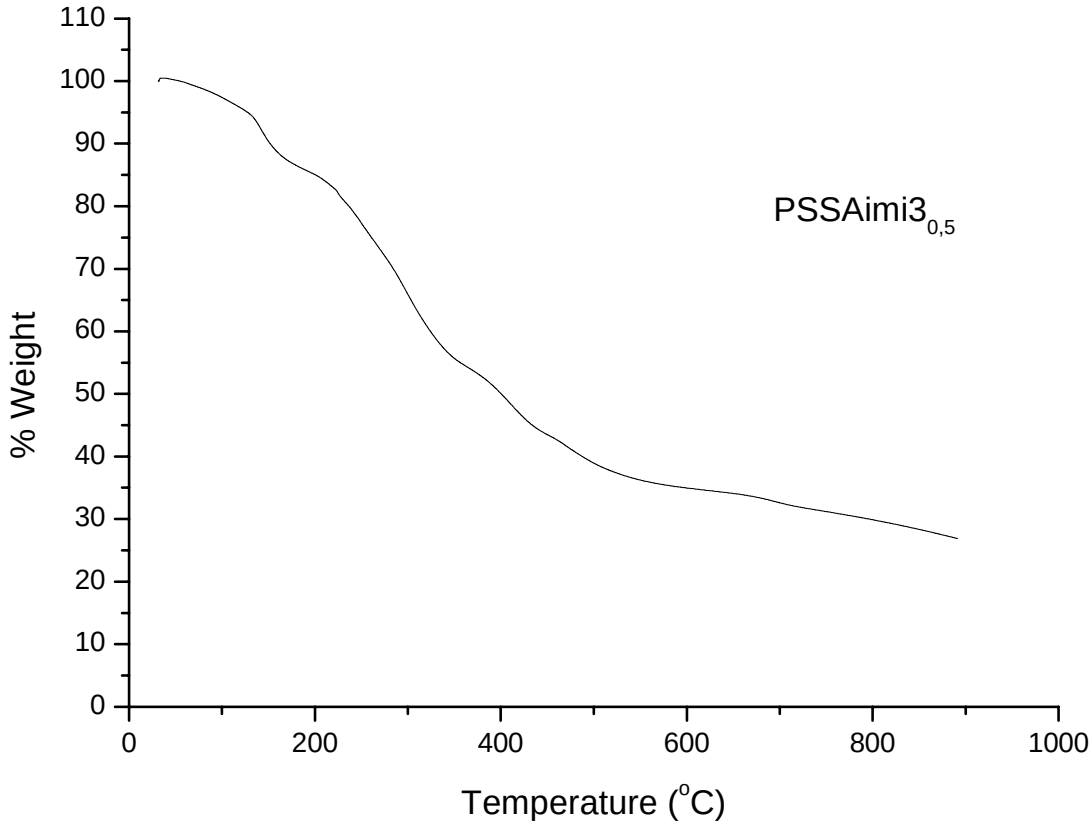

Figure 6.6. TG thermogram of PSSAimi3$_{0,5}$ recorded at a heating rate of 10 ^{o}C/min under a nitrogen atmosphere.

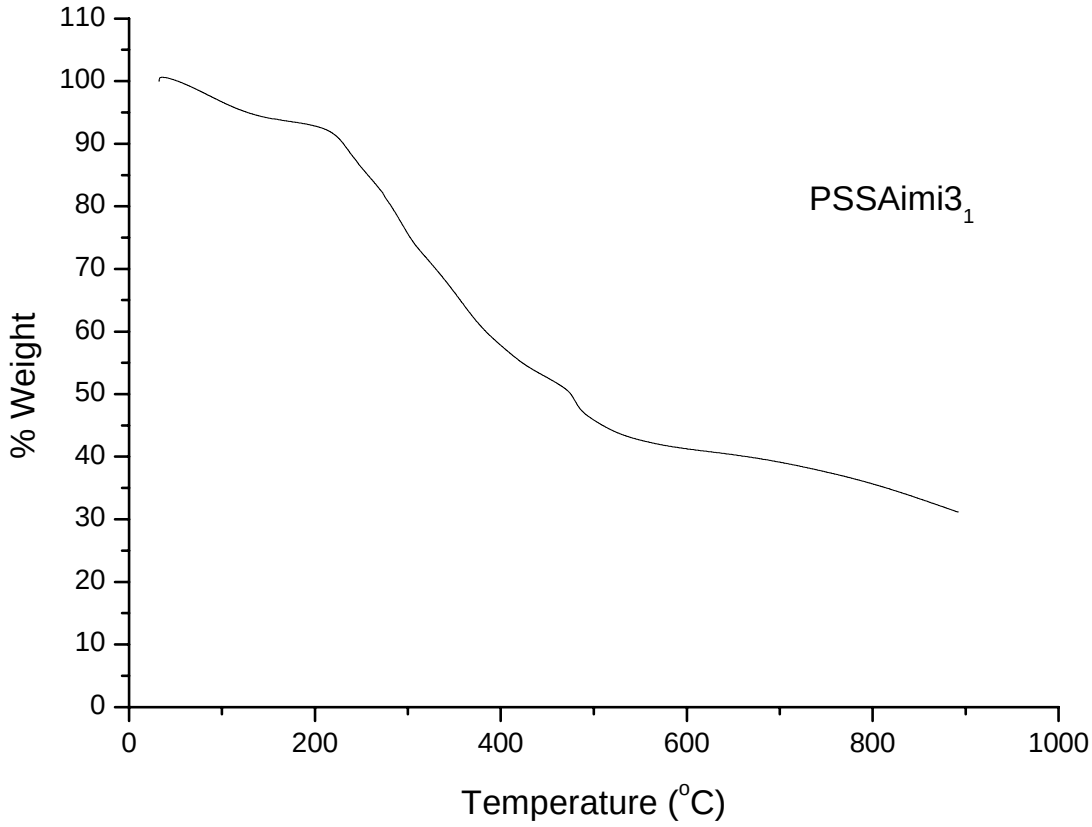

Figure 6.7. TG thermogram of PSSAimi3$_1$ recorded at a heating rate of 10^{o}C/min under a nitrogen atmosphere.

Similar weight change was observed for PSSATri$_1$ and PSSAimi3$_1$ electrolytes within the measured temperature range. The materials seem to be thermally stable at least up to 200 ^{o}C The TG thermograms of PSSATri$_1$ and PSSAimi3$_1$ are shown in Figure 6.8.

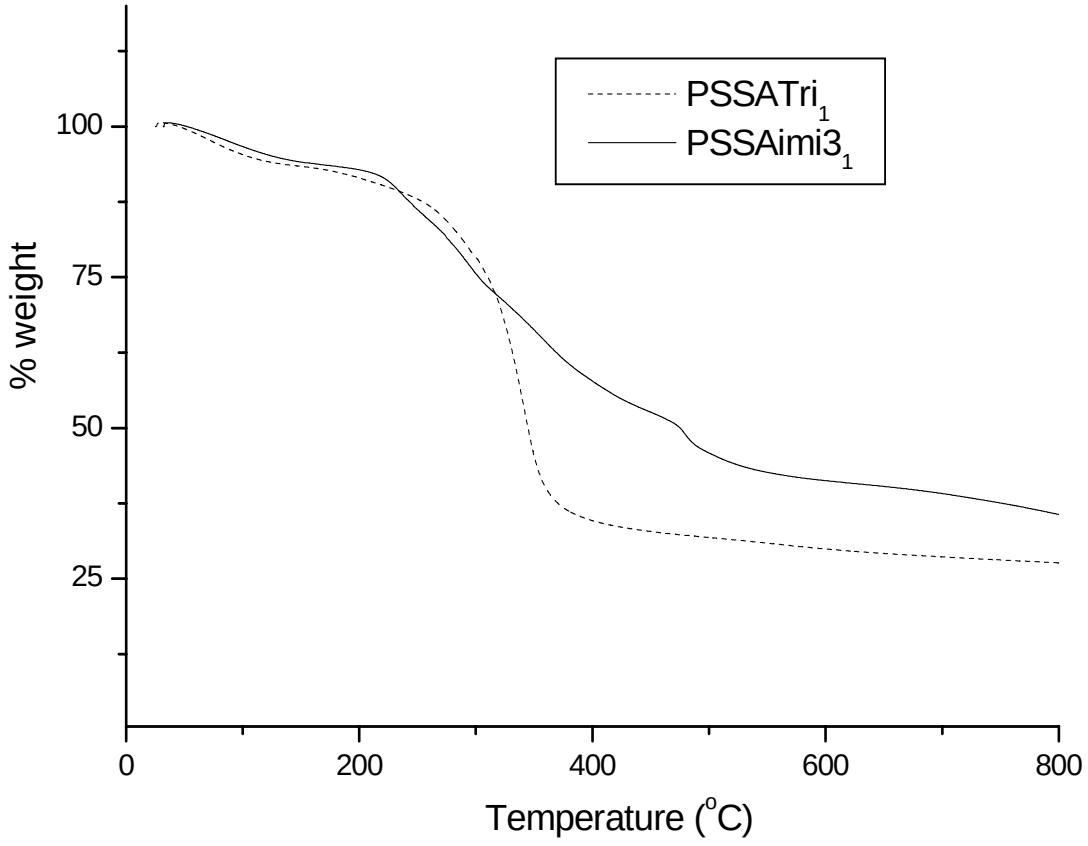

Figure 6.8.TG thermograms of $PSSAimi3_1$ and $PSSATri_1$ recorded at a heating rate of 10°C/minunder a nitrogen atmosphere.

6.3.1.3. Thermogravimetric Analysis (TG) of $CHPVPA_x$

Figure 6.9 shows the thermogravimetry (TG) profiles of the composite membranes. It was previously reported that pure chitosan is thermally stable up to 180°C (Rao et al., 2007). Also the pristine PVPA was reported to be stable until 200 °C (Jiang et al., 1999). The sample $CHPVPA_1$ exhibits a slight weight change up to 180 °C and then the material decomposes. When the composition of PVPA increased to 82%, then the degradation temperature shifts to approximately 150 °C. An elusive weight loss below these temperatures can be attributed to loss of absorbed humidity.

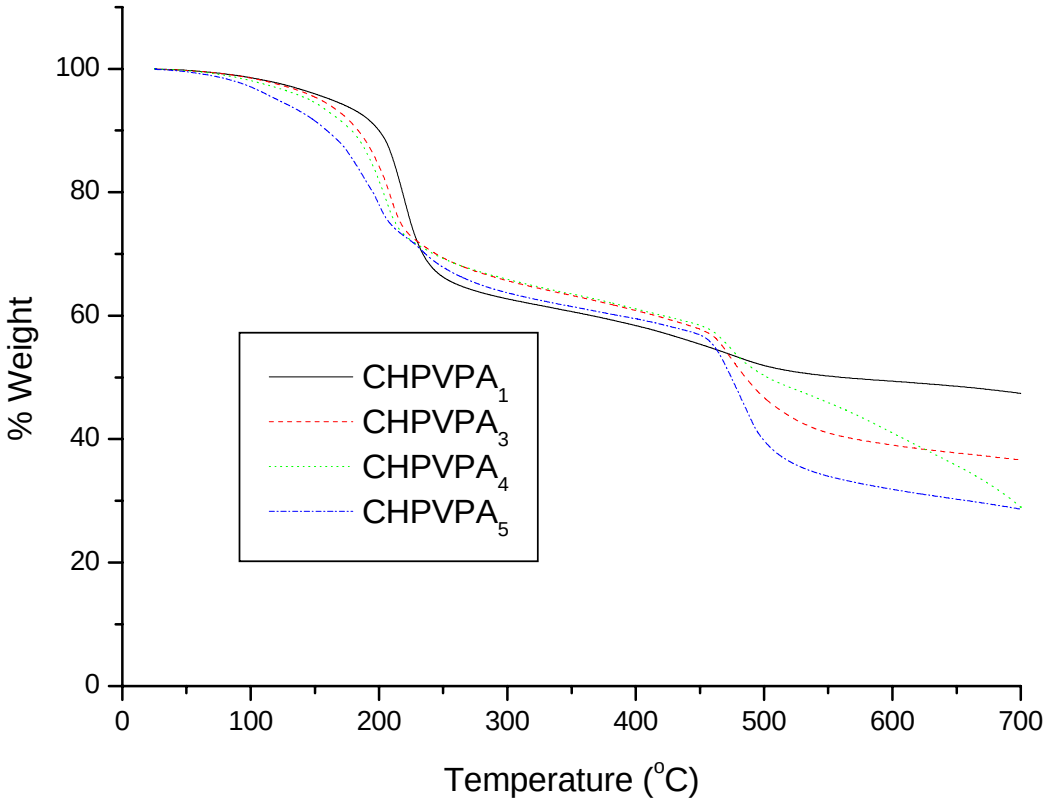

Figure 6.9. TG thermograms of $CHPVPA_x$ membranes recorded at a heating rate of 10°C/min under a nitrogen atmosphere.

6.3.2 Differential scanning calorimetry (DSC)

6.3.2.3. Differential scanning calorimetry (DSC) of $PSSATri_x$

DSC thermograms were recorded by heating cooling cycles form -140 °C to 40 °C and the T_gs were evaluated form the second heating curves at a heating rate of 10 °C/min. The T_g of pristine PS is about 108 °C. However, after doping of PSSA with Tri, the T_g of the $PSSATri_1$ appears at -50 °C (figure 6.10) and $PSSATri_{1.5}$ appears at -42 °C respectively (Figure 6.11).

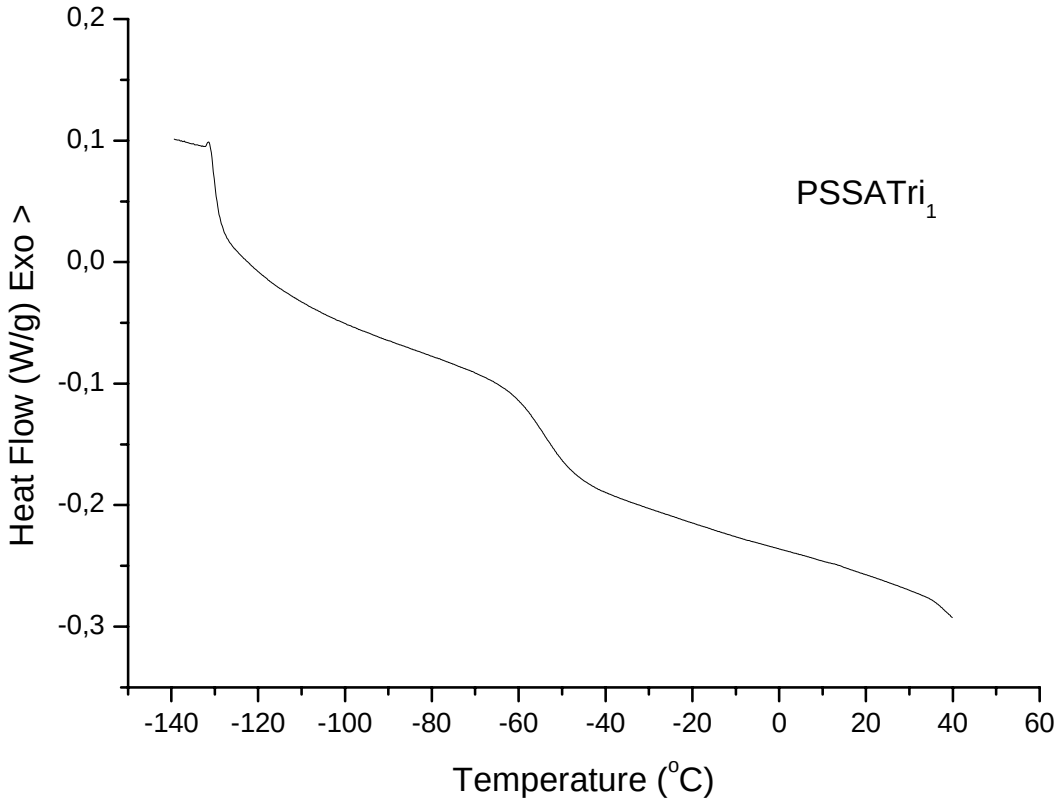

Figure 6.10. The DSC curve of $PSSATri_1$ .Temperature scanning rate is 10 ^{o}C /min. Second heating curve was evaluated.

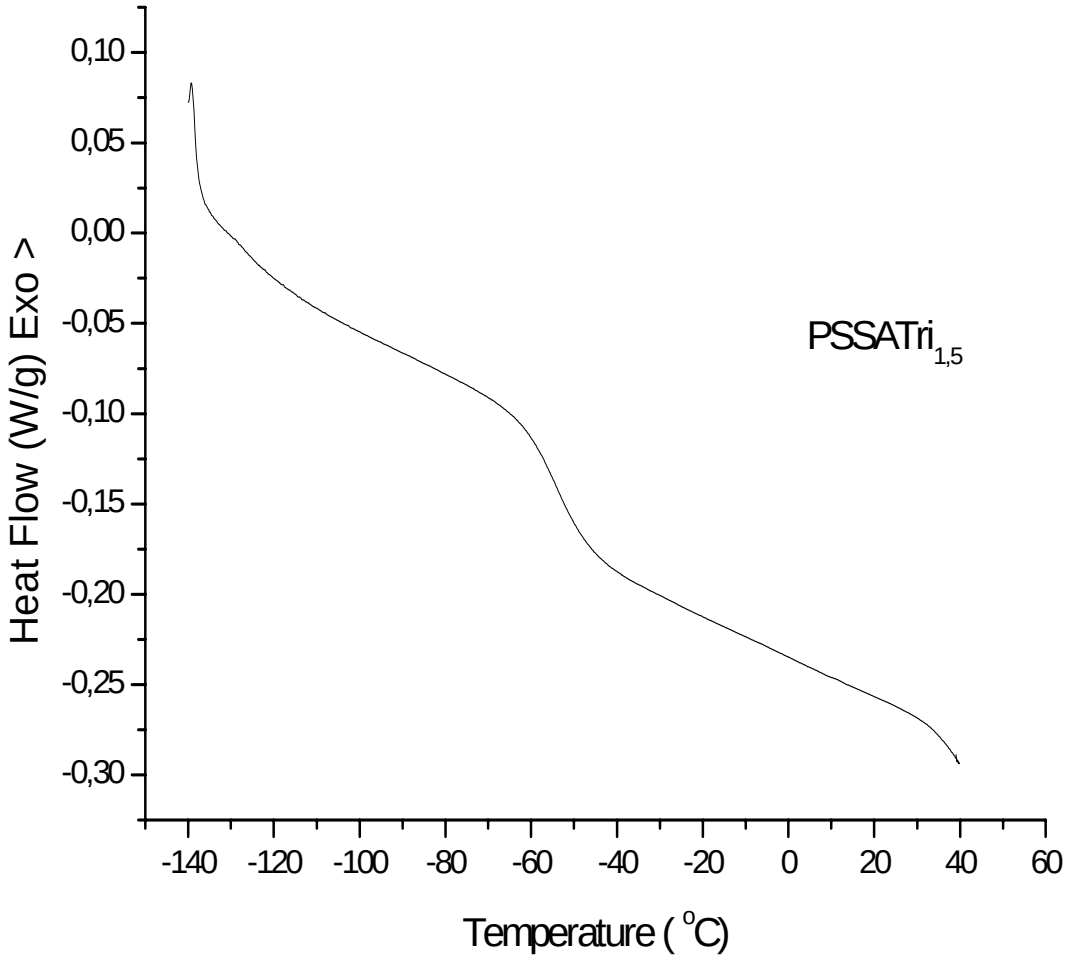

Figure 6.11. The DSC curve of $PSSATri_{1.5}$, Temperature scanning rate is 10 °C /min. Second heating curve was evaluated.

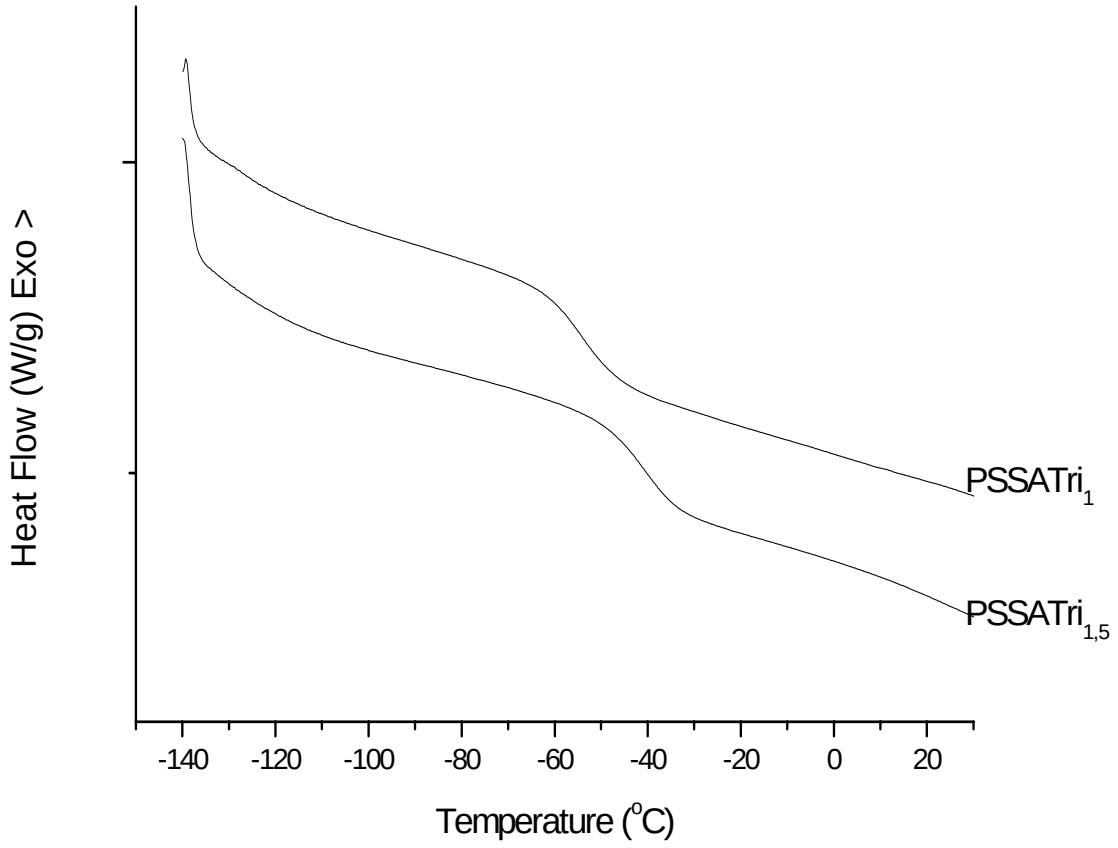

Figure 6.12.Comparison of the DSC curves of $PSSATri_1$ and $PSSATri_{1.5}$, Temperature scanning rate is 10 °C /min. Second heating curves were evaluated.

6.3.2.4. Differential scanning calorimetry (DSC) of $PSSAimi3_x$

DSC thermograms were recorded by heating cooling cycles form -140 °C to 40 °C and the T_gs were evaluated form the second heating curves at a heating rate of 10 °C/min. Previously we have reported the glass transition temperature of benzimidazole doped PSSA ($PSSABnIm_{1.5}$) as 147 °C (Bozkurt, 2005). However, after doping of PSSA with imi3, the T_g of the $PSSAimi3_1$ appears -36 °C (Figure 6.13) and $PSSAimi3_{0.5}$ appears -38 °C respectively (Figure 6.14).

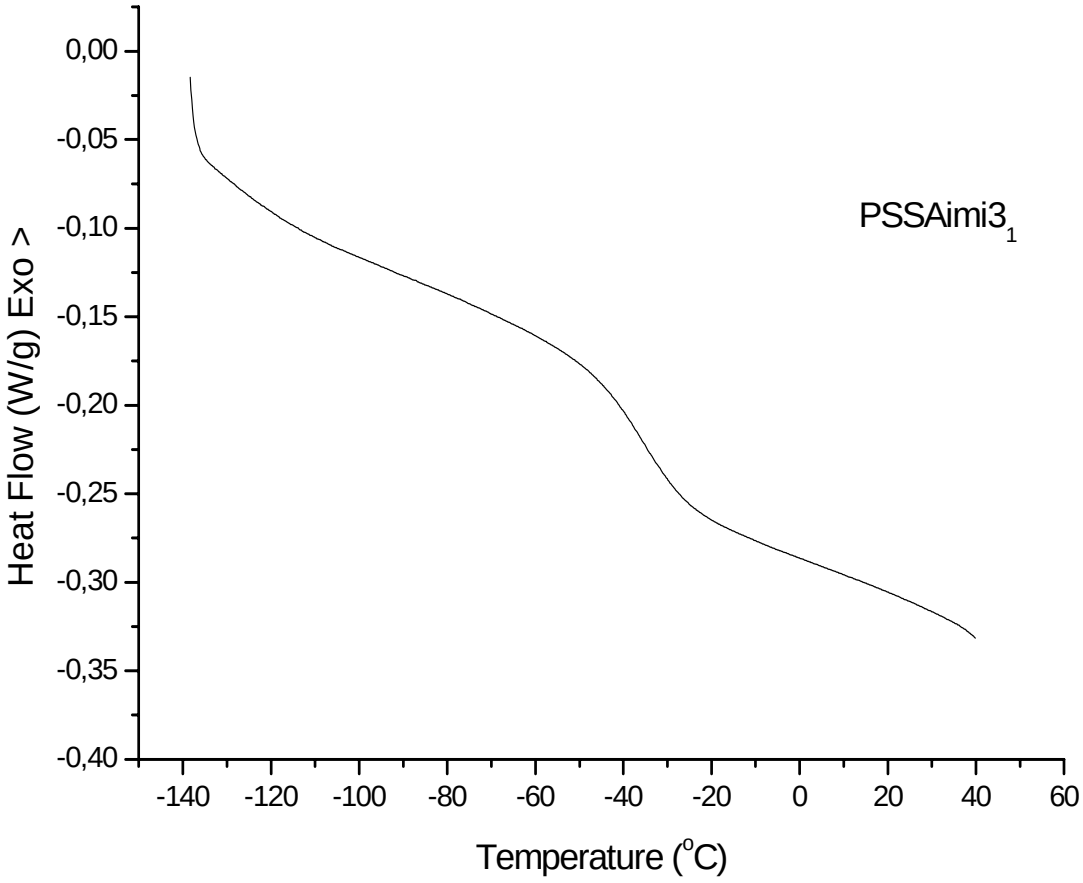

Figure 6.13. The DSC curve of PSSAimi3$_1$. Temperature scanning rate is 10 ^{o}C /min. Second heating curve was evaluated.

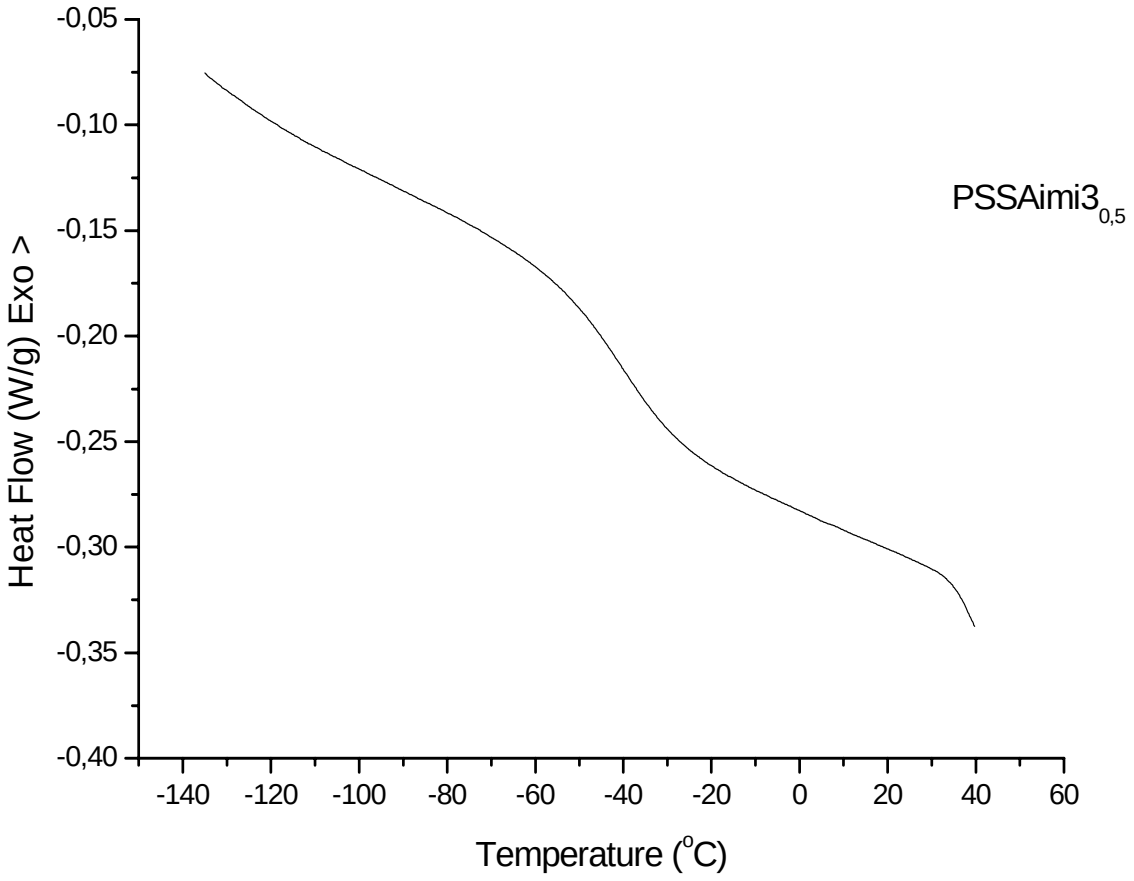

Figure 6.14. The DSC curve of PSSAimi3$_{0.5}$. Temperature scanning rate is 10 ^{o}C /min. Second heating curve was evaluated.

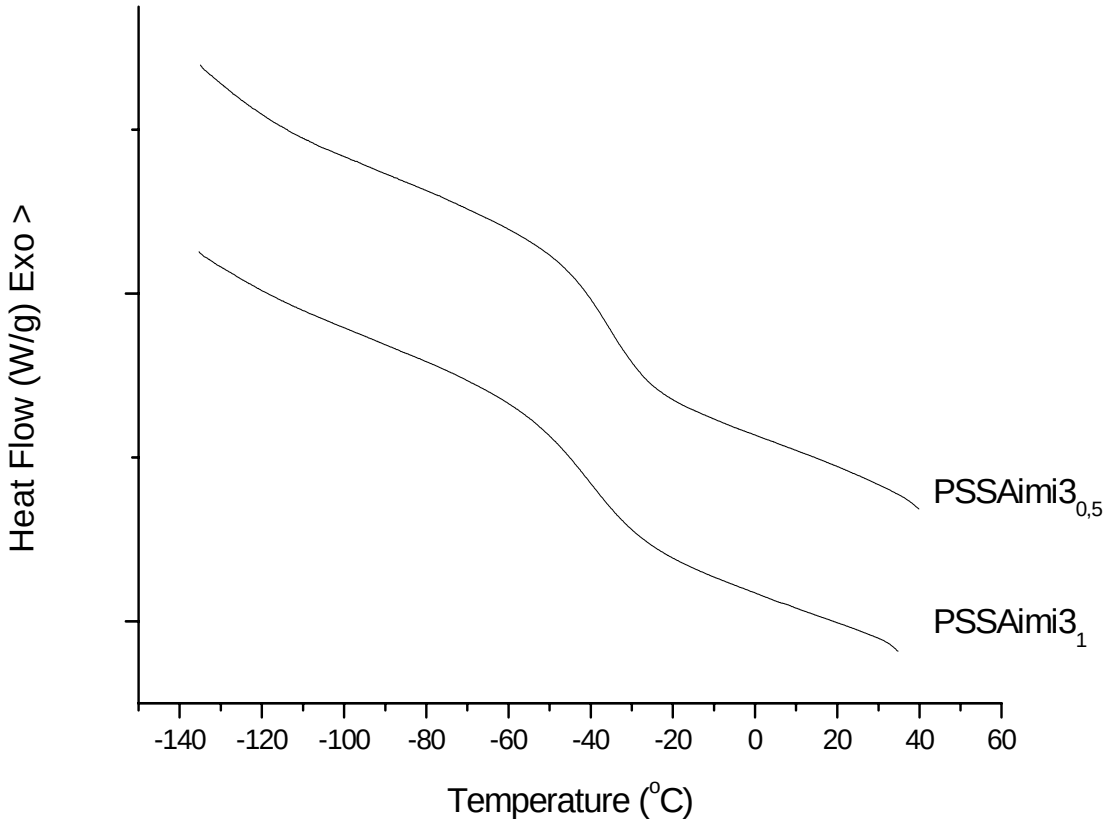

Figure 6.15. Comparison of the DSC curves of PSSAimi3$_{0.5}$ and PSSAimi3$_1$. Temperature scanning rate is 10 ^{o}C /min. Second heating curves were evaluated.

After doping of PSSA with Tri and imi3, the T_gs of the PSSATri$_1$, PSSATri$_{1.5}$ and PSSAimi3$_1$ appears at -50 ^{o}C, -42 ^{o}C and -36 ^{o}C, respectively (Figure 6.16). This behavior can be expressed by the plastization of the host polymer through doping. The presence of single glass transition is the evidence of the homogeneity of these materials.

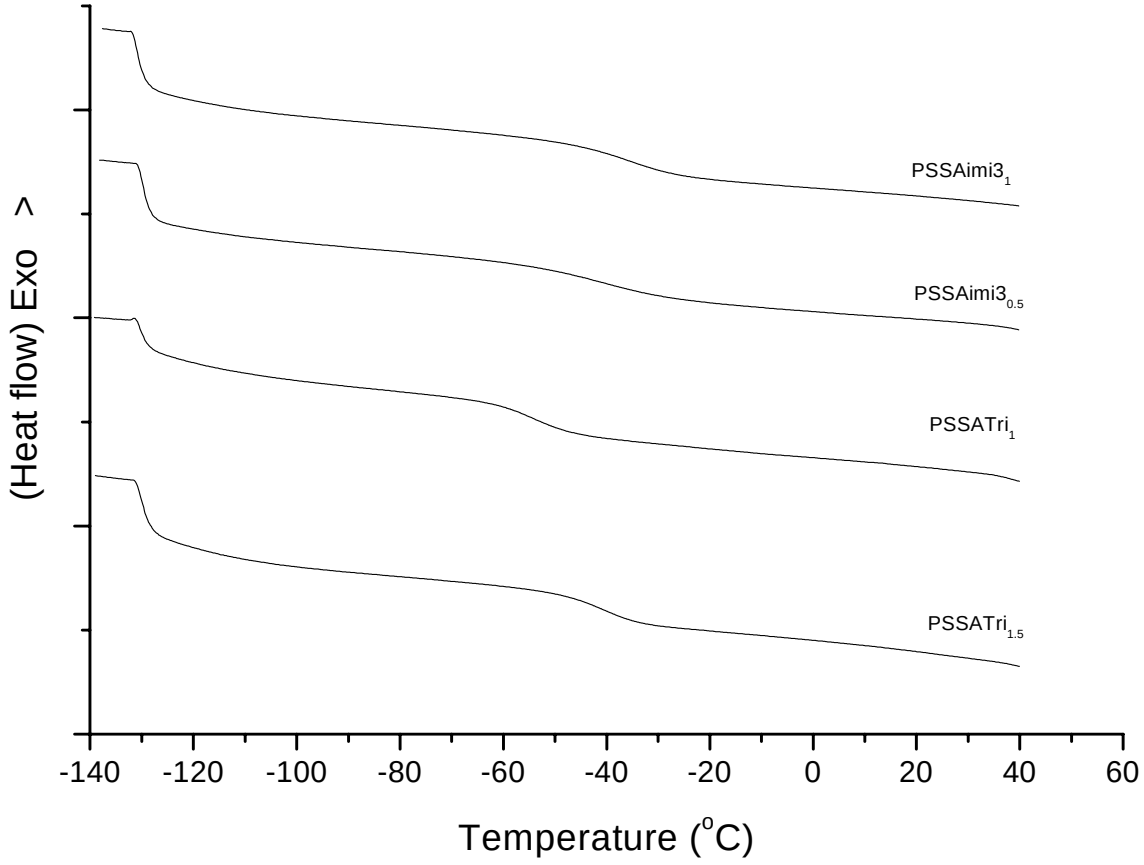

Figure 6.16. Comparison of the DSC curves of PSSATri$_1$, PSSATri$_{1.5}$, PSSAimi3$_{0.5}$ and PSSAimi3$_1$. Temperature scanning rate is 10 ^{o}C /min. Second heating curves were evaluated.

6.3.2.5. Differential scanning calorimetry (DSC) of CHPVPA$_x$

DSC measurements were carried out to determine the glass transition temperatures (Tg) of the composites and the results are shown in Figure 6.17 No distinct Tg was observed up to 125 ^{o}C. The reason for such a high Tg may be due to ionic cross-linking which results in the restrictions of segmental motions of the polymer chains. The same problem in detecting Tg's has also been encountered in the copolymers of vinylphosphonic acid) and 4(5)-vinylimidazole (Bozkurt et al., 2003).

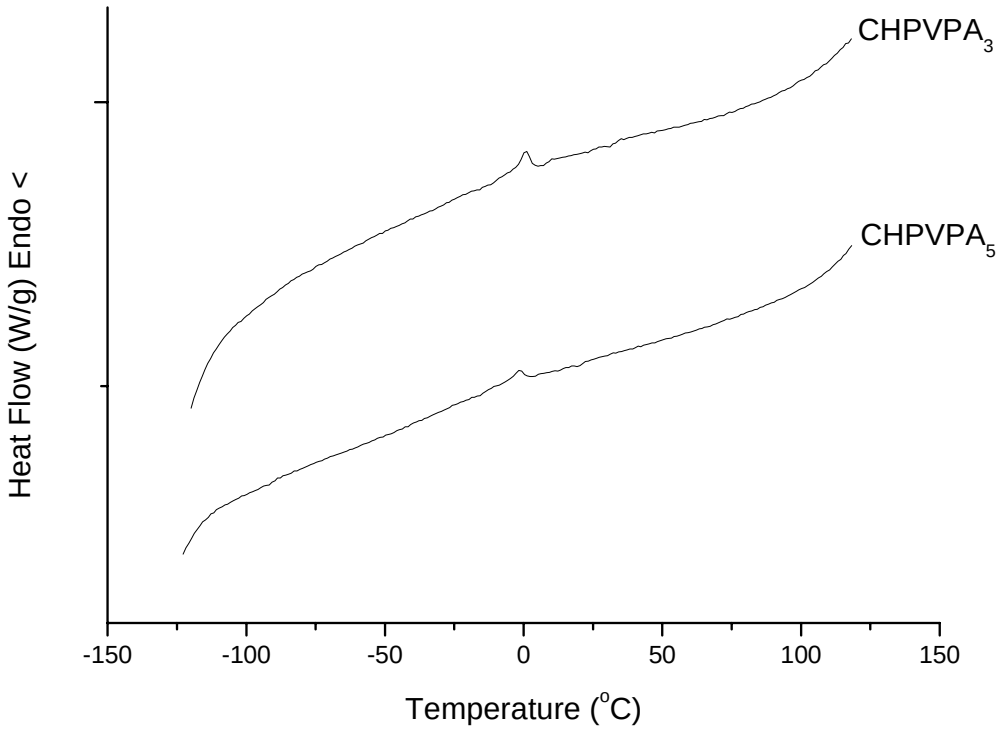

Figure 6.17. DSC curves of $CHPVPA_3$ and $CHPVPA_5$. Temperature scanning rate is 10 °C /min. Second heating curves were evaluated.

6.4. X-RAY DIFFRACTION (XRD) STUDIES

6.4.1. X-Ray diffraction (XRD) studies of the $CHPVPA_x$

X-Ray diffraction of chitosan and $CHPVPA_x$ composite membranes are shown in Figure 4. The broad peaks observed in the XRD pattern around 15° and 25° of 2θ indicate the average intermolecular distance of the crystalline part of pure chitosan (Rao et al., 2007, Kolh and Kannan, 2003). In contrast, composite membranes show greater amorphous morphology. This behavior was described as the elimination of interchain hydrogen bonding between amino groups and hydroxyl groups in chitosan (Kim and Lee, 1993).

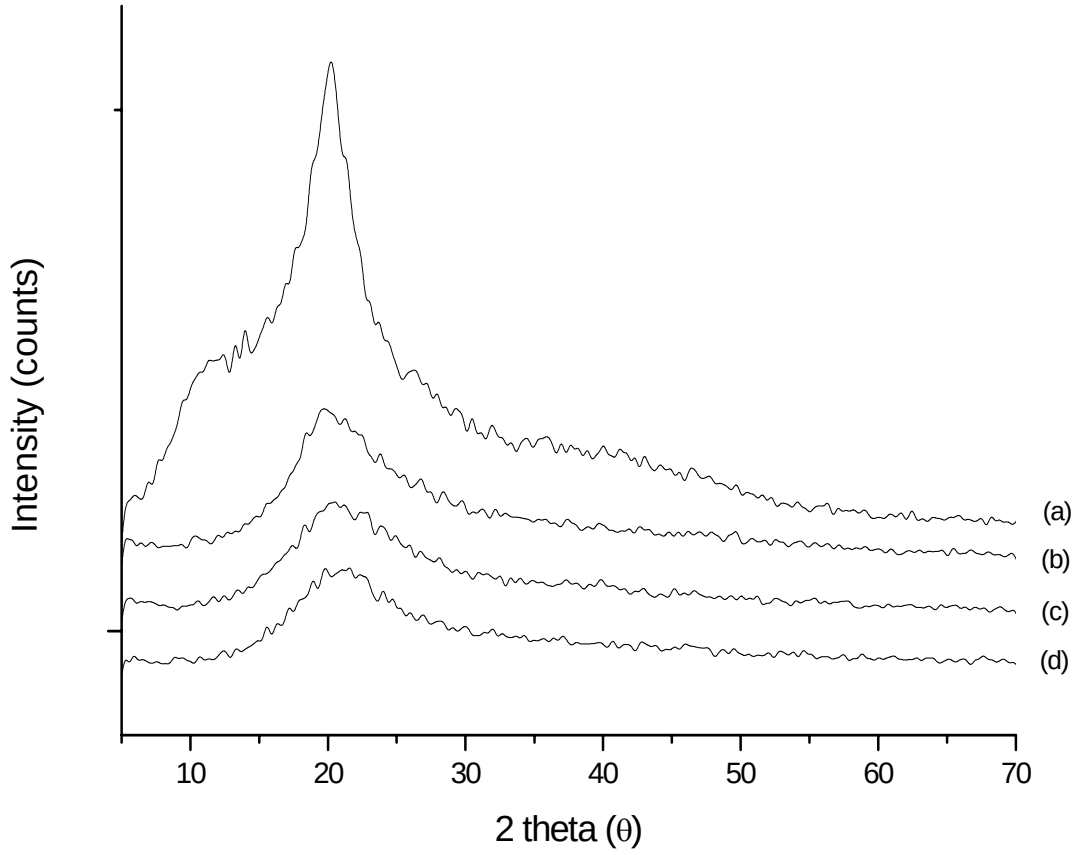

Figure 6.18.XRD patterns of (a) pure chitosan, (b)CHPVPA$_1$, (c)CHPVPA$_2$ and (d)CHPVPA$_4$

6.5. METHANOL PERMEABILITIES

6.5.1. Methanol Permeabilities of CHPVPA$_X$ Membranes

Methanol permeability of the composite membranes was determined using a diaphragm diffusion cell which was described in a previous work (Gasa et al., 2006). Methanol permeabilities were calculated using the following equation (Eq.6.1):

$$P = [W\ (g) \times l\ (cm)] / [M_W\ (g/mol) \times A\ (cm^2) \times t\ (s)] \quad (6.1)$$

where, P is the methanol permeability, W is the permeated amount of methanol, *l* is the thickness of the membrane, M_w is the molecular weight of methanol, A is the area the cell hole and t is the time.

Figure 6.19 is the plot of the mass of methanol that diffused through the composite membrane, $CHPVPA_5$ as a function of time. The molar flux (g/s) was obtained from the slope of this plot and methanol permeabilities were calculated as 3.39 $x10^{-9}$ mol/s.cm at 20 ^oC and 5.42 $x10^{-9}$ mol/s.cm at 40 ^0C. In the same system methanol permeability of Nafion 112 was found to be $1.89x10^{-9}$ mol/s.cm. Previously the methanol permeability of the composites base on N-methylene phosphonic chitosan and poly (vinyl alcohol) was reported to be $9.45x10^{-8}$ cm^2/s (Binsu et al., 2006).

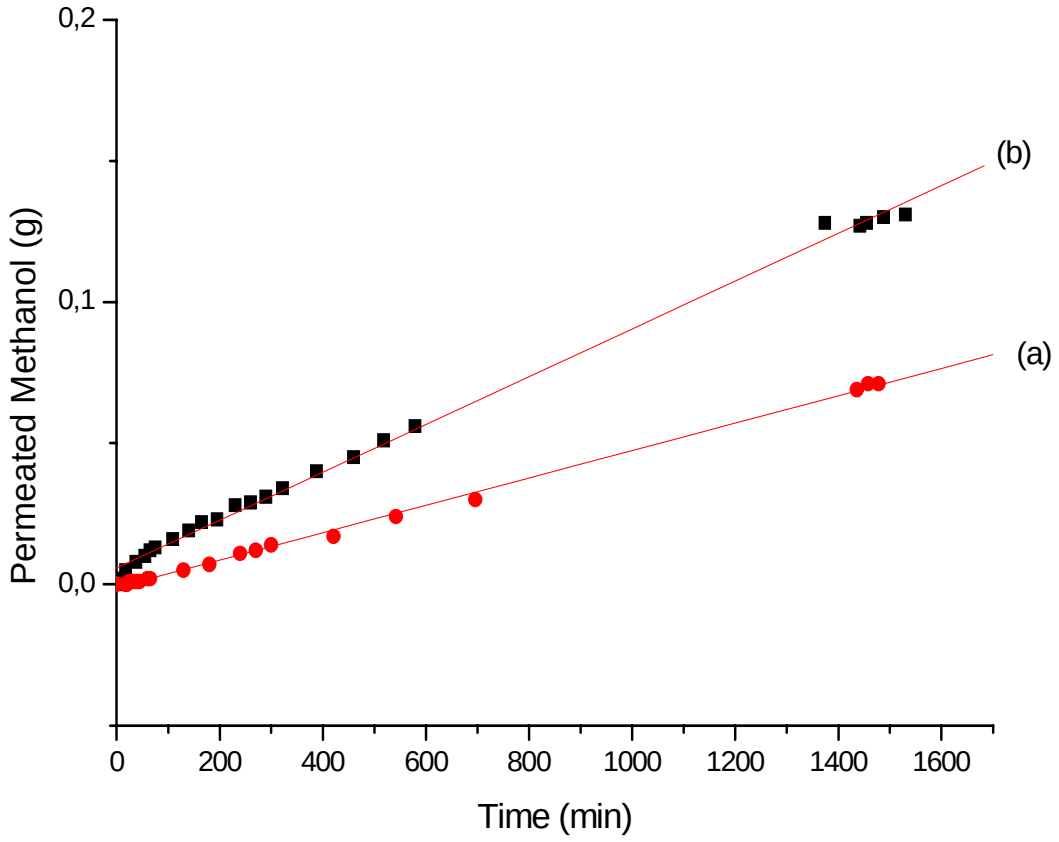

Figure 6.19. Mass flow of methanol through composite membrane, $CHPVPA_5$ at (a) 20^oC and (b) 40^oC.

6.5.2. Water/methanol uptake

The solvent uptake measurements were made according to literature (Li et al., 2004, Smitha et al., 2006). The pre-weighed films (dry W) of the membranes was soaked into methanol / water (12 mol/L) solution and the % swelling was determined. To get rid off any external liquid, the sample was wiped out and the sample weighed after different time intervals until a constant weight (Wwet). The final solvent uptake value was determined by equation, (Eq.6.2):

$$\%\text{Uptake} = [(W_{wet} - W_{dry}) \times 100] / W_{dry} \quad (6.2)$$

As can be seen in Figure 6.20, increased methanol uptake with molar ratio of PVPA/Chitosan is thus reasonably increased. This finding is primarily ascribed to ionic crosslinking where the materials become more rigid at lower PVPA composition, i.e., x=2. The addition of PVPA increased the swelling character of the composites.

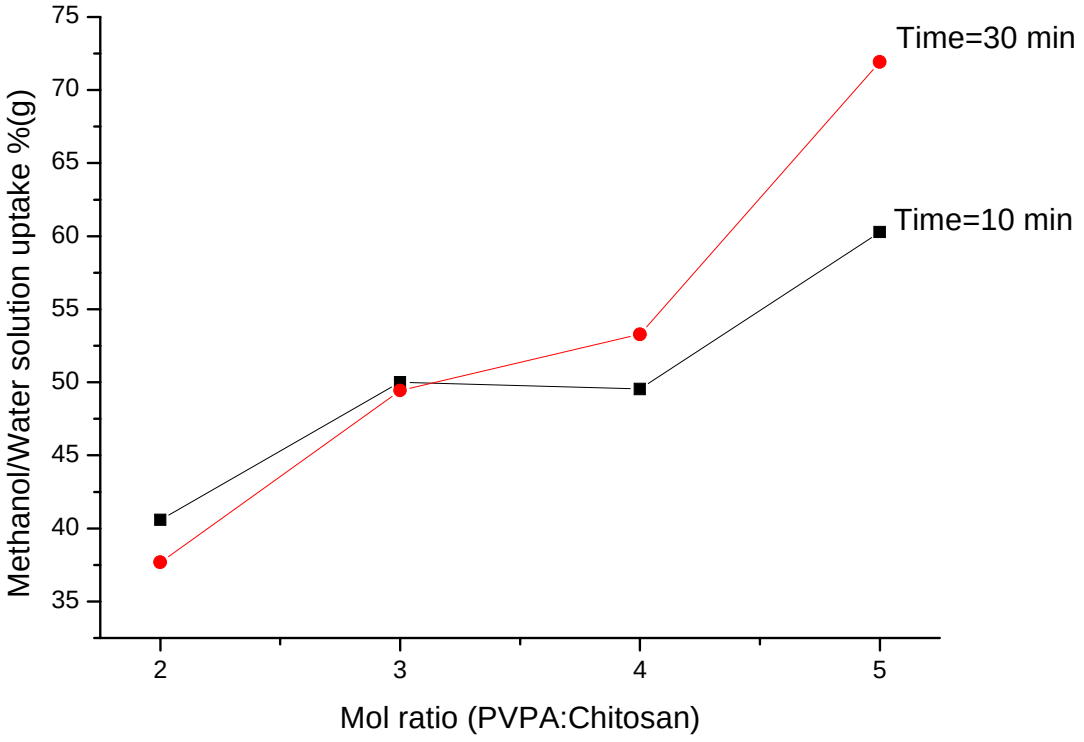

Figure 6.20. Solvent Uptakes of CHPVPA$_x$ membranes at the time of 10 min and 30 min in 12 mol/L methanol/water solution at 25 ^{o}C.

6.6. CONDUCTIVITY OF POLYMER ELECTROLYTES

Polymer electrolytes and polyelectrolytes are known to conduct the electricity by the transport of free ions. The electrical conductivity measurement of these materials are performed with both, direct current (DC) and alternating current (AC) measurements.The former method is accomplished by sandwiching the material between two nonblocking or blocking electrodes and a DC voltage is applied. AC measurements, is the most popular approach for the determination of electrical properties of polymer electrolytes. In this method a sinusoidal voltage is applid to a cell which functions as a capacitor and the resulting impedance is determined.

One inherent advantage of studying materials through their electrical properties is that electrical measurements can be made over a very wide range of frequencies with a high degree of precision. Thus the dielectric constant and loss of solid polymers are often known from 10^{-4} Hz up to optical frequencies. Taken together with the possibility of varying

temperature and pressure, the breadth of the experimental technique becomes very impressive, and researches have made full use of this tool in probing underlying molecular behaviour.

In considering the methods of measurement we must distinguish two basic types, namely lumped-circuit and distributed-circuit methods. The aim of lumped-circuit methods, which are always used at lower frequencies, is to determine the equivalent electrical circuit of a specimen at a given frequency. We can see directly how the components of the complex permittivity of the material may be expressed in terms of an equivalent parallel circuit. Thus let the specimen be represented by a capacitance C_p in parallel with a resistance R_p, as show in fig.6.21(a) the total impedance Z will then be given by

$$1/Z = 1/R_P + \mathrm{i}\,\omega\, C_p \tag{6.3}$$

Application of the alternating voltage represented by the real part of $V=V_o\, e^{i\omega t}$ will produce an out-of-phase or capacitive current I_c:

$$\begin{aligned} I_c &= \text{Imaginary part } [V/Z] \\ &= \mathrm{i}\,\omega\, C_p V \end{aligned} \tag{6.4}$$

And an in-phase or resistive current I_R:

$$\begin{aligned} I_R &= \text{Real part } [V/Z] \\ &= V/R_p \end{aligned} \tag{6.5}$$

$$I_c = \mathrm{i}\,\omega\, C_o\, \varepsilon^{l}\, V \tag{6.6}$$

$$I_R = \omega\, C_o\, \varepsilon^{u}\, V \tag{6.7}$$

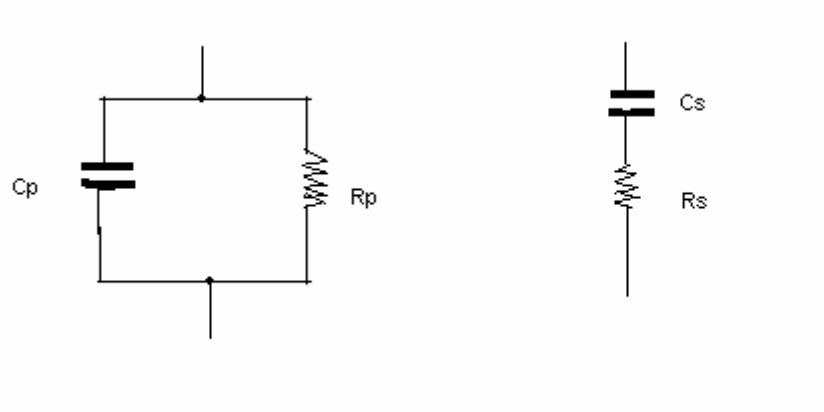

(a) (b)

Figure.6.21. Equivalent electrical circuits of dielectric specimens: (a) parallel, (b) series.

Comparing equations (6.4) and (6.5) with equations (6.6) and (6.7), respectively,

$$\varepsilon' = C_p / C_o \tag{6.8}$$

$$\varepsilon'' = 1/ R_p C_o \omega \tag{6.9}$$

and

$$\tan\delta = \varepsilon'' / \varepsilon' = 1/ R_p C_p \omega \tag{6.10}$$

Alternatively, the specimen may be regarded in terms of a series circuit. If the equivalent series components of capacitance and resistance are C_s and R_s, respectively (see fig. 6.21(b)), the total impedance will be given by

$$Z = R_s + 1/ i \omega C_s \tag{6.11}$$

If we again compare out-of-phase and in-phase currents after application of the alternating voltage, we obtain

$$\varepsilon' = C_s / C_o(1+\tan^2\delta) \tag{6.12}$$

$$\varepsilon'' = R_s C_s / C_o(1+\tan^2\delta) \tag{6.13}$$

and

$$\tan\delta = \varepsilon'' / \varepsilon' = R_s C_s \omega \tag{6.14}$$

We can therefore calculate the dielectric constant and loss of a material from measured values of either equivalent series or parallel circuit components of a specimen.

The reciprocal of the specimen resistance in the equivalent parallel circuit for a given frequency is sometimes called the AC conductance G_p. It is a combination of DC conductance, by which we mean any real flow of charge through the sample under the influence of the applied field, and the anomalous conductance due to any time-dependent polarization processes. The contribution that a true DC conductivity σ (conductivity is defined as the reciprocal of resistivity which is the resistance between opposite face of a unit cube of a unit cube of material) will make to the dielectric loss at an angular frequency ω can be readily calculated as follows for the material in a parallel-plate capacitor. Substituting for resistance in equation (6.9):

$$\varepsilon'' = G_p / C_o \omega \tag{6.15}$$

If the capacitor plates have area A and separation s:

$$G_p = \sigma A / s \quad \text{and} \quad C_o = \varepsilon_o A / s \tag{6.16}$$

And hence

$$\varepsilon'' = \sigma / \varepsilon_o \omega \tag{6.17}$$

This shows how DC conductivity causes ε'' to rise rapidly at low frequencies. At high frequencies the electromagnetic wavelength inevitably becomes comparable with sample dimension, and lumped-circuit methods must be abandoned in favor of distributed-circuit methods in which the sample becomes the medium for propagation of electromagnetic waves.

Dielectric constant and loss must then be obtained from the observed wavelength and attenuation characteristics (Blythe, 1979).

The proton conductivity studies of the samples were performed using a SI 1260-Schlumberger impedance spectrometer at the Max-Planck Institute for Polymer Research, Mainz, Germany. The samples were placed between gold electrodes and their conductivities were measured in the frequency range 1 Hz to 1 MHz at 10 ^{o}C intervals. The temperature was controlled with a Novocontrol cryosystem, which is applicable between -150 and 400 ^{o}C with a precision of 0.01 ^{o}C. Frequency dependent AC conductivities (σ_{ac} (ω)) were measured using the Eq (6.18).

$$\sigma'(\omega) = \sigma_{ac}(\omega) = \varepsilon''(\omega)\,\omega\,\varepsilon_o \qquad (6.18)$$

where σ' (ω) is the real part of conductivity, $\omega = 2\pi f$ is the angular frequency, ε_o is the vacuum permittivity (ε_o = 8.852 x 10^{-14} F/cm), and ε'' is the imaginary part of the complex dielectric permittivity (ε^*). Then the DC conductivity is derived from σ_{ac} versus F data by linear fitting and extrapolating the frequency independent AC conductivity plateaus to zero frequency.

6.6.1. Proton conductivity of PSSATri$_x$

The frequency dependence AC conductivity, σ_{ac} (ω) of the materials was measured at several temperatures using impedance spectroscopy within the range of 0.1 Hz - 1 MHz. The curve consists of two well-defined regions; a low frequency zone (f<100 Hz) is related to electrode polarization due to the blocking effect of the gold electrodes. At higher frequencies (f>100 Hz), frequency independent plateaus are generated which corresponds to conduction processes in the bulk of samples.

Figures 6.22, 6.23 and 6.24 are the frequencies dependence σ_{ac} (ω) for PSSATri$_x$. Similar regions can be observed in Figures, except the dispersion region in the low temperature (T< 30 ^{o}C) and high frequency region (f > 10^4 Hz).

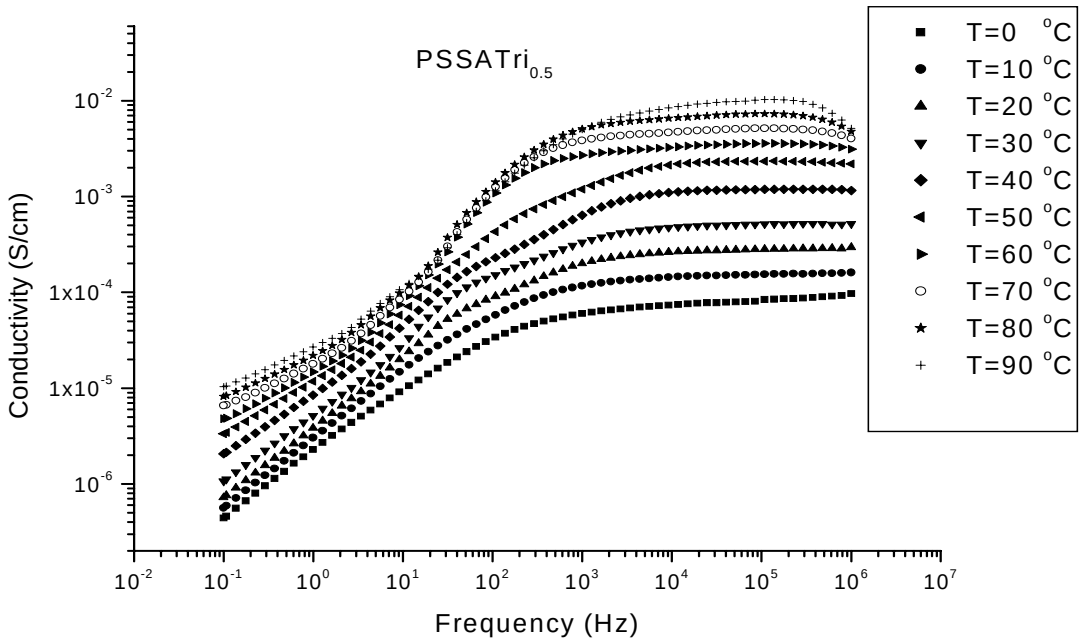

Figure 6.22. AC conductivity versus Frequency (Hz) for $PSSATri_{0,5}$ at various temperatures.

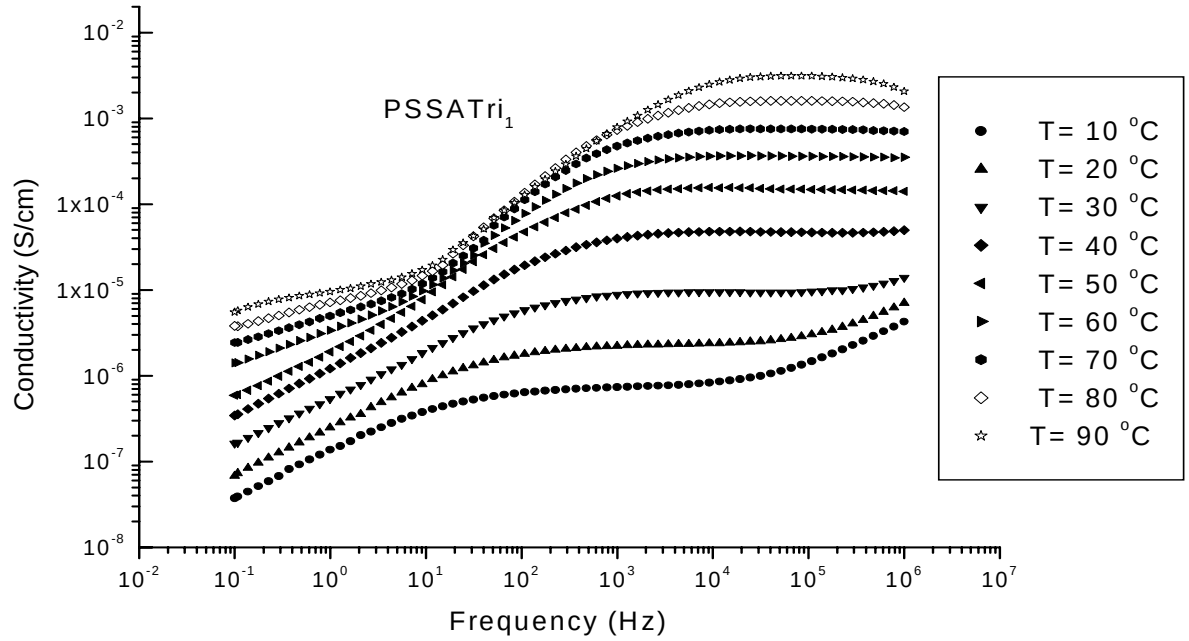

Figure 6.23. AC conductivity versus Frequency (Hz) for $PSSATri_1$ at various temperatures.

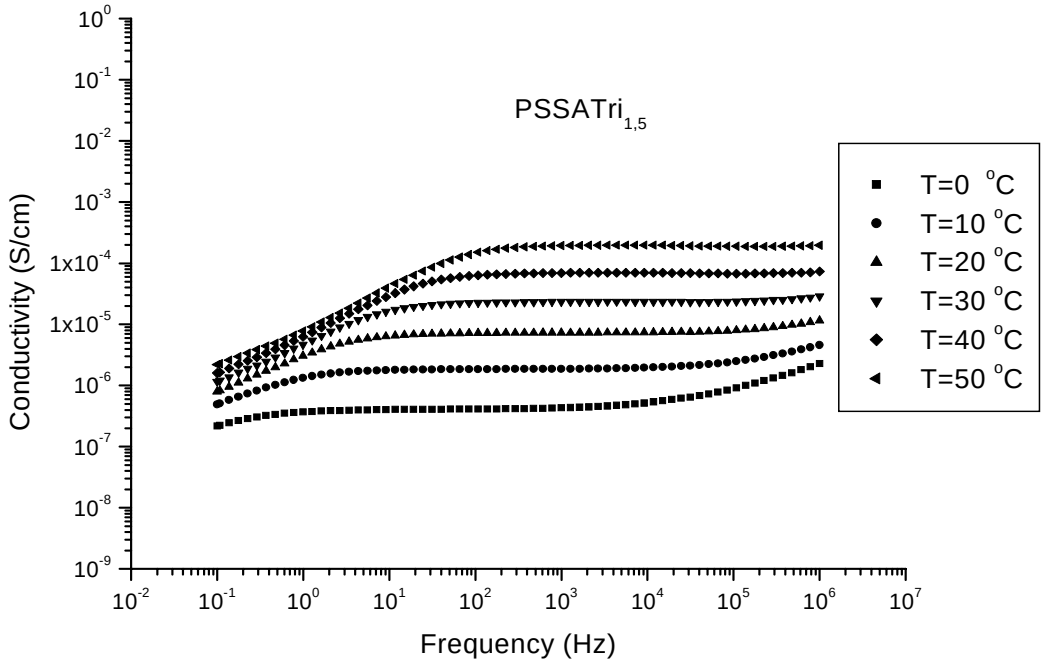

Figure 6.24 AC conductivity versus Frequency (Hz) for $PSSATri_{1,5}$ at various temperatures.

The molecular structure of 1H-1,2,4-Triazole, Tri is similar to other heterocyclic structures such as imidazole or pyrazole, but it comprises three nitrogen in the five-membered ring Therefore conduction mechanism is expected to be similar to those heterocyclic systems. To investigate the proton conductivity of Tri in acidic polymers, polystyrenesulfonic acid, PSSA was doped with Tri. The proton conductivity of anhydrous $PSSATri_1$ electrolyte increased with increasing temperature. The proton exchange between polymer and Tri was confirmed by by FTIR spectroscopy. The proton exchange reaction between adjacent 1H-1,2,4-Triazoles is described as structure diffusion (Grotthuss mechanism) where Tri acts as proton solvent in the conduction process (Günday et al., 2006). As reported, in polyelectrolyte/1H-1,2,4-Triazole systems the heterocyclic groups form hydrogen bonding network and promote long range proton transport that is far better than imidazole (Zhou et al., 2005).

Recently, the proton conductivity of anhydrous sulfonated polysulfone/Tri electrolytes were reported (Li et al., 2005). It was noticed that there is no significant conductivity change

with the concentration of Tri especially at higher temperatures. The proton conductivity of the sulfonated polysulfone/Tri electrolytes reached 1.5 x 10^{-3} S/cm at 100 ^{o}C and 5 x 10^{-3} S/cm at 140 ^{o}C.

In a very recent study, the efficiency of Tri was demonstrated as proton solvent in the anhydrous Poly(vinylphosphonic acid)/Tri (PVPATri$_x$) and poly(2-acrylamido-2-methyl-1-propane sulfonic acid)/Tri (PAMPSTri$_x$) electrolytes (x is the doping ratio) (Gündayet al., 2006). These homogeneous polymer electrolyte membranes show a maximum proton conductivity of 2.3x10^{-3} S/cm for PVPATri$_{1.5}$ at 120 ^{o}C and of 9.3x10^{-4} S/cm for PAMPSTri$_2$ at 140 ^{o}C in the anhydrous state.

6.6.2. Proton conductivity of PSSAimi3$_{0.5}$

The insertion of imidazole terminated oligoetilen oxide (imi3) increased the conductivity of dry PSSA and proton conductivity of PSSAimi3$_{0.5}$ was found to be approximately 10^{-4} S/cm at ambient temperature (Figure 6.25). In this system, imi3 plasticized the material and proton transport expected to occur between imidazole units through intermolecular proton transport (structure diffusion). Thus, long range proton transport can be enhanced by the protonic defects that form local disorder through hydrogen bonding network, i.e., Him-(HimH+)-imH) (Kreuer et al., 1998).

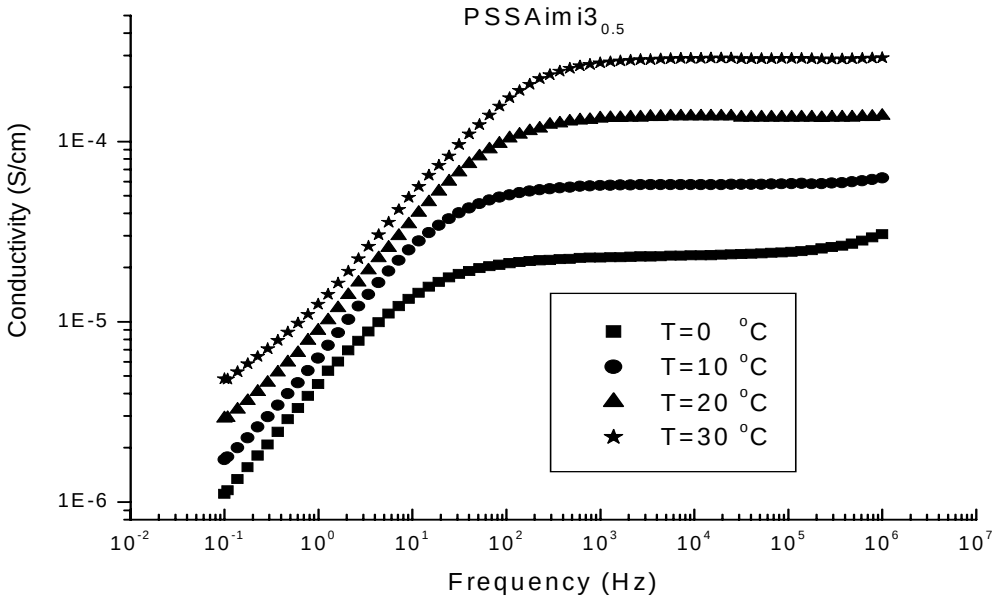

Figure 6.25. AC conductivity versus Frequency (Hz) for PSSAimi3$_{0.5}$ at various temperatures.

6.6.3. DC conductivity of PSSATri$_x$ and PSSAimi3$_x$

The frequency independent plateau regions correspond to DC conductivity, σ_{dc} which is calculated by linear fitting and extrapolating to zero frequency.

Figure 6.27 shows the temperature dependence of the DC conductivity, σ_{dc} as a function of reciprocal temperature for the PSSA doped with imi3 and Tri. The conductivity isotherms belong to those samples which yield highest conductivity within the same series, i.e., PSSATri$_x$ and PSSAimi3$_x$. The conductivity data were measured by heating and cooling cycles for a given sample, suggesting reproducibility of the conductivity data. The results are also compared with PSSABnIm$_{1.5}$ (Bozkurt, 2005). The temperature dependence of DC conductivity yielded curved lines which can be described by Vogel-Tamman-Fulcher (VTF) equation (PSSATri$_1$ and PSSABnIm$_{1.5}$).

Also proton conductivity of anhydrous materials based on BnIm doped PSSA was reported (Bozkurt, 2005). The PSSABnIm$_x$ blends showed a maximum conductivity of 5x10^{-4} S/cm at 150 ^{o}C in the anhydrous state (Figure 6.26). Clearly, the proton conductivity of the anhydrous PSSATri$_{1.5}$ electrolyte is at least five orders of magnitude higher than that of PSSABnIm$_{1.5}$ at room temperature. This result shows that 1H-1,2,4-Triazole is a promising protogenic solvent in terms of proton conductivity compared to benzimidazole. PSSATri$_1$ showed a highest conductivity of 0.016 S/cm at 150 ^{o}C.

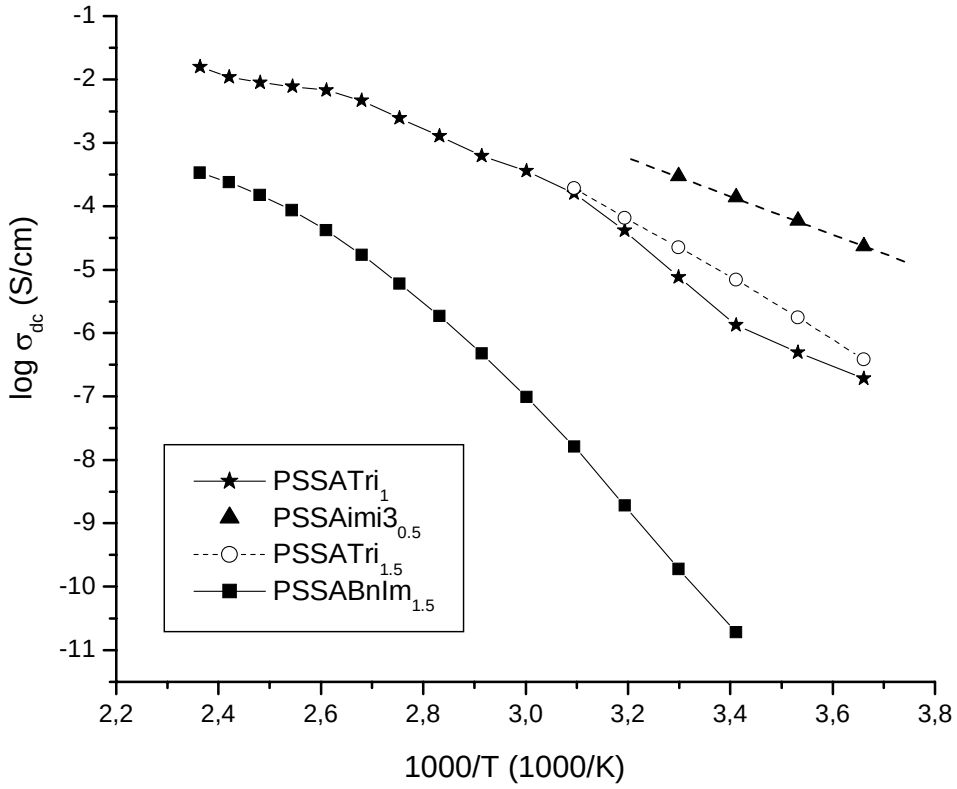

Figure 6.26. Variation of the proton conductivities of PSSATri$_1$, PSSATri$_{1.5}$, PSSAimi3$_{0.5}$ and PSSABnIm$_{1.5}$ as a function of reciprocal temperature.

6.6.4. Conductivity of CHPVPAx

The frequency dependence of AC conductivity, σ_{ac} (ω) of the materials was measured at several temperatures using impedance spectroscopy. Figure 6.27 shows the σ_{ac} (ω) of the CHPVPA$_5$ versus frequency at various temperatures. It can be observed from the figure that conductivity seems to be almost constant in the frequency range over 1-3 decades,

corresponding to DC conductivity, σ_{dc}. The temperature dependence of the σ_{dc} was obtained by linear fitting of the plateau values to real axis.

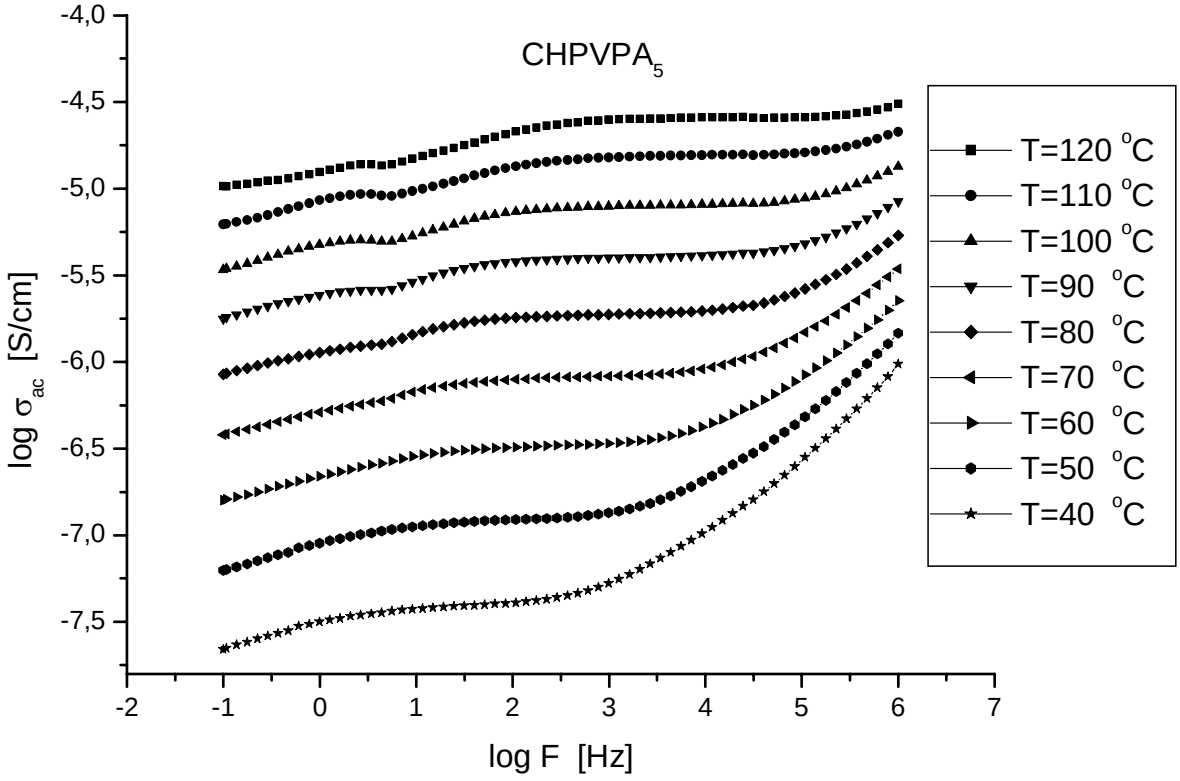

Figure 6.27. AC conductivity versus Frequency (Hz) for $CHPVPA_5$ at various temperatures.

The temperature dependence of DC conductivity of $CHPVPA_2$, $CHPVPA_3$ and $CHPVPA_5$ are shown in Figure 6.28. The DC conductivity of the samples increases linearly with temperature which can be described by Arrhenius equation (Eq.6.19):

$$\sigma = \sigma_o \exp(-E_a/kT) \qquad (6.19)$$

where σ_o is the pre-exponential factor, E_a is the activation energy, k is the Boltzmann constant.

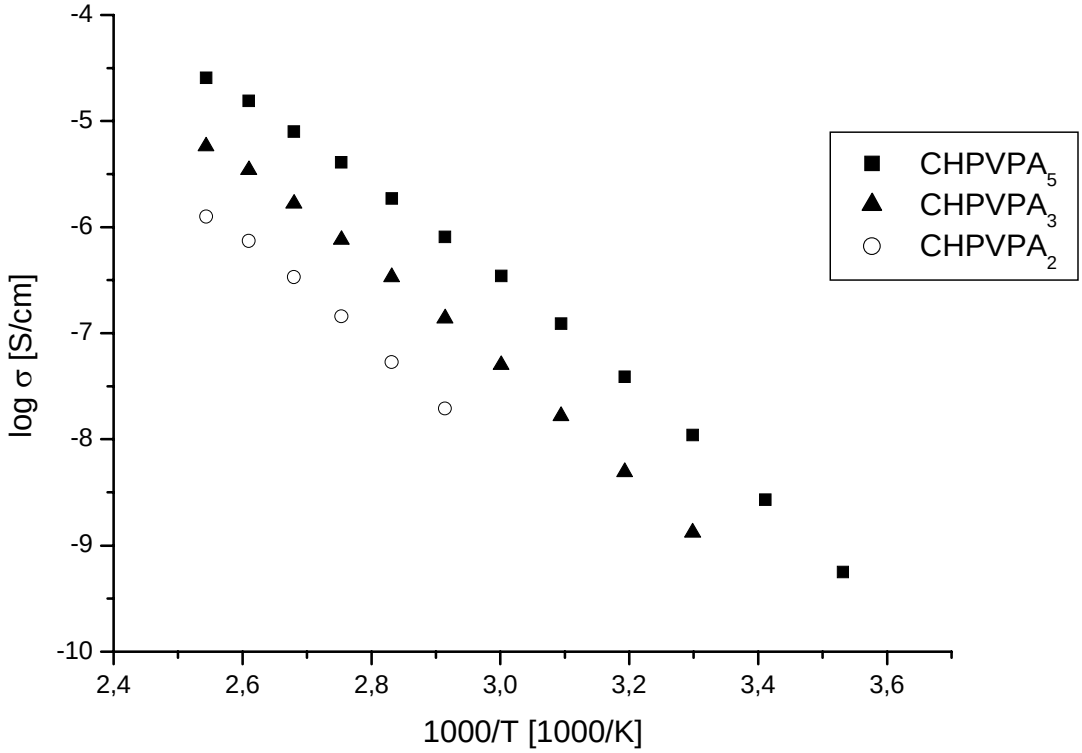

Figure 6.28. Variation of the proton conductivities of $CHPVPA_5$ as a function of reciprocal temperature.

Proton conductivity and activation energy of these composite membranes are listed in Table 6.2.

Table 6.2. Maximum anhydrous proton conductivities and Arrhenius parameters (logσo, Ea) for the chitosan/PVPA composite membranes.

Samples	log σ_o(S/cm)	E_a (eV)	Conductivity (S/cm)
$CHPVPA_5$	7.53053	0.9330	$2.5x10^{-5}$ at 120°C
$CHPVPA_3$	7.21568	0.9629	$5.8x10^{-6}$ at 120°C
$CHPVPA_2$	6.79652	0.9852	$1.3x10^{-6}$ at 120°C

Through preparation of the composite membranes, proton donor and acceptor functions were immobilized into the matrix where the effective proton conduction mechanism can be described as Grotthuss-type diffusion rather than vehicular transport.

Protons which are generated form PVPA molecule transfer to the amino group of chitosan resulting in the electrostatic interaction between $–P–O^-$ and H_3N^+-, as confirmed by FT-IR. As the PVPA composition increases, the materials become more amorphous and the conductivity the composites increases in a similar manner.

Previously, proton conductivity of the chitosan–MP (methanediphosphonic acid) composite materials was reported (Yamada and Honma, 2005). Especially, the chitosan–200 wt. % MP composite material showed the proton conductivity of $5x10^{-3}$ S cm^{-1} at 150 ^oC. In contrast, the pure chitosan film and lightly mixed material (mixing ratio of ≤100 wt.% MP), did not show any measurable proton conductivity (<10^{-8} S cm^{-1} at 150 ^oC). Additionally, the proton conductivity of the pure MP material was $8x10^{-5}$ S cm^{-1} at 150 ^oC under anhydrous conditions. They also reported that pristine chitosan without the addition of dopant did not show any measurable proton conductivity.

Copolymers of vinylphosphonic acid (VPA) and 4-vinylimidazole (4-VIm) were reported (Bozkurt et al., 2003). The conductivity of the copolymers was ranging from 10^{-6} to 10^{-12} S/cm within the measured temperature regime. The reason of the low conductivity was explained by the ionic crosslinking which restricted the segmental relaxations as well as blocking of the free nitrogens in alternating copolymers.

Also chitosan acetate–salt complexes were used to obtain some insight on the mechanism of ionic conductivity in chitosan-based polymer electrolytes (the chitosan acetate, plasticized chitosan acetate and chitosan acetate containing salt) (Osman et al., 2001). The conductivity in these systems was reported to be due to the mobile ions from the salt. Highest proton conductivity in plasticized film containing salt was $4.0x10^{-5}$ S cm^{-1} and for the plasticized films not containing salt was $3x10^{-10}$ S cm^{-1}.

In solid chitosan/PVPA systems, the proton conduction is expected to occur within the neighboring protonated and non-prototonated units. The composite materials showed a relatively better proton conductivity of $3x10^{-5}$ S/cm at 120 ^{o}C in the anhydrous state.

CHAPTER 7

CONCLUSIONS

Novel anhydrous proton conductors were produced by doping of polystyrenesulfonic acid, PSSA with 1H-1,2,4-Triazole and imi3 at various molar ratios. Transparent, homogeneous and elastic films were produced. FT-IR confirmed proton exchange reactions between host polymer and proton solvents and also hydrogen bond network formation. The $PSSATri_x$ and $PSSAimi3_x$ electrolytes are thermally stable up to at least 200 ^oC. The homogeneity of the materials and plastisizing effect of dopants were proved by DSC. After doping of PSSA with Tri and imi3, the T_gs of the $PSSATri_1$, $PSSATri_{1.5}$ and $PSSAimi3_1$ appears at -50 ^oC, -42 ^oC and -36 ^oC, respectively.

From FT-IR and conductivity isotherms it can be concluded that proton conductivity occurs through structure diffusion (Grotthuss mechanism). The proton conductivity of $PSSAimi3_{0.5}$ is approximately 10^{-4} S/cm at room temperature and that of $PSSATri_1$ reaches to a maximum value of 0.016 S/cm at 150 ^oC. Although it was demonstrated that both Tri and imi3 are efficient proton solvents in the PSSA host matrix and yielded promising conductivities for fuel cell application, 1H-1,2,4-Triazole doped membranes showed better conductivity performance above 100 ^oC.

Polysalts of chitosan/PVPA were prepared by in situ polymerization of vinyl phosphonic acid (VPA) in the existence of chitosan. PVPA was successfully utilized as the proton source in chitosan. The resultant composites showed low methanol permeability, better mechanical and thermal properties. The sample $CHPVPA_1$ exhibits a slight weight change up to 180 ^oC and then the material decomposes. When the composition of PVPA

increased to 82%, then the degradation temperature shifts to approximately 150 ^{o}C. DSC measurements were carried out to determine the glass transition temperatures (Tg) of the composites. No distinct Tg was observed up to degradation temperature. The XRD results showed that the materials are completely amorphous.

Proton conducting properties of these anhydrous polymer composite electrolytes increased in parallel with PVPA composition. Chitosan-PVPA composite material showed a relatively high proton conductivity of $2.5x10^{-5}$ S/cm at 120 ^{o}C. The immobilization of acidic units via in situ polymerization is rather interesting and may solve the dopant exclusion problem which was observed especially in PBI/H_3PO_4 systems.

REFERENCES

Acheson R. M., An Introduction to the Chemistry of Heterocyclic Compounds, John Wiley, Canada, 1976.

Ajayan P.M., Schadler L.S., Braun P.V., Nanocomposite Science and Technolocy, Wiley-VCH, pp 112, 2006.

Appleby A. J., Foulkes F. R., Fuel Cell Handbook, Van Nostrand Reinhold, New York, 1989

Asensio J.A., Borros S., Romero Gomez, J. Polym. Sci. Part A: Polym. Chem. Vol. 40, pp 3703, 2002.

Bae B. and Kim D., Journal of Membrane Science, Vol. 220, pp. 75, 2003.

Bae J.M., Honma I., Murata M., Yamamoto T., Rikukawa M., Ogata N., Solid State Ionics Vol. 147, pp. 189, 2002.

Bailly C, Williams DJ, Karasz FE, Macknight WJ. Polymer; Vol. 28, pp. 1009, 1987.

Ball S.C., Platinum Met. Rev. Vol. 49, pp. 27, 2005.

Besse S., Capron P., Diat O., et al., J. New Mater. Electrochem. Syst., Vol. 5, pp. 109, 2002.

Bozkurt, A., Meyer, W. H., Solid State Ionics, Vol. 138, pp. 259, 2001.

Bozkurt A., Meyer W.H., Gutmann J., Wegner G., Solid State Ionics, Vol. 164 pp. 169, 2003.

Bozkurt, A., Meyer, W. H., Wegner, G., Journal of Power Sources, Vol. 123, pp. 126, 2003.

Bozkurt A, Turk J Chem., Vol. 29, pp.117, 2005.

Bozkurt A. and Pakula T., Chemical Physics Letters, Vol. 422, pp. 496, 2006.

Bozkurt A., Ise M., Kreuer K.D., Meyer W.H. and Wegner G., Solid State Ionics, Vol.125, pp. 225, 1999.

Bouchet R. and Siebert E., Solid State Ionics, Vol.118, pp. 287, 1999.

Bingöl B., Meyer W.H., Wagner M., Wegner G., Macromol. Rapid Commun., Vol. 27, pp. 1719, 2006.

Binsu V.V., Nagarale R.K., Shahi V.K., Ghosh P.K., Reactive & Functional Polymers, Vol. 66, pp. 1619, 2006.

Blythe A.R., Electrical properties of polymers, Cambridge University Press 1979, pp. 68-71

Bloys van Treslong C.J., Staverman A.J., Rec. Trav. Chim., Pay-Bas, Vol. 93(6), pp. 171, 1974.

Braun D., Cherdron H., Rehahn M., Ritter H., Voit B., Polymer Synthesis: Theory and Practice; Fundamentals, Methods, Experiments; Fourth Edition, pp. 127, 2004.

Bredas J.L., Chance R.R., Silbey R., Phys Rev B; Vol. 26 pp. 5843, 1982.

Buckley, A., Stuetz, D. E., Serad, G. A., In Encyclopedia of Polymer Science and Engineering, Second Edition, Vol. 11, pp. 572–601, New York, Wiley & Sons, 1988.

Carter R., Wycisk R., Yoo H., Pintauro P.N., Electrochem. Solid State Lett. Vol. 5, pp. A195–A197, 2002.

Chalk A.J., Hay A.S., J. Polym. Sci. A;Vol. 7, pp. 691, 1968

Chin, D.T., Chang, H.H., Journal of Applied Electrochemistry, Vol. 19(1), pp. 95, 1989.

Crofts A., Biophysics 354, Biological Energy Conversion, 1996,

Daniel, M.F., Desbat, B., Cruege, F., Trinquet, O., Lass`egues, J.C., Solid State Ionics, Vol. 28, pp. 637, 1988.

DesMarteau, D.D., Journal of Fluorine Chem., Vol. 72, pp. 203, 1995.

Ding, J., Chuy, C., Holdcroft, S., Adv Funct Mater., Vol. 12, pp. 389, 2002.

Dippel, T., Kreuer, K. D., Lass`egues, J. C., Rodriguez, D., Solid State Ionics, Vol. 61(1–3), pp. 41, 1993.

Energy Policy Act, 2005, http://web.mit.edu/fuelcells/

Flint S.D., Slade R.C.T., Solid State Ionics, Vol. 97, pp. 299, 1997.

Fontanella, J.J., Wintersgill, M.C., Wainright, J.S., Savinell, R.F., Litt, M., Electrochimica Acta, Vol. 43(10–11), pp. 1289, 1998.

Fuell Cell Hand Book, Parsons Inc., West Virginia, 2000.

Gautier-Luneau I., Denoyelle A., Sanchez J.Y., Poinsignon C., Electrochim Acta, Vol. 37, pp.1615, 1992.

Gasa J.V., Weissand R.A., Shaw M.T., Journal of Polymer Science: Part B: Polymer Physics, Vol. 44, pp. 2253, 2006.

Gillham, J. K., Macromolecule Science, Vol. 1, pp. 83, 1972.

Glipa, X., Bonnet, B., Mula, B., Jones, D. J., Rozi`ere, J., Journal of Material Chem., Vol.9(12), pp. 3045, 1999.

Gupta B., Buchi F.N., Scherer G.G., Solid State Ionics; Vol. 61, pp. 213, 1993.

Günday S.T., Bozkurt A., Meyer W.H. and Wegner G., J.Polym. Sci. Polym Phys, Vol. 44, pp.3315, 2006.

Gowariker V.R., Vishwanathan N.V., Sridhar J., Polymer Science, New Age International, New Delhi, 1999

Guo X., Fang J., Watari T., Tanaka K., Kita H., Okamoto K., Macromolecules Vol. 35, pp. 6707, 2002.

Hatakeyama T. and Quinn F.X., Thermal Analysis Fundamentals and Applications to Polymer Science; Second Edition

Higuchi M., Minoura N., Kinoshita T., Chem. Lett., pp. 227, 1994.

Hogarth, M., Glipa, X., "High Temperature Membranes For Solid Polymer Fuel Cells", ETSU F/02/00189/REP DTI/Pub URN 01/893 , 2001.

Hoogers G., Fuel Cell Technology Handbook, CRC Press, Washington, DC, 2003.

Hofmann M.A., Ambler C.M., Maher A.E., et al., Macromolecules, Vol. 35, pp. 6490, 2002

Honma I., Takeda Y., Bae J.M., Solid State Ionics, Vol. 120, pp. 255, 1999.

Ismail A.F., Zubir N., Nasef M.M., Dahlan K.M. and Hassan A.R., Journal of Membrane Science, Vol. 254, pp. 189, 2005.

Jang L. K., Nguyen D., Geesey G.G., Water Res., Vol. 33, pp. 2826, 1999.

Jannasch P., Current Opinion in Colloid and Interface Science, Vol. 8, pp. 96, 2003.

Jiang D.D., Yao Q., McKinney M.A., Wilkie C.A., Polym. Degrad. Stabil., Vol. 63, pp. 423, 1999.

Johnson B.C., Ylgor I., Iqbal M., Wrightman J.P., Lliyd D.R., McGrath J.E., J. Polym. Sci: Polym. Chem., Ed. 1984

Karadedeli B., Bozkurt A., Baykal A., Physica, Vol. B 364, pp. 279, 2005.

Kawahara M., Rikukawa M., Sanui K., Ogata N., Solid State Ionics, Vol. 136, pp. 1193, 2000.

Kawahara M., Morita J., Rikukawa M., Sanui K., Ogata N., Electrochim Acta., Vol. 45, pp. 1395, 2000.

Kim J.H., Lee Y.M., Polymer, Vol. 34(9), pp. 1952, 1993.

Kim J.D., Honma I., Solid State Ionics, Vol. 176, pp. 979, 2005.

Kolhe P., Kannan R.M., Biomacromolecules, Vol. 4, pp. 173, 2003.

Kotov, S.V., Pederesen, S.D., Qui, W.Z.M., Burton, D.J., Jornal of Fluorine Chem., Vol. 82, pp. 13, 1997.

Kobayashi T., Rikukawa M., Sanui K., Ogata N., Solid State Ionics; Vol. 106, pp. 219, 1998.

Kreuer, K.D., Weppner W., Rabenau A., Angew. Chem., Int. Ed., Vol. 21, pp. 208, 1982.

Kreuer, K.D., Journal of Molecular Structure, Vol.177, pp 265, 1988.

Kreuer K.D., Dipel, T.H., Meyer, W.H., Maier, J., "Perfluorinated Ionemer Membranes", Proceedings of the First International Symposium on Material Research Society, 10-21 April, Vol. 293, pp. 273-282, Mainz, 1993.

Kreuer, K.D., Chemistry Materials, Vol. 8, pp.610, 1996.

Kreuer K.D., Fuchs A., Ise M., Spaeth M. and Maier J., Electrochim. Acta, Vol.43, pp. 1281, 1998.

Kreuer, K.D., Proceedings of the sixth Asian Conference on Solid State Ionic: Science and Technology, 29 November-4 December, pp. 263, New Delhi, 1998.

Kreuer, K.D., Solid State Ionics, Vol. 136–137, pp. 149, 2000.

Kreuer, K.D., Journal of Membrane Science, Vol. 185, pp. 29, 2001.

Larminie J., Dicks A., Fuel Cell Systems Explained, Wiley, West Sussex, 2000.

Lass`egues, L.C., Desbat B., Trinquet O., Cruege F., Poisignon C., Solid State Ionics, Vol. 35(1–2), pp. 17, 1989.

Lassegues J.C., Grondin J., Hernandez M. and Maree B., Solid State Ionics, Vol. 145 pp. 37, 2001.

Li S., Zhou Z., Zhang Y. and Liu M., Chem. Mater., Vol. 17, pp. 5884, 2005.

Li S., Krishnan L., Srinivasan S., Benziger J., Bocarsly A.B., Journal of Membrane Science, Vol. 243, pp. 327, 2004.

Ling J., Savadogo O., J. Electrochem. Soc. Vol. 151, pp. A1604, 2004.

Liu, W., Ruth, K., Rusch G., Journal of New Material Electrochemical Systems, Vol. 4, pp. 227, 2001.

Lide DR, Handbook of Chemistry and Physics, Boca Raton: CRC Press, 1995

Li S., Zhou Z., Zhang Y., Liu M., Chemistry of Materials, Vol. 17, pp. 5884, 2005.

Manthiram Y.F.A. and Guiver M.D., Electrochemistry Communications, Vol.8, pp. 1386, 2006.

Miyatake K., Iyotani H., Yamamoto K., Tsuchida E., Macromolecules; Vol. 29, pp. 6969, 1996.

Munson R.A., Lazarus M.E., Journal of Physical Chemistry, Vol. 71(10), pp. 3245, 1967.

Munson R.A., Journal of Physical Chemistry, Vol. 68(11), pp. 3374, 1964.

Murthy N.S., Minor H., Polymer, Vol. 31, pp. 996, 1990.

Münch W., Kreuer K.D., Silvestri W., Maier J., Seifert G., Solid State Ionics, Vol. 145, pp. 437, 2001.

Neburchilov V., Martin J., Wang H., Zhang J., Journal of Power Sources Vol. 169, pp. 221, 2007.

Nicholas P. Cheremisinoff, Ph.D.; Polymer Characterization Laboratory Techniques and Analysis

Osman Z., Ibrahim Z.A., and Arof A.K., Carbohydrate Polymers Vol. 44, pp. 167, 2001.

Osugi N., Dong T., Hexig B. and Inoue Y., Journal of Applied Polymer Science, Vol. 104, pp. 2939, 2007.

Peled E., Duvdevani T., Aharon A., Melman A., Electrochem. Solid-State Lett., Vol. 3, pp. 525, 2000.

Ponce M.L., L.A.S. de, Prado A., Silva V., Nunes S.P., Desalination, Vol. 162, pp. 383, 2004.

Pourcelly G., Oikonomou A., Hurwitz H.D., Gavach C., Journal of Electroanalytical Chemistry, Vol. 287, pp. 43, 1990.

Przyluski J., Wieczorek W., Synthetic Metals, Vol. 45, pp. 323, 1991.

Pu H., Meyer W.H, Wegner G., Journal of Polymer science: Polymer Physics, Vol. 40(7), pp. 663, 2002.

Qingfeng L., Hjuler H.A., Bjerrum N.J., Journal of Applied Electrochemistry, Vol. 31, pp. 773, 2001.

Qi Z., Pickup P.G., J. Chem. Soc. Chem. Commun.:15., 1998.

Qi Z., Lefebvre M.C., Pickup P.G., J. Electroanal Chem.; Vol. 9, pp. 459, 1998.

Rao P.S., Sridhar S., Wey M.Y., Krishnaiah A., Ind. Eng. Chem. Res., Vol. 46, pp. 2155, 2007.

Rikukawa M., Morita J., Sanui K., Ogata N., Proceedings of the Fifth International Symposium on Polymer Electrolytes, p.32, 1996.

Rieke P.C., Vanderborgh N.E., Journal of Membrane Science, Vol. 32, pp. 313, 1987.

Rikukawa M. and Sanui K., Prog. Polym. Sci., Vol.25, pp. 1463, 2000.

Rodriguez D., Jegat C., Trinquet O., Grondin J., Lass`egues J.C., Solid State Ionics, Vol. 61(1–3), pp. 193, 1993.

Savadogo O, Varela F.J.R, Journal of New Material Electrochemical Systems, Vol. 4(2), pp. 93, 2001.

Savett S.C., Atkins J.R., Sides C.R., Harris J.L., Thomas B.H., Creager S.E., Pennington W.T., DesMarteau D.D., Journal of Electrochemical Society, Vol. 149, pp. A1527, 2002.

Saxena A., Kumar A., Shahi V.K., Journal of Colloid and Interface Science, Vol. 303 pp. 484, 2006.

Sevil F., Bozkurt A., Journal of Physics and Chemistry of Solids, Vol. 65, pp. 1659, 2004.

Senadeera G.K.R., Gareem M.A., Skaarup S., West K., Solid State Ionics, Vol. 85, pp. 37, 1996.

Schuster M.F.H., Meyer W.H., Annu. Rev. Mater.Res., Vol. 33 pp. 233, 2003.

Schuster M., Meyer W.H., Wegner G., Herz H.G., Ise M., Kreuer K.D., and Maier J., Solid State Ionics Vol. 145, pp. 85, 2001.

Schoolman D., Trinquet O., Lass`egues J.C., Electrochimica Acta, Vol. 37(9), pp. 1619, 1992.

Silva V.S., Weisshaar S., Reissner R., Ruffmann B., Vetter S., Mendes A., Madeira L.M., Nunes S., J. Power Sources Vol. 145 pp. 485, 2005.

Singleton R.W., Noether H.D., Tracy J.F., Journal of Polymer Science: Polymer Symposium, Vol. 19, pp. 65, 1967.

Smitha B., Sridhar S., Khan A.A., Journal of Membrane Science Vol. 259, pp. 10, 2005.

Smitha B., Sridhar S., Khan A.A., Journal of Power Sources, Vol. 159, pp. 846, 2006.

Soczka-Guth T., et al., International Patent WO99/29763 (1999)

Sun J., Jordan L.R., Forsyth M. and MacFarlane D.R., Electrochim. Acta, Vol. 46 pp. 1703, 2001.

Steele B.C.H. and Heinzel A., Nature Photonics, Nature 414, pp. 345, 2001.

Stevens J.R., Wieczorek W., Raducha D., Jeffrey K.R., Solid State Ionics., Vol. 97, pp. 347, 1997.

Tanaka R., Yamamoto H., Kawamura S., Iwase T., Electrochimica Acta.,Vol. 40(13), pp. 2421, 1995.

Tanaka R., Yamamoto H., Shono A., Kubo K., Sakurai M., Electrochimica Acta, Vol. 45(8–9), pp. 1385, 2000.

Tang H., Pintauro P.N., Journal of Applied Polymer Science, Vol. 79, pp. 49, 2001.

Vink H., Macromol. Chem. and Physics, Vol. 182, pp.279, 1981.

Voet D., and Voet J.G., Biochemistry, John Willey &Sons, New York,1992.

Vogel C., Meier-Haack J., Taeger A., Lehmann D., On the stability of selected monomeric and polymeric aryl sulfonic acids on heating in water (Part I), Fuel Cells 4 (4) pp. 320–327, 2004.

Wainright J.S., Wang J.T., Weng D., Savinell R.F., Litt M., Journal of Electrochemical Society, Vol. 142(7), pp. L121, 1995.

Wasmus S., Daunch A., Moaddel H., Rinaldi P.L., Litt M., Presented at 187 th Electrochem. Soc. Meet, Reno, Abstr. 466, 1995.

Wang F., Hickner M., Kim Y.S., Zawodzinski T.A., McGrath J.E., J. Membr. Sci., Vol. 197, pp. 231, 2002.

Wieczorek W., Stevens J.R., Polymer, Vol. 38, pp. 2057, 1997.

Yamada M., Honma I., Chem. Phys. Chem., Vol. 5, pp. 724, 2004.

Yamada M., Honma I., Polymer, Vol. 45, pp. 8349, 2004.

Yamada M., Honma I., Angew Chem, Int Ed., Vol. 43, pp. 3688, 2004.

Yamada M., Honma I., Journal of Physical Chemistry, Vol. 108, pp. 5522, 2004.

Yamada M., Honma I., Polymer, Vol. 46, pp. 2986, 2005.

Yamada M., Honma I., Electrochim. Acta, Vol.48, pp. 2411, 2003.

Yamada M., Honma I., Electrochimica Acta, Vol. 50 pp. 2837, 2005.

Yamada M., Honma I., Polymer, Vol. 46, pp. 2986, 2005.

Yang C., Costamagna P., Srinivasan S., Benziger J. and Bocarsly A.B., Journal of Power Sources, Vol.103, pp. 1, 2001.

Yeo R.S., McBreen J.C., Journal of Electrochemical Society, Vol. 130, pp.533, 1983.

Zhou Z., Li S., Zhang Y., Liu M. and Li W., Journal of American Chemical Society Vol. 127, pp. 10824, 2005.